1-1-2013

Welding Parameters, Distortion and Mechanical Properties of AA7075 Lap Joints in SSFSW

Hejun Yu
University of South Carolina

WELDING PARAMETERS, DISTORTION AND MECHANICAL PROPERTIES OF AA7075 LAP JOINTS IN SSFSW

by

Hejun Yu

Bachelor of Science
North China University of Technology, 2008

Submitted in Partial Fulfillment of the Requirements

For the Degree of Master of Science in

Mechanical Engineering

College of Engineering and Computing

University of South Carolina

2013

Accepted by:

Anthony P. Reynolds, Major Professor

Xiaodong Li, Committee Member

Lacy Ford, Vice Provost and Dean of Graduate Studies

DEDICATION

This work is dedicated to the honor of my parents, Lu Xia and Chunyu Yu, their endless love and support for me made it all possible.

Also to my friends who have supported me through the trials of graduate school. It was a rough road, but I never would have made it without the encouragement. Yuchen Huang and many others.

ACKNOWLEDGEMENTS

I am grateful to my adviser, Dr. Reynolds for his wisdom advice and kindness support on my academic and research. I thank Dr. Wei Tang for his diligent effort to my experiments and thesis. I also would like to thank Mr. Dan Wilhelm, FSW lab technician and talented craftsman, for his help and mentorship in the experiment procedure. And many thanks to my wonderful team member Piyush Upadhyay, Xiao Li, Xiaomin Huang, Reza-E-Rabby, Clinton Canaday for their patience and assistance on my research. Thanks to Boeing for funding on my research, without funding, this work would not have been possible.

Finally, thanks to those who have always encouraged and supported me during this thesis writing.

ABSTRACT

Friction Stir Welding (FSW), first invented by The Welding Institute of UK (TWI) in 1991, is a solid state welding process which was initially applied to welding Aluminum Alloy. FSW has wide application in industrial sectors. Stationary shoulder friction stir welding (SSFSW) was first developed to weld low thermal conductivity Ti-based alloys, which are hard to weld using conventional friction stir welding. Previous literatures showed SSFSW can produce uniform temperature distribution through thickness during the welding process. Since SSFSW is still under study phase, its advantages and disadvantages are not yet well defined. It is important to study the characteristics of SSFSW for its further application.

The object of this thesis is to develop low distortion and high mechanical properties for AA7075-T6 parallel double-pass lap joints using SSFSW. The effect of welding control parameters and tool design on process response was investigated. Then the microstructure, distortion, and mechanical properties of AA7075 after FSW were studied. The effect of post welding heat treatment (PWHT) on distortion and mechanical properties was also investigated.

The study found that rotation speed affects torque and total power in SSFSW. Z-force was the main factor affecting X-force. Tool design didn't affect process response much. Saddle shape was observed for distortion distribution of SSFSW. PWHT helped to reduce distortion and regain mechanical property. Fine and equiaxed grains were observed in the weld nuggets. Grain size increased with power input for a given welding speed. Microhardness tests revealed higher hardness present at weld nugget zone (WNZ) and base material, and lower hardness present at HAZ. Tensile test showed the maximum ultimate stress (UTS) was 537.37MPa. Most tensile tests failed at the cavity defect area or at HAZ.

TABLE OF CONTENTS

LIST OF TABLES

LIST OF FIGURES

LIST OF ABBREVIATIONS

AA	Aluminum Alloy
AS	Advancing Side
AW	As Welded
BS	Base Material
CFSW	Conventional Friction Stir Welding
FSW	Friction Stir Welding
HAZ	Heat Affected Zone
HV	Vickers Hardness
MLI	Mean Linear Intercept
PWHT	Post Weld Heat Treatment
RS	Retreating Side
SAZ	Shoulder-affected Zone
SEM	Scanning electron microscopy
SSFSW	Stationary Shoulder Friction Stir Welding
TMAZ	Thermo-mechanically Affected Zone
TWI	The Welding Institute

UTS	Ultimate Tensile Strength
WNZ	Welding Nugget Zone

CHAPTER 1 INTRODUCTION

1.1.Background

Friction Stir Welding (FSW), first invented by The Welding Institute of UK (TWI) in 1991, is a solid state welding process which was initially applied to welding Aluminum Alloy. The FSW welding process is that a non-consuming rotating pin tool heat and plasticize the base materials by friction, which result in forging of the materials together [1]. The advantages of FSW include: 1) being able to weld unweldable materials by traditional fusion welding method, like Aluminum Alloy 2XXX and 7XXX [2], 2) decrease severe distortion and residual stress happened in fusion welding [3][4], 3) have Fine recrystallized microstructure [5], 4) no solidification cracking encountered in fusion welding [6]. FSW has become a widely used welding technique in automotive, shipping and aerospace industries. However, conventional FSW (CFSW) is also facing many challenges, such as: 1) Generating flash on welding surface [5], 2) heterogeneous heat input on metal material, which may lead to surface overheating with rotating shoulder[7].

Stationary Shoulder FSW was developed by TWI for welding low thermal conductivity Titanium Alloys. With the non-rotational shoulder, SSFSW has the potential

of 1) generating no flash, 2) reducing heat input at the top of CFSW joint, 3) producing a more uniform heat input to the welded material. The mechanism of SSFSW was shown in Figure 1.1 [8]. The stationary shoulder and stationary tool head are fixed. They are located outside the rotating pin. The stationary shoulder slides over the surface of the material during the welding process instead of rotating, therefore stationary shoulder generates much less heat input than rotating shoulder [8].

SSFSW is still under research state, heat generation and material flow on the welding material and between the tool parts are still unclear. So it's important to study SSFSW process and its welding performance for its further application. In this work, the welding parameter for AA7075-T6 parallel pass lap joint in SSFSW is studied to find the optimum welding condition to achieve low distortion, good microstructure, hardness, and tensile strength.

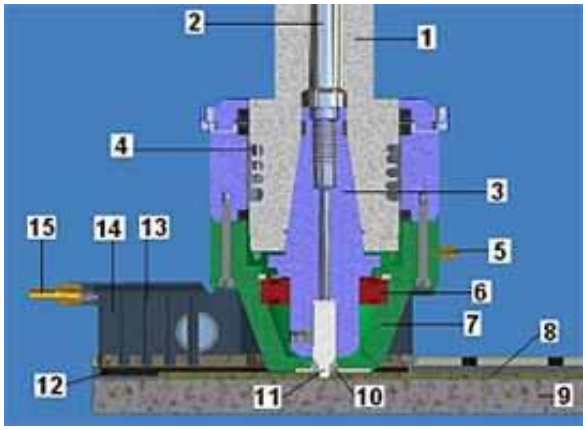

Figure 1.1 Stationary Shoulder FSW mechanism [8]

1) Rotating spindle, 2) Draw bar, 3) ISO 50 Tool holder, 4) Water cooling jackets, 5) Argon input, 6) Support bearing, 7) Stationary tool head, 8) Ti workpiece 9) Backing plate, 10) Sliding shoe, 11) Rotating pin, 12) Sliding seal, 13) Argon supply, 14) Gas chamber, 15) Inert gas input

1.2.AA7075-T6

Aluminum Alloy 7075-T6 (AA7075-T6), first introduced by Alcoa in 1943, is an Al-Zn-Mg-Cu alloy. It has high strength and corrosion resistance with addition of chromium. T6 means the alloy is solution heat-treated and then artificially aged to a peak aged condition [9]. Alloy 7075 sheet and plate have wide application on aircraft and aerospace structures where both high strength and corrosion resistance are required. AA7075-T6 offer moderately good strength to toughness relationships and act as the standard of comparison for more recent 7XXX series alloy developments. General chemical composition of AA 7075-T6 was shown in Table 1.1.The mechanical properties of AA 7075-T6 including strength, hardness and temperature were shown in Table 1.2[10][11].

Component	Wt. %	Component	Wt. %	Component	Wt. %
Al	87.1 - 91.4	Mg	2.1 - 2.9	Si	Max 0.4
Cr	0.18 - 0.28	Mn	Max 0.3	Ti	Max 0.2
Cu	1.2 - 2	Other, each	Max 0.05	Zn	5.1 - 6.1
Fe	Max 0.5	Other, total	Max 0.15	ASM Material Date	

Table 1.1 Chemical composition of AA7075-T6 [10]

Alloy	Solution Heat treat temperature	Aging temperature	Strength		
			Tensile Yield	Ultimate Tensile	Hardness (Vickers)
AA 7075-T6 sheet	482 ℃	121 ℃ (24H)	503 MPa(T6)	572 MPa(T6)	175(T6)

Table 1.2 Mechanical properties of AA7075-T6 [11]

1.3.Lap Joint of FSW

Lap joint is a joint between two overlapping plates. In FSW, the rotating tool pin is plunged through the top plate and partially into the bottom plate. Lap joint has wide applications in automotive and aircraft industries. it is often used in parts assemblies. It can substitute fastener (rivets or bolts) replacement for shorter time. Figure 1.2 demonstrates the lap joint in friction stir welding process [12].

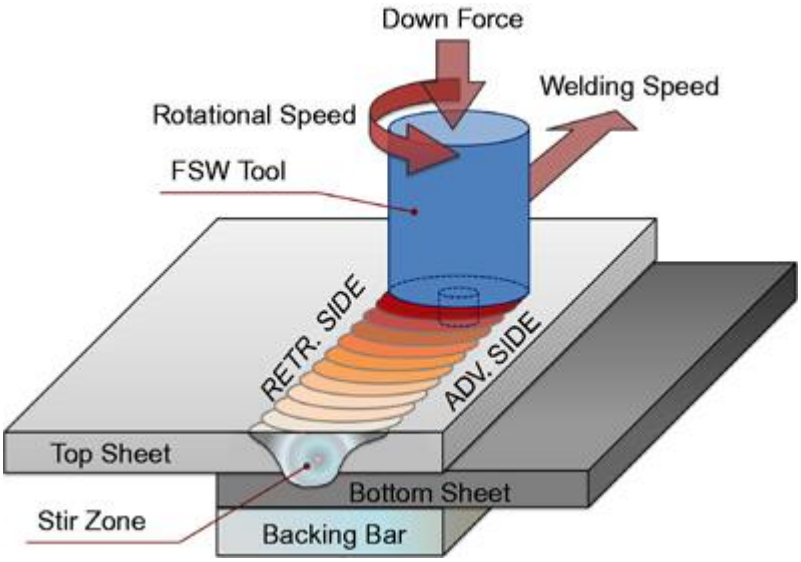

Figure 1.2 Schematic picture of lap joint in Friction Stir Welding [12]

1.4.Tool Design

Tool design is important in FSW because it affects heat generation, material flow, and welding quality. In conventional FSW, the rotating shoulder generates considerable heat, while in SSFSW, the stationary shoulder generates much less heat compared to CFSW shoulder, which is mainly contributed by friction on the welding surface. SSFSW

rotating tool pin generates large portion of total heat. So the effect of tool design may be very different for SSFSW from CFSW. Cylinder and taper pin with thread were both used in this study to compare their effect on SSFSW process. Study on CFSW showed that using tapered tools with thread can achieve defect free welds [7]. Non-flat and tri-flat design pin were both adopted in the study.

Previous literature showed the effect of tool design on microstructure and mechanical properties of the material are not very obvious. For AA6061-T6, grain size on the bottom of stir zone was slightly smaller for triangular prism tool than that for the column shape tool, while tensile strength didn't change with tool shape [13]. For this reason, the effect of tool shape was only compared in process response part in this study.

1.5. Welding parameters

Welding control parameters include rotation speed, welding speed and downward force (Z-force). It's important to select right welding parameters so that optimum process response (torque, X-direction force, power) and welding quality can be achieved. Torque is an indicator of shear stress around the tool. Reducing torque minimize the total power required, thus enhance the energy efficiency. X-force is an indicator of tool failure. Excessive X-force will cause tool failure [7].

Torque decreases with increasing rotation speed due to higher temperature caused by higher heat generation rate (heat input/time), whose indicator is power input. The effect

of welding speed on torque is not significant in conventional FSW [14]. Although increasing rotation speed sometimes showed the tendency to reduce X-force, the relationship between X-force and rotation speed is not clear [15]. The process responses under different welding control parameters are extensively compared in this study, in order to find a locally optimum welding parameter combination for AA7075 SSFSW.

1.6. Thermal Cycle

Thermal cycle in FSW depends on process parameter like rotational and welding speed and forges force. The peak temperature in the stir zone is proportional to rotation speed, whereas the cooling rate is dependent on welding speed. Cooling rate can also be increased by employing rapid cooling techniques such as welding under water and in the presence of cold fluids. Mahoney et al measured temperature distribution Peak temperature distribution adjacent to a friction stir weld on a 6.35mm AA7075 plate [16] (See Figure 1.3).

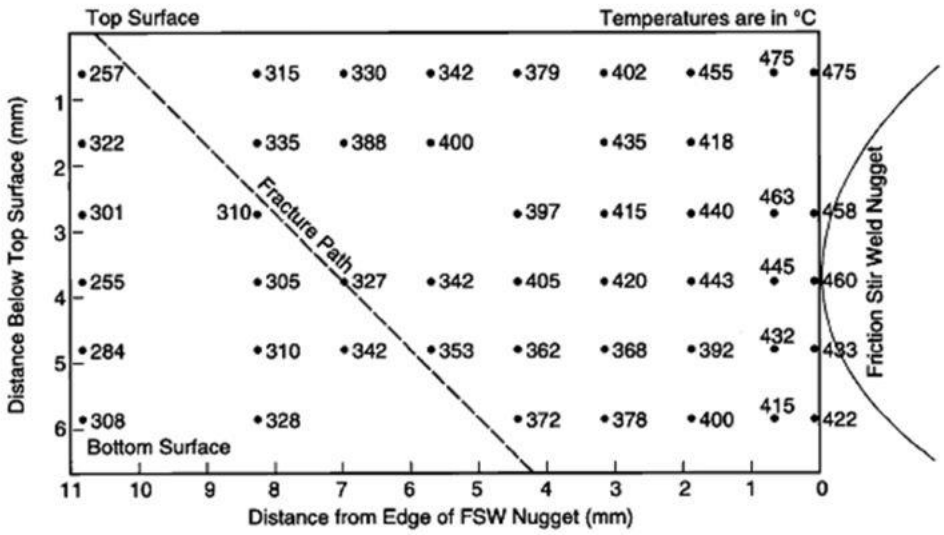

Figure 1.3 Peak temperature distribution adjacent to a friction stir weld in AA7075 T651 [16]

1.7.Precipitation

AA7075-T6 gain strength during precipitation hardening. Usually, 7XXX series aluminum alloy is strengthen by a particular precipitate phase, however different precipitate phases can be present simultaneously. For FSW, it is important to find ideal strengthening that can form homogeneous distribution of second phase particle. In the Al–Zn–Mg 7XXX series Al alloys, the supersaturated solid–solution decomposes in the following sequence [17].

Supersaturated solid solution → GP zone → η′(MgZn2) → η($MgZn_2$)

AA7075 precipitation begin in supersaturated solid solution, Guinier-Preston(GP) Zone usually happen at 140 ℃. From 140 ℃ to 220 ℃, GP Zone gradually give rise to forming η' phase, which is believed to have peak aged strength. At higher temperature, Coarsen η tend to form, which lead to loss of strength. Around 450 ℃- 475 ℃, precipitates dissolve into the aluminum matrix.

The precipitate stability process of 7XXX series Aluminum Alloy is listed below [18].

1) Strengthening (coherent) η phase begin to dissolve when T ≥ 190 ℃.
2) Incoherent η phase precipitates between 215 and 250 ℃.
3) When temperature is around 250 °C η begin to coarsen.
4) The temperature for η phase dissolution is at T≥320 ℃.
5) Incoherent η phase forms at around 350 ℃, the solute depleting from the matrix at fastest speed.

After heat treatment of 120 ℃ (T6), TEM analysis showed the presence of fine strengthening precipitates in the nugget similar to the one present in the base metal [19]. The precipitates were severely coarsened in the HAZ by the thermal cycle. The study from Reynolds et al showed minimum hardness was observed where the peak temperature was 350 ℃, which likely associate with solute depletion by η phase precipitation [18].

1.8.Material Flow

Flow pattern of material in FSW affect the thermomechanical histories and welding parameters. Typically there are two kinds of material movement in FSW. One is extrusion around the pin: a) Material on advancing side is highly deformed and sloughs off behind the pin forming arc-shape. b) Material on the retreating side fills in material on its own side and never rotates around the pin [20]. The other is extrusion from upper portion of the pin welding path, which material is forced down by the pin thread and deposited in the weld nugget by compressive pressure [21].

A low welding speed to rotation speed ratio, also referred as hot weld, often caused more vertical material transport. On the other hand, a high welding speed to rotation speed ratio, also referred as “cold weld”, often caused less vertical transport [22].

1.9.Post Weld Heat Treatment (PWHT)

Post weld heat treatment is an artificial aging process intended to help heat-treatable alloys, like AA7075-T6, to regain initial mechanical properties. Study in PWHT showed

significant reduced distortion and strength of welding sheets. Aging process let the alloy form intermetallic particles, which can improve hardness according to the particle hardening mechanisms [23] . Post Weld Heat treatment (PWHT) effect on distortion and mechanical properties will be discussed at result and discussion part.

1.10. Microstructure

Threadgill et al. first classify conventional Friction Stir Welding microstructure into four distinct zones. 1) Weld Nugget: stirring zone by pin rotation, fully recrystallized area. 2) Heat Affect Zone (HAZ): material zone which is close to welding area, have thermal effect but no plastic deformation. 3) Thermo-mechanically Affected Zone (TMAZ): transition zone between HAZ and weld nugget that have plastic deformation without recrystallization and thermal effect. (It is usually difficult to distinguish the precise boundary between TMAZ and WNZ.) 4) base material: material zone that is remote from the welding area and nearly keep the original microstructure and mechanical properties. [5]

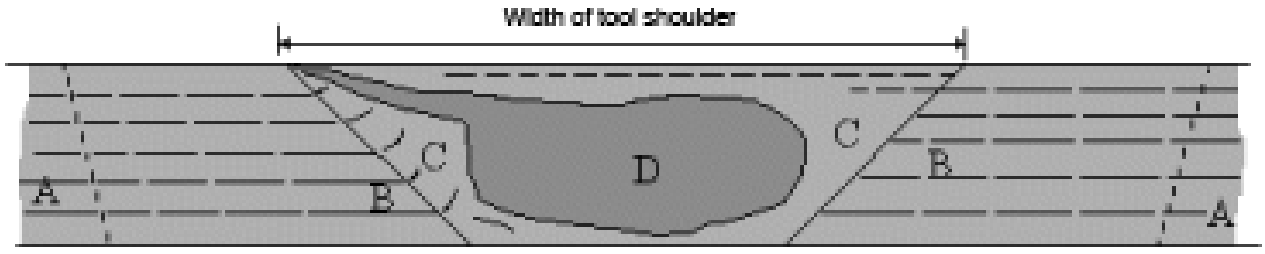

Figure 1.4 Various microstructural regions in the cross section of a CFSW [5]

A: base material, B: heat-affected zone (HAZ), C: thermo-mechanically affected zone (TMAZ), D: welding nugget zone (WNZ).

The microstructure of AA7075 after Conventional FSW process has been extensively studied in the industry. It is known that base material and HAZ showed unrecrystallized pancake shape microstructure [24]. WNZ exhibited equiaxed recrystallized fine grain, where density dislocation is relatively small [2].

Figure 1.5 (from this study) showed the metallographic cross section AA7075-T6 in SSFSW and CFSW. Microstructure regions of lap joint (AA7075) SSFSW was similar to conventional FSW, it was still classified into four distinct zones. It should be noticed that the typical flash was produced by CFSW.

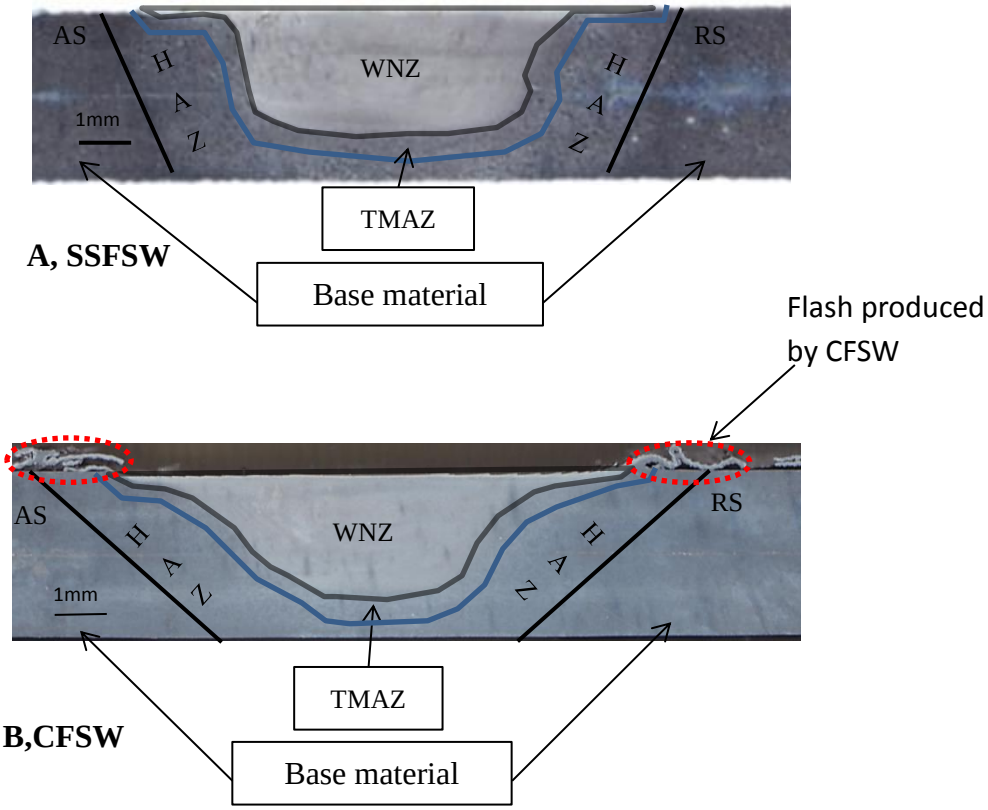

Figure 1.5 Comparison between SSFSW&CFSW microstructure regions of lap joint(AA7075) by tapered tri-flats tools

1.11. Defects

Defects in FSW result from improper process temperature, material flow and joint geometry. Common defect in FSW is wormhole, which often happens in cold weld due to excessive welding speed. Lap joint FSW may likely introduce top sheet thinning defect and kissing bond defect. Sheet thinning is the up/down-turning of original joint line faying surface caused by excessive vertical flow (hot weld), which may decrease shear strength. The kissing bond defect is separation of the interfaces due to insufficient heat transferred (cold weld) [7].

1.12. Distortion

Although FSW is a low distortion and residual stress welding method, there are situations that distortion of different degree can happen in FSW. With the wide application of FSW, studies on distortion are needed more. Literatures on distortion on Aluminum Alloy revealed that the distortion after FSW process generally displays a saddle shape. This is caused by extrusion difference between top and bottom surface during FSW process [25]. The downward tool pressure can release some of the local plastic deformation due to welding thermal cycles and constraint, hence help reduce the distortion [26].

1.13. Residual Stress

Residual stress and distortion are important aspects for Aluminum Alloy FSW. Residual stress is the remained stress within welds after removing the external forces and thermal input. Tensile residual stress is known to decrease fatigue life and corrosion resistance. It is mainly caused by uneven expansion and contraction due to heating. The hole drilling technique can be used to gain the residual stress profiles for 7075-T6 aluminum alloys [27]. Several studies showed that high residual stress happen in HAZ. Richards et al. studied active cooling method to achieve low residual stress [28]. Heat treatment can effectively remedy the internal stress and they were able to enhance the tensile strength of AA7075 after FSW up to 10% [29].

1.14. Mechanical Properties

AA7075-T6 is designed to have high hardness and strength. So its mechanical property after FSW process is especially important. Hardness distributions in 7XXX (precipitation hardening alloy) depend on local thermal history and heat treatment. Hardness distribution usually has a "W" shape curve with the lowest point occurring in HAZ [5]. In HAZ hardness decrease due to the accelerated ageing and recovering due to the weld thermal cycle [30]. The highest hardness often happens at the nugget area, there is a sudden decrease in hardness on both side of the nugget, falling through TMAZ, and lowest hardness happens at the HAZ [18][31].

Tensile properties of the weld have been proven to be related to the hardness distribution, so the location of fracture in transverse tension is also at hardness minimum in HAZ [32].

1.15. Literature Reviews on SSFSW

SSFSW is quite new technique, there are only a few published papers on SSFSW, and most of them study on the microstructure and texture aspects of SSFSW. Davies, et al studied the microstructure of Ti-6Al-4V in SSFSW process [8]. Ahmed, et al demonstrated that by welding with a stationary shoulder, the shoulder-affected region in the weld crown of an AA6082 weld was reduced in size, which is significant for HAZ reduction [33]. Li, et al studied AA2219-T6 in SSFSW, they found microstructure and hardness distribution of AA2219-T6 demonstrate asymmetry property [34]. Another literature by Li, et reported the relationship between rotation speed and microstructure and tensile properties for AA2219-T6 in SSFSW. They found defect free joint were obtained under rotation speed from 600 rpm to 900 rpm. Tensile strength reached maximum of 69% base material at 800RPM. Defect-free joints were fracture at minimum hardness area in WNZ, whereas the joints with defect fracture at defect location [35]. Martin, et al applied SSFSW to T-joint corner weld, and was able to achieve defect free weld [36].

CHAPTER 2 EXPERIMENTAL PROCEDURE

2.1.Friction Stir Welder

All the Aluminum Alloy welds in this study were welded using MTS FSW Process Development System (See Figure 2.1).

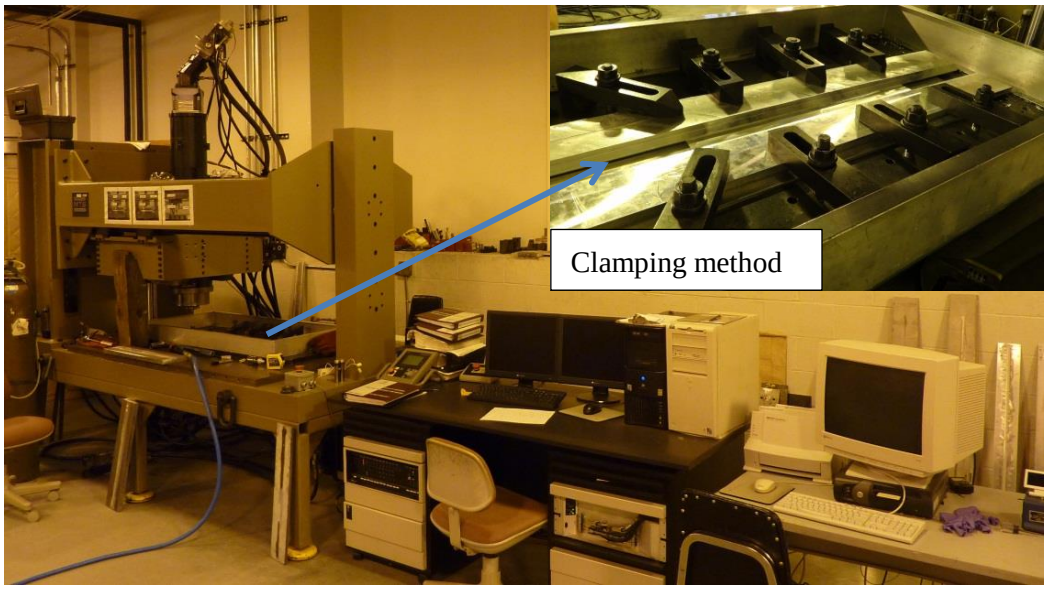

Figure 2.1 MTS FSW Process Development System

MTS FSW Process Development System is a hydraulically powered semi-automatic machine. Welding parameters can be preprogramed on the machine with customized control screen. The platform has room for a maximum 1m ×1m weld plate. There are two control modes for the machine: load control and position control. Load control mode is

suggested for welding Aluminum Alloy in the experiment. Load control mode adjust the downwards force (Z-force) to keep the tool touching or below the material surface. When proper Z-force is applied in FSW, smooth welds surface can be produced. The spindle that runs on the hydraulic servo motor has the rated torque of 169N·m at peak rotation speed 3000rpm. Greater toque can be achieved by reducing the gear at range of one to five and one to three. X direction travel speed can reach up to 2286 mm/min. The maximum downward force (Z-force) that the machine can apply is 133.4kN, which is accomplished by two hydraulic actuators.

2.2.Material and Sheet Preparation

AA7075-T6 sheets, produced by ALCOA, were received from Boeing Phantom Works with two sets of dimensions: 1206.5mm x 152.4mm x 1.6mm and 1206.5mm x 38.1mm x 1.6mm (See Figure 2.2). Then alloy sheets were cut into shorter length from 377.8mm to 604.8mm using a vertical band saw. The lengths of the weldments are listed in table 2.3. The cut edges of the welds were deburred with a steel file. Any surface oxidation around the welding area of the sheets was removed to using a DeWalt (DW402) 114 mm Angle Grinder with 3M Bristle Disks ensures welding performance. Then all the welding sheets were wiped clean with a dry clean cloth.

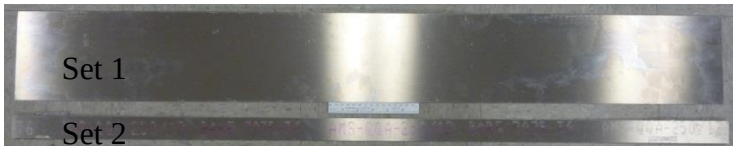

Figure 2.2 Received AA7075-T6 welding sheet (two sets)

2.3. Welding Tools

Stationary shoulder tool was made from two assemble pieces: stationary shoulder and rotating shank with threaded pin. Conventional shoulder tools also contained two assembling pieces: rotational shoulder and pin. For SSFSW, shoulder had diameters of 11.4mm and 12.7mm. Cylinder pin w/o flats and 8^0 taper pin were each fabricated with thread. Both left-hand (LH) and right-hand (RH) thread form were adopted on SSFSW tool pin to compare the difference. For CFSW, only one set of geometry was chosen because it simply acted as calibration for each SSFSW experiment group in this study. The rotational shoulder diameter was 10.2mm, 3.50 taper RH thread pin were fabricated. Both shoulder and tool pin was made from H13 tool steel, tool pin was austenized and quenched. Detail geometry of welding tools in each group was listed in Table 2.1.

Tool Design	Tool 1	Tool 2	Tool 3	Tool 4
Shoulder Type	Stationary Shoulder			Rotating Shoulder
Shoulder Diameter	11.4mm (0.45inch)		12.7mm (0.5inch)	10.2mm (0.4inch)
Pin Shape	Cylinder		8^{o} taper	3.5^{o} taper
Pin Flat	Non-flat	Tri-flats, Flat Depth: 0.38mm (0.015inch)		
Pin Top Diameter	3.8mm (0.15inch)		5.1mm (0.2inch)	4.4mm (0.172inch)
Pin Bottom Diameter			5.7mm (0.225inch)	4.6mm (0.182inch)
Pin Length	2.0mm (0.08inch)			
Thread form	1.57 threads/mm(40 threads/inch)			
	Right-hand thread (RH)		Left-hand thread & Right-hand thread (LH & RH)	Right-hand thread (RH)

Table 2.1 Various tool design used in each experiment

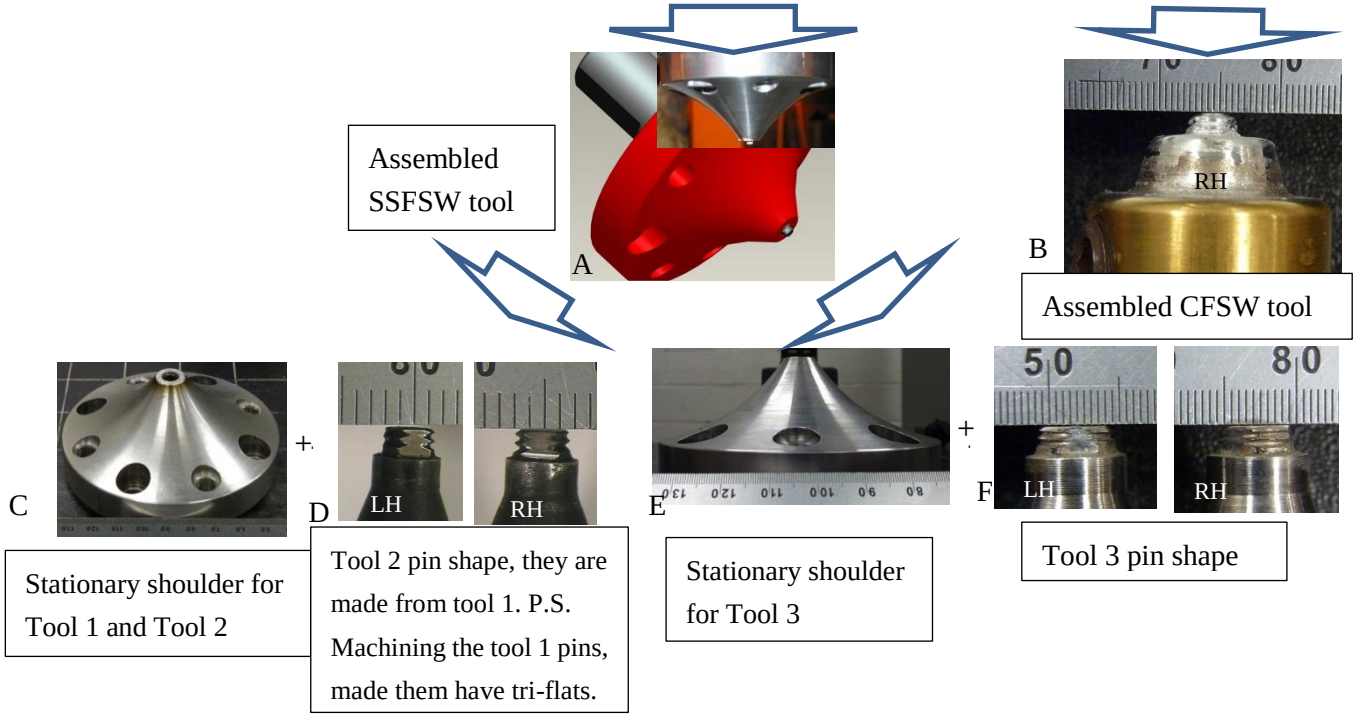

Figure 2.3 Picture of stationary shoulder, pin shape and pin flats.

In order to compare the change of tools shape due to abrasion during welding process, tool pin were cleaned in 16 % NaOH solution at 95 ℃ for up to 30 minutes. Then the cleaned tools were compared by BASIC BENCH contour projector (See Figure 2.4)

Figure 2.4 Comparison between LH&RH threaded pin by BASIC BENCH contour projector

2.4.FSW Process

2.4.1. **Weldment Placement**

The narrow sheets bands (38.1mm wide reinforcement) were placed on the center of the wider sheets (152.4mm wide bottom sheet). Tool steel was placed under bottom sheet as backing plate material for reinforcement.

Figure 2.5 showed the schematic picture of double parallel lap joint FSW process. It should be kept in mind that advancing size (AS) is when pin rotation direction is the same as welding direction, retreating size (RS) is when pin rotation direction is the oppsite to welding direction.

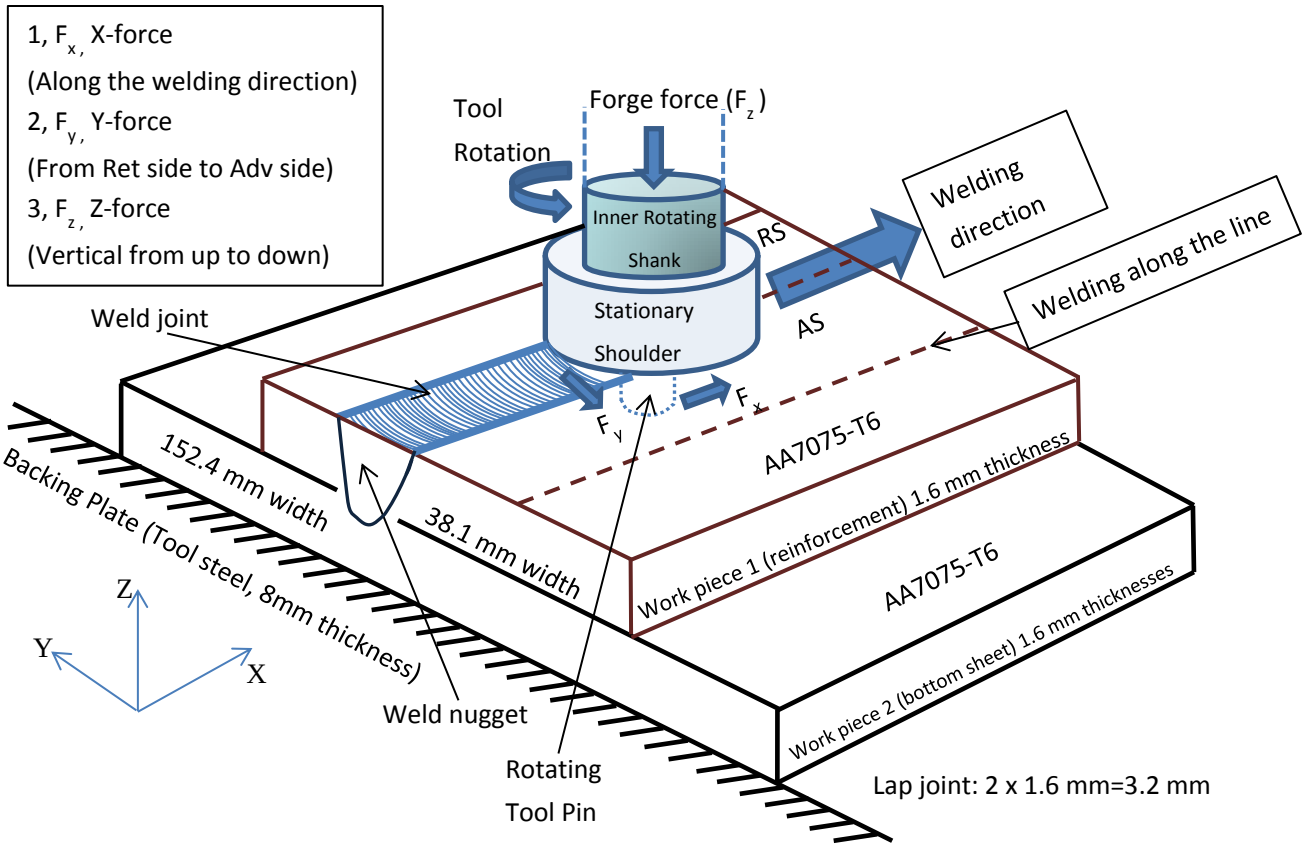

Figure 2.5 Schematic picture of double parallel Lap joints SSFSW

2.4.2. **Clamping**

Clamping constrain the top (reinforcement) and bottom welding sheet. Clamping is an important step, because clamping too loose will lead to displacement of the welds during FSW process, tight clamping will decrease the distortion of the welding sheet after FSW [37]. #3754-3756 welding sheets used weld-start-only-clamping method, which clamp only the bottom sheet with hold downs at weld start for top sheet (reinforcement).(See Figure 2.6)

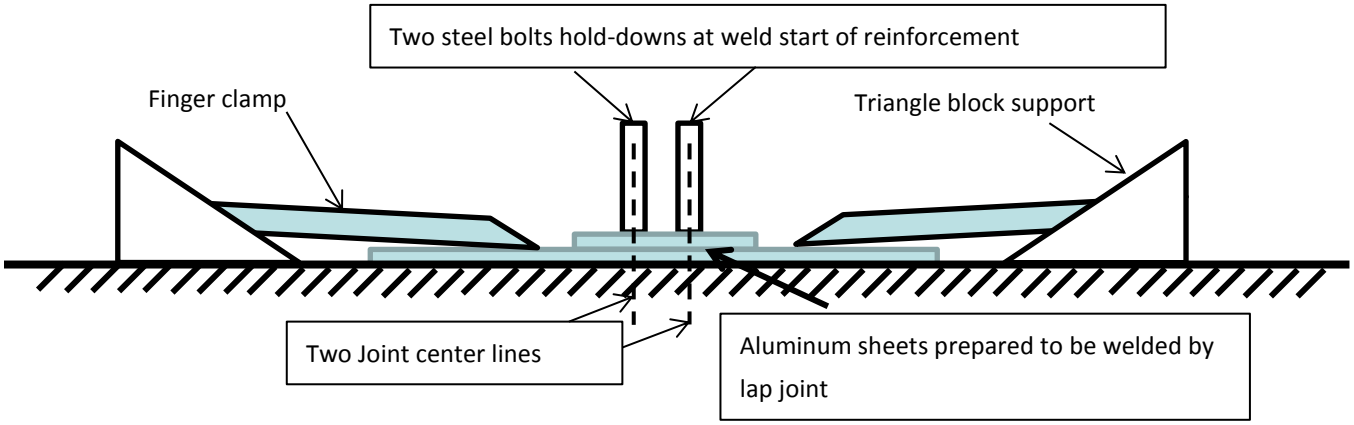

Figure 2.6 Schematic picture of weld-start-only-clamping method

However the reinforcement started deformation (bent away from bottom sheet) during welding process and welding pathway was not parallel to alignment mark. So continues clamping method was used for the rest of experiments, which clamp all along the weld path using aluminum parallel (See Figure 2.7 and Figure 2.8).

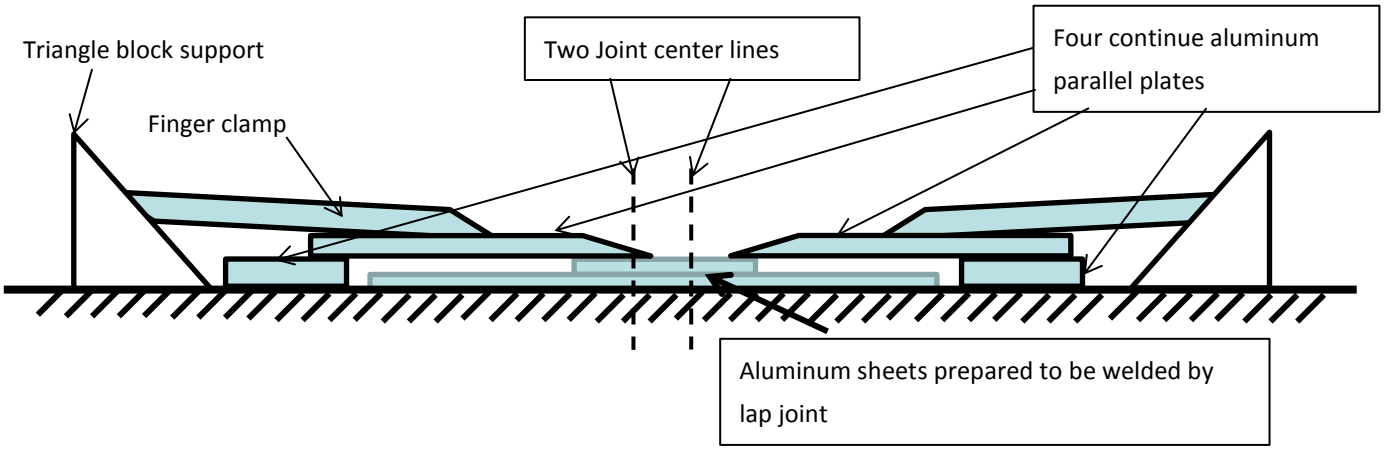

Figure 2.7 Schematic picture of continuous clamping method

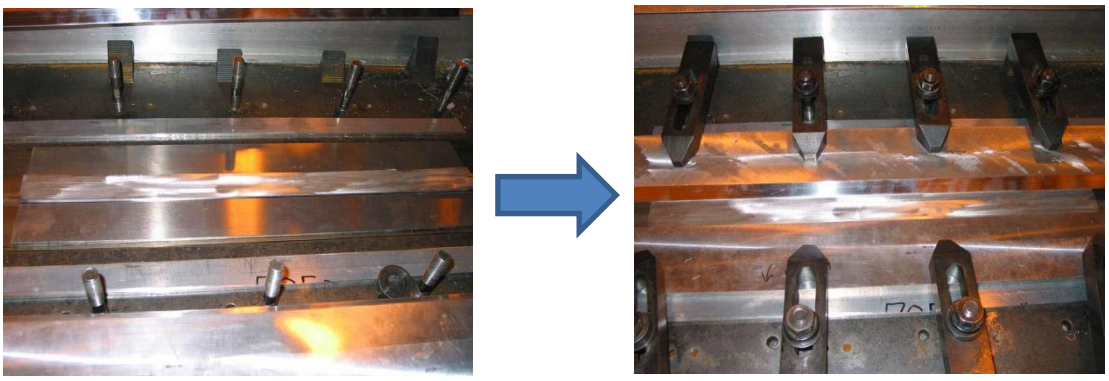

Figure 2.8 Picture of continues clamping method (before and after)

2.4.3. **Welding Direction and Pin Rotation Direction**

Both the same and the opposite welding directions and pin rotation direction were tested to find the optimum welding direction for less distortion.

a. Same welding direction with Right-Hand (RH) thread form pin tool

Both lap joint welds were in the same welding direction with RH thread form tool. (See Figure 2.9)

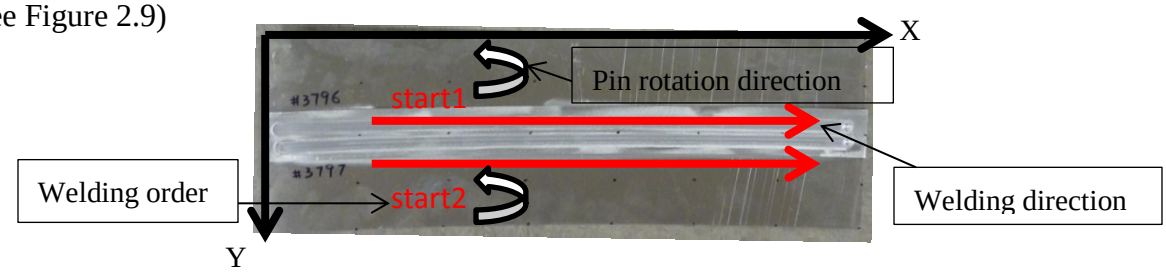

Figure 2.9 Picture of same welding direction with RH thread pin tool

b. Same welding direction with Left-Hand/Right-Hand (LH/RH) thread form pin tool

Both lap joint welds were in the same welding direction with LH and RH thread form pin tool respectively. (See Figure 2.10)

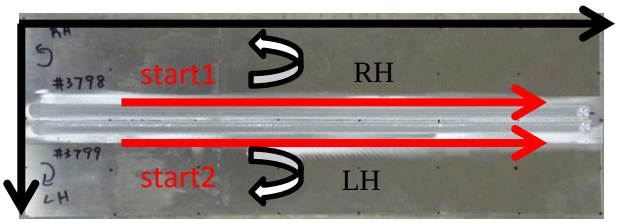

Figure 2.10 Picture of same welding direction with LH and RH thread pin tool

c. Opposite welding direction with Left-Hand (LH) thread form pin tool

Both lap joint welds were in the opposite welding direction with RH thread form pin tool.(SeeFigure 2.11)

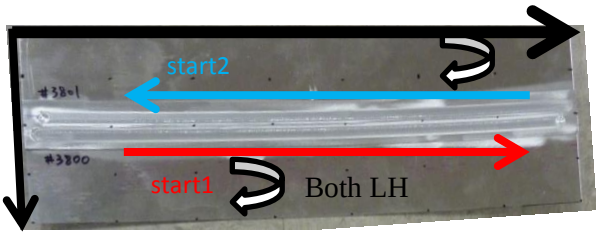

Figure 2.11 Picture of opposite welding direction with LH thread pin tool

d. Opposite welding direction with Right-Hand (RH) thread form pin tool

Both lap joint welds were in the opposite welding direction with RH thread form pin tool. (See Figure 2.12)

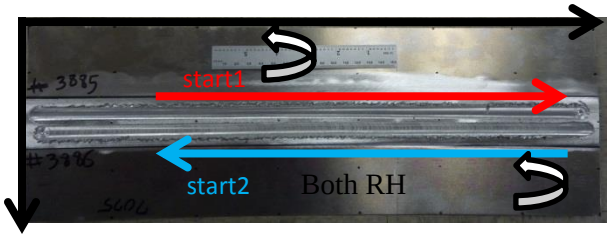

Figure 2.12 Picture of opposite welding direction with RH thread pin tool

2.4.4. **Welding Parameters**

Different rotation rate, welding speed and Z-force were applied to the weldments to study their effects on process response, which including torque, X-force and power. The following Table 2.2 showed the welding control parameters, welding length and tool types used in FSW process.

7075-T6 sheet thickness 1.6mm(0.063in)		Head Angle 0°			
Tool 1 Stationary Shoulder Lap Joint					
Weld No.	Pin Design	Weld Length	Rotation Speed rpm	Welding Speed mm/sec , ipm	Z force kN , lbs
#3754	Thread (RH)	124.5mm (4.9in)	-2000	4.23 , 10	6.23 , 1400
#3755	Thread (RH)	238.8mm (9.4in)	-1000	4.23 , 10	9.79 , 2200
#3756	Thread (RH)	238.8mm (9.4in)	-500	4.23 , 10	11.57 , 2600
#3757A	Thread (RH)	A+B+C=355.6mm (14in)	-500	4.23 , 10	10.68 , 2400
#3757B	Thread (RH)		-500	4.23 , 10	8.90 , 2000
#3757C	Thread (RH)		-500	4.23 , 10	7.12 , 1600
#3758A	Thread (RH)	A+B+C=355.6mm (14in)	-1000	4.23 , 10	9.79 , 2200
#3758B	Thread (RH)		-1000	6.35 , 15	10.68 , 2400
#3758C	Thread (RH)		-1000	8.47 , 20	11.57 , 2600
#3759A	Thread (RH)	A+B+C=381mm (15in)	-1200	6.35 , 15	9.79 , 2200
#3759B	Thread (RH)		-1500	6.35 , 15	9.79 , 2200
#3759C	Thread (RH)		-1800	6.35 , 15	12.46 , 2800
#3760A	Thread (RH)	A+B+C=381mm (15in)	-1200	8.47 , 20	9.79 , 2200
#3760B	Thread (RH)		-1500	8.47 , 20	9.79 , 2200
#3760C	Thread (RH)		-1800	8.47 , 20	9.79 , 2200
Tool 2 Stationary Shoulder Lap Joint					
Weld No.	Pin Design	Weld Length	Rotation Speed rpm	Welding Speed mm/sec , ipm	Z force kN , lbs
#3761A	Thread+3 flats (RH)	A+B+C=381mm (15in)	-1000	4.23 , 10	11.57 , 2200
#3761B	Thread+3 flats (RH)		-1000	6.35 , 15	13.34 , 3000
#3761C	Thread+3 flats (RH)		-1000	8.47 , 20	13.34 , 3000
#3762A	Thread+3 flats (RH)	A+B+C=381mm	-1200	6.35 , 15	9.79 , 2200

#3762B	Thread+3 flats (RH)	(15in)	-1200	8.47 , 20	9.79 , 2200
#3762C	Thread+3 flats (RH)		-1500	8.47 , 20	9.79 , 2200
#3763	Thread+3 flats (RH)	576.6mm (22.7in)	-1500	8.47 , 20	9.79 , 2200
#3764	Thread+3 flats (RH)	208.3mm (8.2in)	-1500	8.47 , 20	9.79 , 2200
#3794	Thread+3 flats (RH)	213.4mm (8.4in)	-1500	8.47 , 20	9.79 , 2200
Tool 3 Stationary Shoulder Lap Joint					
Weld No.	Pin Design	Weld Length	Rotation Speed rpm	Welding Speed mm/sec , ipm	Z force kN , lbs
#3795A	Thread+3 flats (RH)	114.3mm (4.5in)	-1500	8.47 , 20	17.79 , 4000
#3795B	Thread+3 flats (RH)	241.3mm (9.5in)	-1500	8.47 , 20	18.68 , 4200
#3796	Thread+3 flats (RH)	431.8mm (17in)	-1500	8.47 , 20	14.23 , 3200
#3797	Thread+3 flats (RH)	431.8mm (17in)	-1500	8.47 , 20	14.23 , 3200
#3798	Thread+3 flats (RH)	431.8mm (17in)	-1500	8.47 , 20	14.23 , 3200
#3799	Thread+3 flats (LH)	431.8mm (17in)	1500	8.47 , 20	14.23 , 3200
#3800	Thread+3 flats (LH)	431.8mm (17in)	1500	8.47 , 20	14.23 , 3200
#3801	Thread+3 flats (LH)	431.8mm (17in)	1500	8.47 , 20	14.23 , 3200
Tool 4 Conventional Shoulder Lap Joint					
Weld No.	Pin Design	Weld Length	Rotation Speed rpm	Welding Speed mm/sec , ipm	Z force kN , lbs
#3880-3882(dummy)	Thread+3 flats (RH)	Non-Lap joint(dummy)			
#3883	Thread+3 flats (RH)	431.8mm (17in)	-1500	8.47 , 20	6.67 , 1500
#3884	Thread+3 flats (RH)	431.8mm (17in)	-1500	8.47 , 20	6.67 , 1500
#3885	Thread+3 flats (RH)	431.8mm (17in)	-1500	8.47 , 20	6.67 , 1500
#3886	Thread+3 flats (RH)	431.8mm (17in)	-1500	8.47 , 20	6.67 , 1500

Table 2.2 Tool design, weld length and welding control parameters of each welding sheet

FSW procedures were carried out with Z-axis force control method, since load control mode was suggested for welding Aluminum. Real time torque was measured by Torque transducer. These data can be recorded on PDS as a function of time. The frequency of time recorded can be adjusted to fit the experiment. The maximum frequency of time recorded was 1000Hz. In the present experiments, rotation speed,

welding speed, Z-force and X-force recorded frequency was 100HZ. The torque recorded frequency was about 55HZ-57HZ.

2.5.Post-weld Heat Treatment (PWHT)

In order to reduce distortion and enhance the mechanical properties after welding process, T6 Post-weld Heat Treatment was adopted. Welding sheet was heat treated at 121 ℃ for 24 hours in a Blue M electric convection oven (for whole weldments) or a Memmert oil bath equipment(for small size cut specimen) to stabilize the welds.

In order to further reduce the distortion further, clamps were introduced to T6 heat treatment process. Vise grip clamps were used to fix the stacked welding sheets. Two rectangular AA7050 blocks were place on both outside surfaces. The gap between two lap joint welding sheets was filled by narrow regular aluminum sheets.(See Figure 2.13)

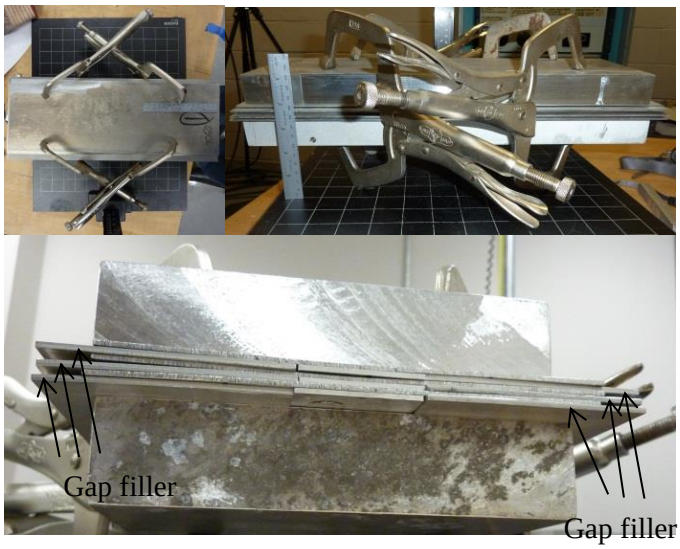

Figure 2.13 Picture of clamping for PWHT

2.6.Distortion Measurement

Distortion was measured before and after PWHT to study the effect T6 heat treatment on weldment distortion. The dimension of welding sheet as weld was 457mm (18in) by 152mm (6in). They were individually marked evenly using permanent marker (See Figure 2.14). Each sheet had 8 virtual columns and 5 virtual rows. There were 8 dots on each row, and 5 dots on each column. The parallel increment was 65.3mm. The vertical increment was 38.1mm.The Cartesian coordinate system was established for the sheet, whose up left corner was set as the origin.

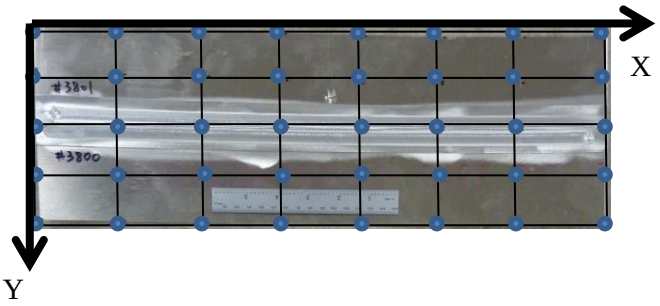

Figure 2.14 Preparation of welding sheet for distortion measurement

The Brown & Sharpe Gage 2000 coordinate measuring machine was used to measure the distortion. (See Figure 2.15).The weldment was clamped at the middle of the welding sheet. The tip of the clamp touched the edge of reinforcement. The Z position datum plane was aligned to the surface of the machine stage. The machine displayed the coordinate value on the control screen when the marked dot on the weldment was gently touched by the machine probe. In order to plot contour map for distortion, bottom

weldment surface Z-axis value was calculated by subtracting sheet thickness from measured top weldment surface Z-axis value. It should be noticed that the bottom surface Z-axis value under the weldment reinforcement area equaled top Z value minus twice the single sheet thickness value due to lap joint.

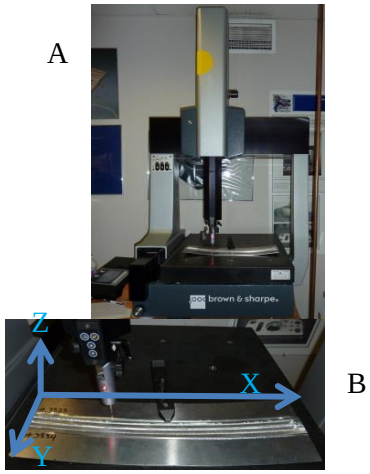

Figure 2.15 The Brown & Sharpe Gage 2000 coordinate measuring machine and coordinate setting

2.7.Metallographic Examination Preparation

Before applying optical characterization, Standard metallographic preparation process was implemented to grind and polish samples to specified level. Metallographic samples were cut from weldment using an abrasive water jet cutter. (See Figure 2.16)

Figure 2.16 Bengal water jet cutting machine

Since the samples cut was small and hard to hold it steady while grinding, the samples were placed in an epoxy mold (See Figure 2.17) (formula: Mixing 25 grams resin and 5 grams hardener to make one mount with diameter 31.75mm). A semi-automatic grinder was used to grind the metallographic samples. A sequence of 120, 240, 320, 400, 600 and 800 grade grit silicon carbide paper was used in the grinding process. The samples then went through a polishing process using a semi-automatic polisher with aluminum oxide powder with sizes of 5μm and 3μm followed by colloidal silica (particle sizes ranging from approximately 30 to 100 nm). Then they were etched by Keller's etchant (formula: distilled water 190ml, HNO_3 5ml, HCl 3ml, HF 2ml) for 8-12 second.

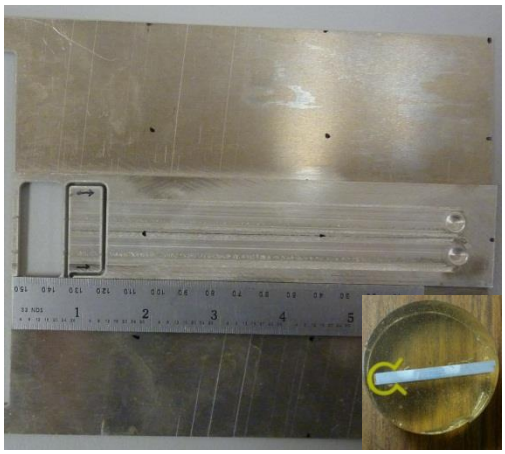

Figure 2.17 Sample cut from weldment and sample placed in the epoxy

2.8. Cross Section Observation

Macrostructure picture of welding sheets was taken by a scanner. Leco Olympus PME3 inverted metallurgical microscope was used to observe the weld microstructure with different magnification times (50x to 500x).One of the oculars on the microscope was replaced by the Canon DSLR EOS T1i. It was used to take metallographic pictures during the observation (See Figure 2.18).

Figure 2.18 Leo Olympus PME3 inverted metallurgical microscope

2.9. Grain Size Measurement

The Mean Linear Intercept method was used to measure grain size. The photos of the metallographic nugget center area were taken at magnifications of 500x to implement grain size measurement. The measured grain size values were then averaged to get the mean grain size value. Also confidence levels of values were calculated using guidelines from the Annual Book of ASTM Standards [38] .

2.10. Microhardness Test

Vickers's hardness was used to measure the microhardness distribution in the metallographic area. Figure 2.19 showed the microhardness test sample with indented marks. The microhardness test area was around 25.4mm x 2.54mm (inside the black dot line square).

Figure 2.19 Mirohardness test area on the sample

Hardness was measured at different thickness level on the cross section of joint. Hardness test was conducted using a Buehler Micromet 1 hardness test machine (See Figure 2.20) with a four-sided diamond shaped Vicker's micro-hardness indenter.

Figure 2.20 Buehler Micromet 1 hardness test machine

The schematic indentation map was showed in the Figure 2.21. The lap joint welding joint specimen thickness was 3.2mm. The gap between each pass was 0.508mm (0.02inch), the distance from first pass to the top line was 0.254mm (0.01inch). Indents were chosen along the nugget center lines, cross section mid-line, on or between the two adjacent passes. Indents were made with spacing ranging from 0.127mm to 1.27mm, using a load of 100gf or 200gf with a loading time of 10 seconds. The spacing ranging and load setting depend on the hardness change gradient. The length of the two diagonals for indents was measured and averaged. Then Vickers hardness was calculated by the following equation (1) and (2)

$d = (d1+d2)/2$ (μm) (1)

$HV = 1854 \times F/d2$ (2)

d: mean value of the diagonals of the indentation(μm) d1: the first diagonal length;

d2: the second diagonal lengths HV: Vickers hardness; F: test load (gf)

Since the hardness test is a contact measurement, in order to avoid residual stress field effects caused by existed indents, the ASTM manual book suggests that a minimum spacing between the two indents is 2.5 times the indent size (see Figure 2.21). When HV change is small, a bigger indent size is suggested to ensure the accuracy of the single indent measurement.

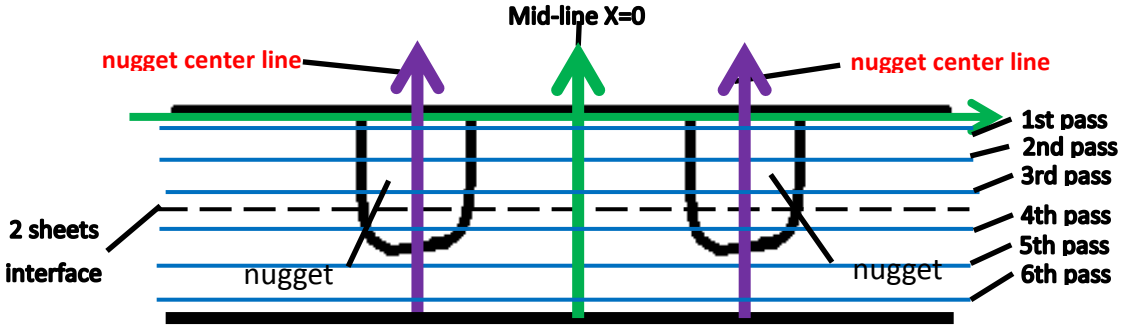

Figure 2.21 Schematic picture of indentation map for hardness test

2.11. Tensile Testing

Tensile test, in which a sample is subjected to axial tension until failure, is an important index for welding quality. Three tensile specimens were cut from middle of the weldment tranverse direction (across the welding pathway) using water jet cutter. The dimension of each specimen was 127mm x 25.4mm.

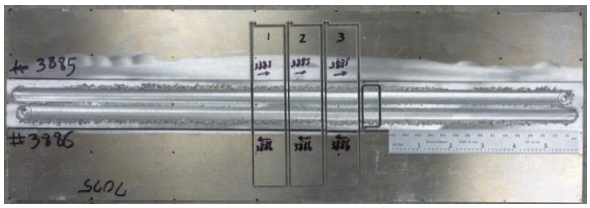

Figure 2.22 Picture of tensile test samples

The transverse tensile testing was conducted using Material Test System 810 (MTS) tensile test machine with displacement control setting 0.0254 mm/sec (0.001 in/sec) at room temperature.

The displacement between two grips was recorded against the applied force.

The applied force is used to calculate the stress σ with equation (3)

$$\sigma = \frac{F_n}{A} \qquad (3)$$

F: the applied force; A: the cross-section of the gauge section.

Tensile test was conducted using MTS 810 tensile test machine. (See Figure 2.23) The machine can calculate the result while the force was increasing, so that the data points can be graphed into a stress-strain curve. For this study, UTS and elongation values of SSFSW and conventional FSW with were measured to find the best condition.

Figure 2.23 MTS 810 tensile test machine

It should be noticed that during the tension test, the applied force (load) went through mid-plane of bottom sheet not through the two sheets interface, due to the specimen grip method (See Figure 2.24).

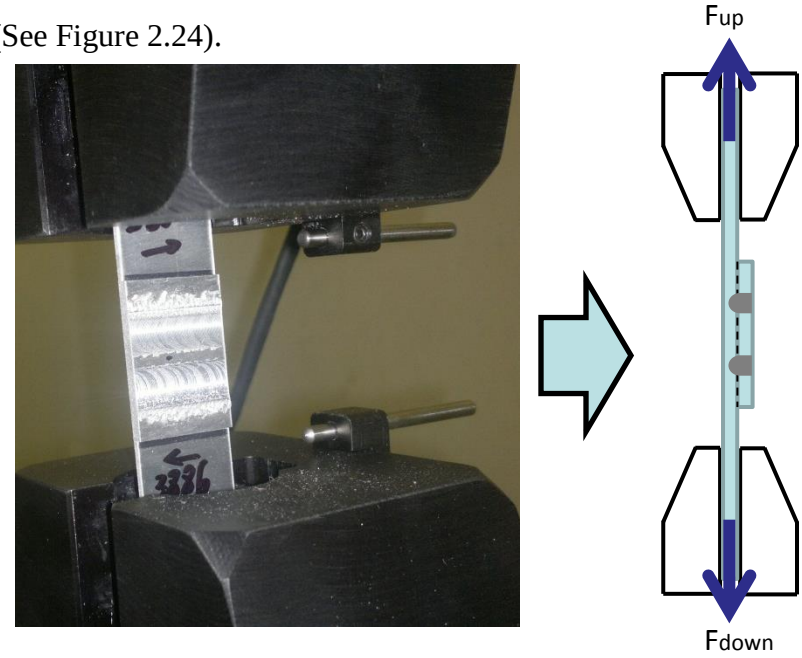

Figure 2.24 Picture and schematic of tensile test process

2.12. SEM Fracture Observation

The fracture sample after tensile test was analyzed using Quanta 200 Environmental Scanning Electron Microscope (ESEM) to investigate the microstructure at fracture cross section area (See Figure 2.25).

Figure 2.25 Quanta 200 Environmental Scanning Electron Microscope (ESEM)

CHAPTER 3 RESULTS AND DISCUSSION

Table 3.1 showed process response under different welding parameters and tool designs. Torque and X-force values were averaged when their control parameters are the same, and error deviation were calculated. Since clockwise rotation with RH thread and counter-clockwise rotation with LH thread resulted in same response magnitude due to symmetry, their absolute values were used in comparison. Result data from #3754-#3756 (different clamping method from other groups), #3764 (tool 2 broken) and #3794 (tool 2 broken, serious surface defect) were not used in the comparison.

Process response values under different welding control parameters and tool designs

7075-T6 sheet thickness 1.6mm(0.063in)		Head Angle 0^{o}								
Tool 1 Stationary Shoulder Lap Joint										
Weld No.	Pin Design	Weld Length	Pin rotation speed rpm	Welding Speed mm/sec	Z force kN	X force kN	(FSW)Torque Nm	Rotation Power W	Travel Power W	Total Power W
#3754	Thread (RH)	124.5mm (4.9in)	-2000	4.23	6.23	2.31	3.76	787.49	9.77	797.27
#3755	Thread (RH)	238.8mm (9.4in)	-1000	4.23	9.79	4.06	6.85	717.33	17.17	734.50
#3756	Thread (RH)	238.8mm (9.4in)	-500	4.23	11.57	4.09	10.69	559.73	17.32	577.05
#3757A	Thread (RH)	A+B+C=355.6mm (14in)	-500	4.23	10.68	3.26	11.92	624.13	13.80	637.93
#3757B	Thread (RH)		-500	4.23	8.90	3.04	12.03	629.89	12.86	642.75
#3757C	Thread (RH)		-500	4.23	7.12	2.60	13.99	732.51	11.00	743.51
#3758A	Thread (RH)	A+B+C=355.6mm (14in)	-1000	4.23	9.79	2.61	9.49	993.79	11.05	1004.84
#3758B	Thread (RH)		-1000	6.35	10.68	3.57	9.39	983.32	22.68	1006.00
#3758C	Thread (RH)		-1000	8.47	11.57	3.68	9.35	979.13	31.14	1010.27
#3759A	Thread (RH)	A+B+C=381mm (15in)	-1200	6.35	9.79	3.90	8.41	1056.83	24.74	1081.57
#3759B	Thread (RH)		-1500	6.35	9.79	4.19	7.45	1170.24	26.63	1196.88
#3759C	Thread (RH)		-1800	6.35	12.46	5.64	5.11	963.21	35.81	999.03
#3760A	Thread (RH)	A+B+C=381mm (15in)	-1200	8.47	9.79	3.83	9.10	1143.54	32.39	1175.93
#3760B	Thread (RH)		-1500	8.47	9.79	3.95	8.32	1306.90	33.44	1340.34
#3760C	Thread (RH)		-1800	8.47	9.79	3.93	5.53	1042.38	33.29	1075.67
Tool 2 Stationary Shoulder Lap Joint										

Weld No.	Pin Design	Weld Length	Pin rotation speed rpm	Welding Speed mm/sec	Z force kN	X force kN	(FSW)Torque Nm	Rotation Power W	Travel Power W	Total Power W
#3761A	Thread+3 flats (RH)	A+B+C=381mm (15in)	-1000	4.23	11.57	4.39	N/A	N/A	18.60	N/A
#3761B	Thread+3 flats (RH)		-1000	6.35	13.34	5.58	N/A	N/A	35.45	N/A
#3761C	Thread+3 flats (RH)		-1000	8.47	13.34	6.06	N/A	N/A	51.29	N/A
#3762A	Thread+3 flats (RH)	A+B+C=381mm (15in)	-1200	6.35	9.79	3.42	8.76	1100.81	21.72	1122.53
#3762B	Thread+3 flats (RH)		-1200	8.47	9.79	3.71	8.32	1045.52	31.37	1076.89
#3762C	Thread+3 flats (RH)		-1500	8.47	9.79	4.07	6.52	1024.16	34.42	1058.58
#3763	Thread+3 flats (RH)	576.6mm (22.7in)	-1500	8.47	9.79	4.02	8.37	1314.76	34.01	1348.76
#3764(pin break)	Thread+3 flats (RH)	208.3mm (8.2in)	-1500	8.47	9.79	3.39 (before pin break)	6.29 (before pin break)	988.03	28.66	1016.69
#3794(pin break)	Thread+3 flats (RH)	213.4mm (8.4in)	-1500	8.47	9.79	2.61 (before pin break)	6.48 (before pin break)	1017.88	22.07	1039.94
Tool 3 Stationary Shoulder Lap Joint										
Weld No.	Pin Design	Weld Length	Pin rotation speed rpm	Welding Speed mm/sec	Z force kN	X force kN	(FSW)Torque Nm	Rotation Power W	Travel Power W	Total Power W
#3795A	Thread+3 flats (RH)	114.3mm (4.5in)	-1500	8.47	17.79	6.02	10.64	1671.54	50.99	1722.53
#3795B	Thread+3 flats (RH)	241.3mm (9.5in)	-1500	8.47	18.68	6.20	9.94	1562.00	52.50	1614.50
#3796	Thread+3 flats (RH)	431.8mm (17in)	-1500	8.47	14.23	5.28	9.78	1536.35	44.66	1581.01
#3797	Thread+3 flats (RH)	431.8mm (17in)	-1500	8.47	14.23	5.13	9.01	1415.19	43.46	1458.65
#3798	Thread+3 flats (RH)	431.8mm (17in)	-1500	8.47	14.23	4.65	9.42	1480.47	39.39	1519.86

#3799	Thread+3 flats (LH)	431.8mm (17in)	1500	8.47	14.23	5.03	-9.36	1469.51	42.59	1512.10
#3800	Thread+3 flats (LH)	431.8mm (17in)	1500	8.47	14.23	5.09	-9.16	1438.74	43.08	1481.83
#3801	Thread+3 flats (LH)	431.8mm (17in)	1500	8.47	14.23	5.00	-8.26	1297.70	42.37	1340.07
Tool 4 Conventional Shoulder Lap Joint										
Weld No.	Pin Design	Weld Length	Pin rotation speed rpm	Welding Speed mm/sec	Z force kN	X force kN	(FSW)Torque Nm	Rotation Power W	Travel Power W	Total Power W
#3880-3882(dummy)	Thread+3 flats (RH)	Non-Lap joint(dummy)								
#3883	Thread+3 flats (RH)	431.8mm (17in)	-1500	8.47	6.67	0.52	9.49	1491.02	4.44	1495.46
#3884	Thread+3 flats (RH)	431.8mm (17in)	-1500	8.47	6.67	0.63	10.22	1605.75	5.34	1611.09
#3885	Thread+3 flats (RH)	431.8mm (17in)	-1500	8.47	6.67	0.72	9.72	1526.36	6.05	1532.41
#3886	Thread+3 flats (RH)	431.8mm (17in)	-1500	8.47	6.67	0.74	10.45	1641.47	6.26	1647.73

Table 3.1 X-force, torque and power under different tool designs and welding control parameters

3.1.Process Response: Torque

Effect of tool profile

Pin profile is an important factor on torque because it can affect heat generation and material flow. Table 3.2 showed the tool design used in each experimental group. The effect of taper on torque was not discussed here, because the experiments adopt these shape all have different with parameters, it was hard to distinguish the source of effect.

	Tool 1	Tool 2	Tool 3	Tool 4
Shoulder Type	Stationary	Stationary	Stationary	Rotational
Pin Shape	Cylinder	Cylinder	Taper (8^o)	Taper (3.5^o)
Pin Flats	Non-flat	Tri-flats	Tri-flats	Tri-flats
Pin diameters	3.8mm	3.8mm	5.1mm(Top diameter) 5.7mm(Bottom diameter)	4.4mm(Top diameter) 4.6mm(Bottom diameter)

Table 3.2 Tool types adopted by different experimental groups

3.1.1. **Stationary Shoulder vs. Rotational Shoulder**

In this study, only tool 4 adopted rotational shoulder, it is acted as a control group. Table 3.3 showed the comparison of process response between SSFSW and conventional FSW.

Weld No.	Tools design	Z-force kN	Torque Nm
Pin rotation speed: ±1500 rpm, Welding speed:8.47 mm/sec			
#3796-3801	Stationary shoulder +Thread+3 flats (LH&RH)+Taper (Tool 3)	14.23	9.17±0.51
#3883-3886	Rotational shoulder+Thread+3 flats (RH)+Taper (Tool 4)	6.67	9.97±0.44

Table 3.3 Torque values under stationary shoulder and rotational shoulder

SSFSW had less torque than CFSW. But the difference is very little. It should be noticed that Z-force applied in SSFSW was bigger than that in CFSW, for the reason that with stationary shoulder, more downward pressure was required to balance the extrusion of material upward for the present study.

3.1.2. **Non-flat vs. Tri-flats**

Table showed the torque under tool with no flat and tool with tri-flats. Resultant data were grouped based on their different input properties.

Weld No.	**Pin Flats**	**Torque (Nm)**	**Torque Difference (%)**
Group 1	Rotation speed:-1200 rpm, Welding speed:6.35 mm/sec, Z-force:9.79 kN		
#3759A	Non-flat (tool 1)	8.41	4.16
#3762A	Tri-flats (tool 2)	8.76	
Group 2	Rotation speed:-1200 rpm, Welding speed:8.47 mm/sec, Z-force:9.79 kN		
#3760A	Non-flat (tool 1)	9.10	-8.57
#3762B	Tri-flats (tool 2)	8.32	
Group 3	Rotation speed:-1500 rpm, Welding speed:8.47 mm/sec, Z-force:9.79 kN		
#3760B	Non-flat (tool 1)	8.32	-10.46
#3762C-3763	Tri-flats (tool 2)	7.45±1.31	

Table 3.4 Torque values under pin with no flat and pin with tri-flat

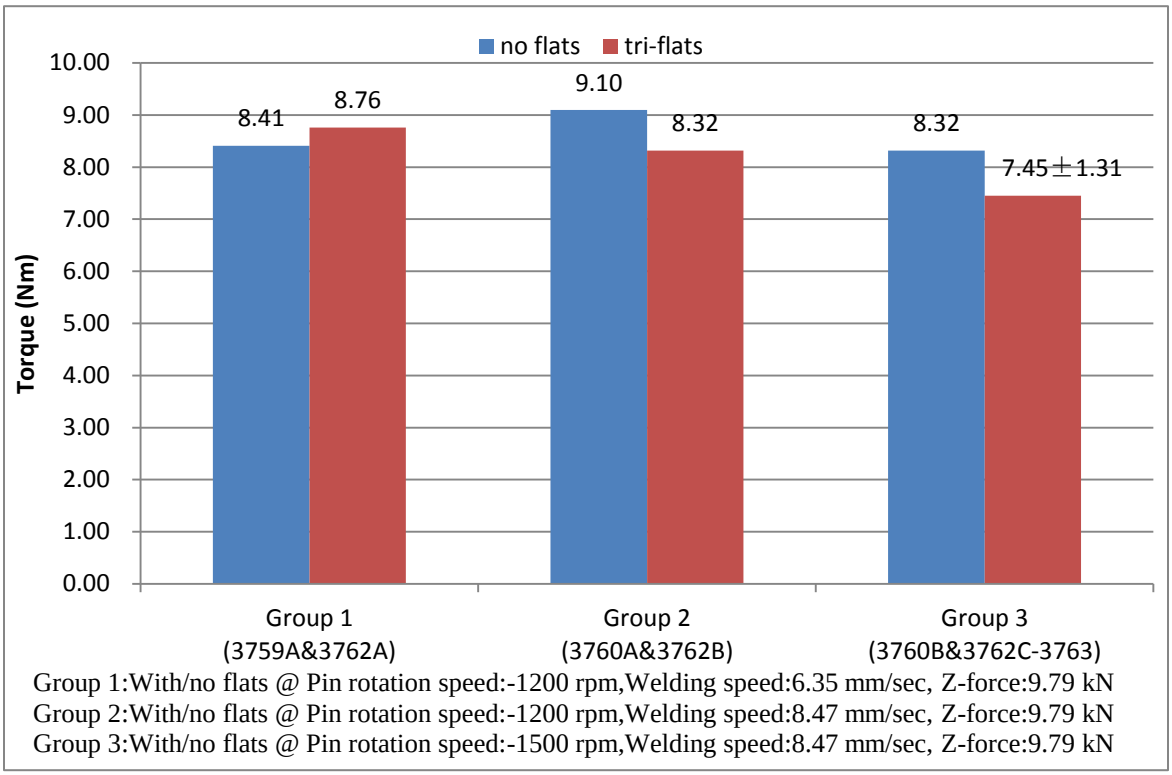

Figure 3.1 The relationship between torque and presence of pin flat

Torque adapting tri-flat pin was slightly reduced in group 2 and group 3, but slightly increased in group 1. The effect of flats on SSFSW was not obvious due to the tiny pins and thin sheets used in the experiments. Further experiment was required to confirm the relationship between pin profile and torque for SSFSW. For the present study of the thin sheets, Tri-flats feature did not affect the torque much.

Effect of Process Parameters

3.1.3. **Effect of Rotation Speed**

Table 3.5 and Figure 3.2 showed the relationship between rotation speed and torque.

Weld No.	Pin Design(Tool 1)	Pin rotation speed (rpm)	Torque (Nm)
Different pin rotation speed @ Welding speed:6.35 mm/sec, Z-force:9.79 kN by Tool 1			
#3759A	Thread (RH)	-1200	8.41
#3759B	Thread (RH)	-1500	7.45
Different pin rotation speed @ Welding speed:8.47 mm/sec, Z-force:9.79 kN by Tool 1			
#3760A	Thread (RH)	-1200	9.10
#3760B	Thread (RH)	-1500	8.32
#3760C	Thread (RH)	-1800	5.53
Weld No.	Pin Design (Tool 2)	Pin rotation speed (rpm)	Torque (Nm)
Different pin rotation speed @ Welding speed:8.47 mm/sec, Z-force:9.79 kN by Tool 2			
#3762B	Thread+3 flats (RH)	-1200	8.32
#3762C-3763	Thread+3 flats (RH)	-1500	7.45 ±1.31
Weld No.	Pin Design(Tool 3)	Pin rotation speed (rpm)	Torque (Nm)
Different pin rotation speed @ Welding speed:8.47 mm/sec, Z-force:14.23 kN by Tool 3			
#3796-3801	Thread+3 flats (LH&RH)	±1500	9.17 ±0.51
Weld No.	Pin Design(Tool 4)	Pin rotation speed (rpm)	Torque (Nm)
Pin rotation speed: -1500 rpm @ Welding speed:8.47 mm/sec, Z-force:6.67 kN by Tool 4			
#3883-3886	Thread+3 flats (RH)	-1500	9.97 ±0.44

Table 3.5 Torque under different pin rotation speed

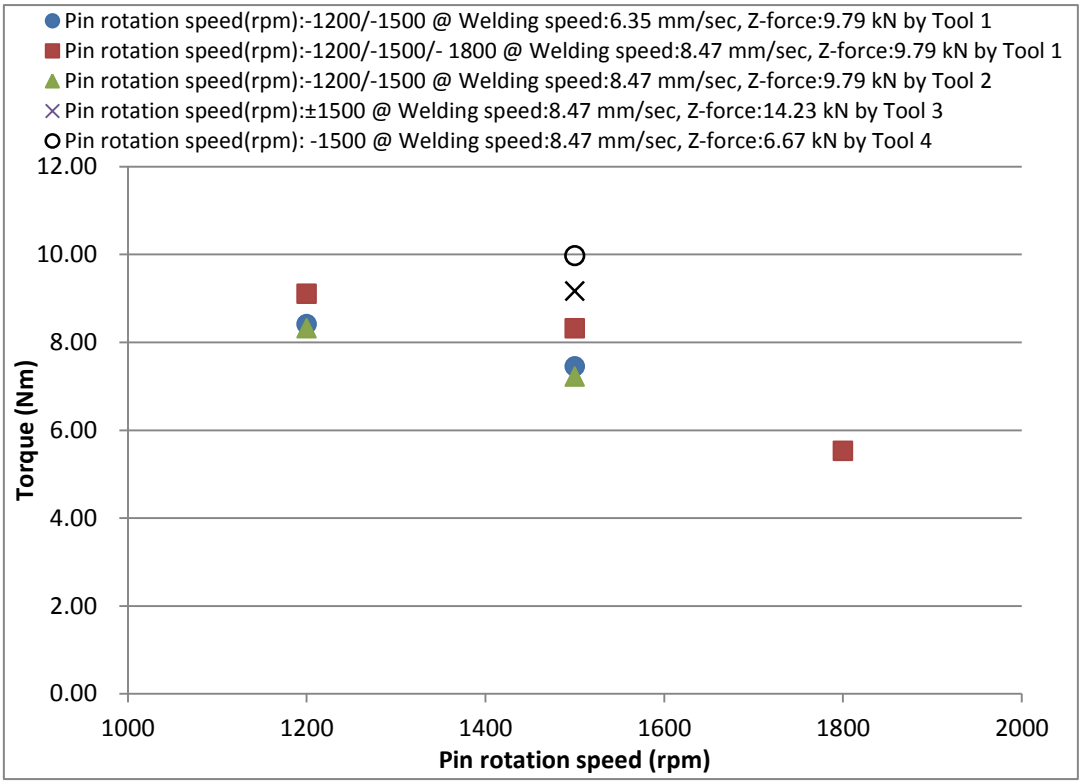

Figure 3.2 The relationship between torque and rotation speed

Results showed torque decreased with increasing rotation speed as expected, which indicated rotation speed was an important factor on torque from SSFSW. This was because increasing rotation speed can increase heat generation rate (power input) and temperature, hence decrease the flow stresses around the tool.

In literatures on conventional FSW, torque also often showed a strong correlation to rotation speed. Torque decreased with increasing rotation speed [5]. It was because pin rotation rate can increase heat generation rate and temperature, which would reduce the shear strength of material contacting the pin. This reducing effect for Stationary shoulder FSW was not as significant as for rotational shoulder FSW, since the stationary shoulder did not contribute to torque much. A more generalize relationship (with different welding

speed and Z-force) between rotation speed and torque was formed to verify this correlation.

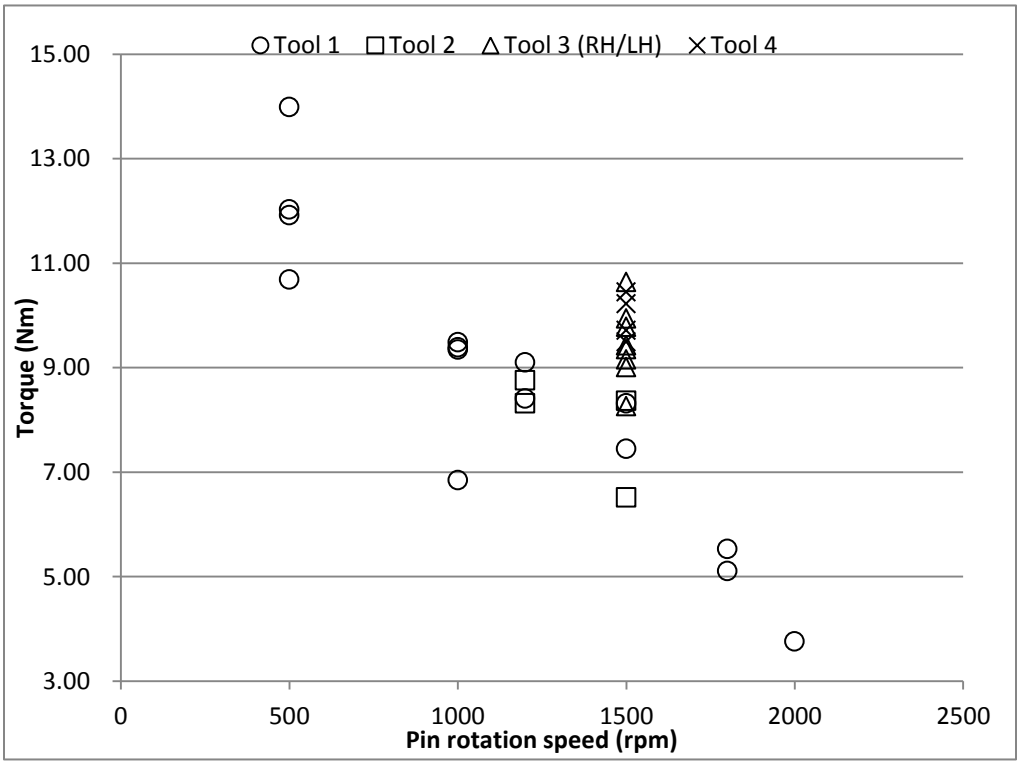

Figure 3.3 The generalized relationship between torque and rotation speed (regardless other parameters being different)

Again, torque decreased with increasing rotation speed in general, which proved that rotation speed was an important factor on torque. Torque in SSFSW can be reduced by increasing rotation speed when tool design and other process parameters keep unchanged.

3.1.4. **Effect of Z-force**

Table 3.6 and Figure 3.4 showed the relationship with Z-force (downward force) and torque. Several literatures studied the effect of Z-force on torque in CFSW [39][40].

Weld No.	Pin Design (Tool 1)	Z force kN	(FSW)Torque Nm
Different Z-force @ Welding speed: 4.23 mm/sec, Pin rotation speed: -500 rpm by Tool 1			
#3756	Thread (RH)	11.57	10.69
#3757A	Thread (RH)	10.68	11.92
#3757B	Thread (RH)	8.90	12.03
#3757C	Thread (RH)	7.12	13.99
Weld No.	Pin Design (Tool 3)	Z force kN	(FSW)Torque Nm
Different Z-force @ Welding speed: 8.47 mm/sec, Pin rotation speed: ±1500 rpm by Tool 3			
#3795A	Thread+3 flats (RH)	17.79	10.64
#3795B	Thread+3 flats (RH)	18.68	9.94
#3796-3801	Thread+3 flats (LH&RH)	14.23	9.17±0.51
Weld No.	Pin Design (Tool 3)	Z force kN	(FSW)Torque Nm
Z-force(kN): 6.67 @ Welding speed: 8.47 mm/sec, Pin rotation speed: -1500 rpm by Tool 4			
#3883-3886	Thread+3 flats (RH)	6.67	9.97±0.44

Table 3.6 Torque under different Z-force (downward force)

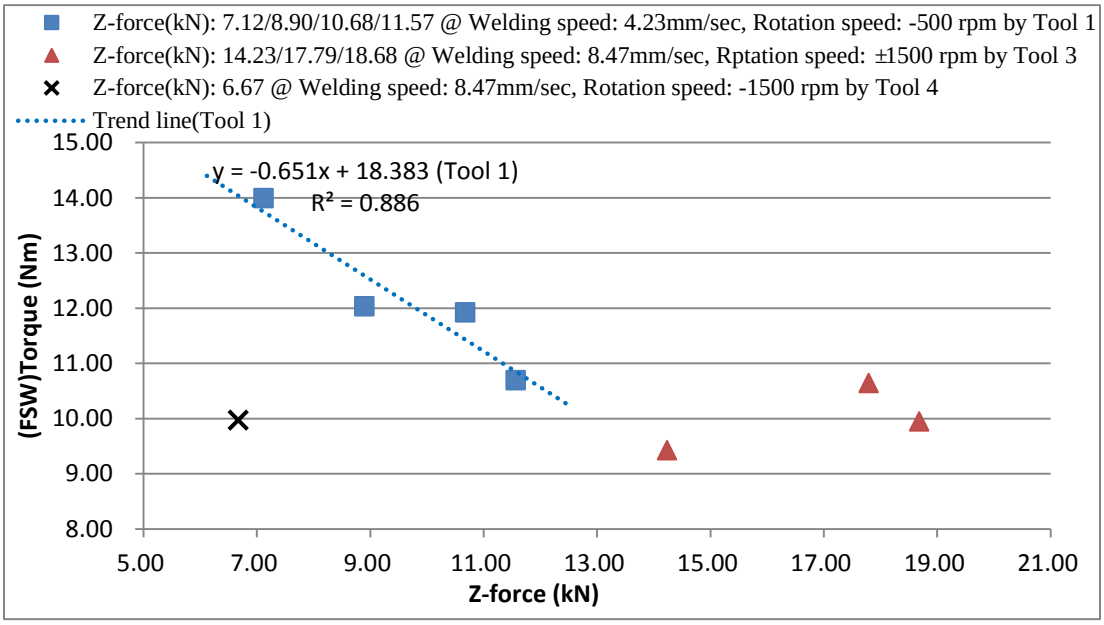

Figure 3.4 The relationship between torque and Z-force at 500 rpm and 1500 rpm

The results showed torque decreased with increasing Z-force at low rotation speed. This indicated Z-force may play a role in torque at low rotation speed (500 rpm for the present welds), but torque did not change much by changing Z-force at high rotation speed (1500 rpm for the present welds). The possible reason was that at the low rotation speed, increasing Z-force helped increase temperature to reduce the torque. While at the high rotation speed, temperature was high enough to make torque reach a plateau. It should be noticed that the samples with low rotation speed had the more serious wormhole defects than the samples with high rotation speed. The decline trend may be caused by the inadequately rotation speed.

3.1.5. **Effect of Welding Speed**

Table 3.7and Figure 3.5 showed the relationship between welding speed and torque. Torque increased with increasing welding speed in most cases, but this effect was minor. Welding speed mainly affected X-force (pin experienced) and travel energy consumption. So the change of torque by welding speed was insignificant. However, welding speed would affect the welding quality and efficiency. If welding speed was too high, the heat input was not enough to soften the metal, there would lead to defects. If welding speed was too low, the welding efficiency would be affected.

Weld No.	Pin Design (Tool 1)	Welding Speed mm/sec	(FSW)Torque Nm
Group 1	Pin rotation speed:-1200 rpm, Z-force:9.79 kN by Tool 1		
#3759A	Thread (RH)	6.35	8.41

#3760A	Thread (RH)	8.47	9.10
Group 2	Pin rotation speed:-1500 rpm, Z-force:9.79 kN by Tool 1		
#3759B	Thread (RH)	6.35	7.45
#3760B	Thread (RH)	8.47	8.32
Weld No.	Pin Design (Tool 2)	Welding Speed mm/sec	(FSW)Torque Nm
Group 3	Pin rotation speed:-1000 rpm, Z-force:13.34 kN by Tool 2		
#3761B	Thread+3 flats (RH)	6.35	N/A
#3761C	Thread+3 flats (RH)	8.47	N/A
Group 4	Pin rotation speed:-1200 rpm, Z-force:9.79 kN by Tool 2		
#3762A	Thread+3 flats (RH)	6.35	8.76
#3762B	Thread+3 flats (RH)	8.47	8.32

Table 3.7 Torque under different Z-force (downward force)

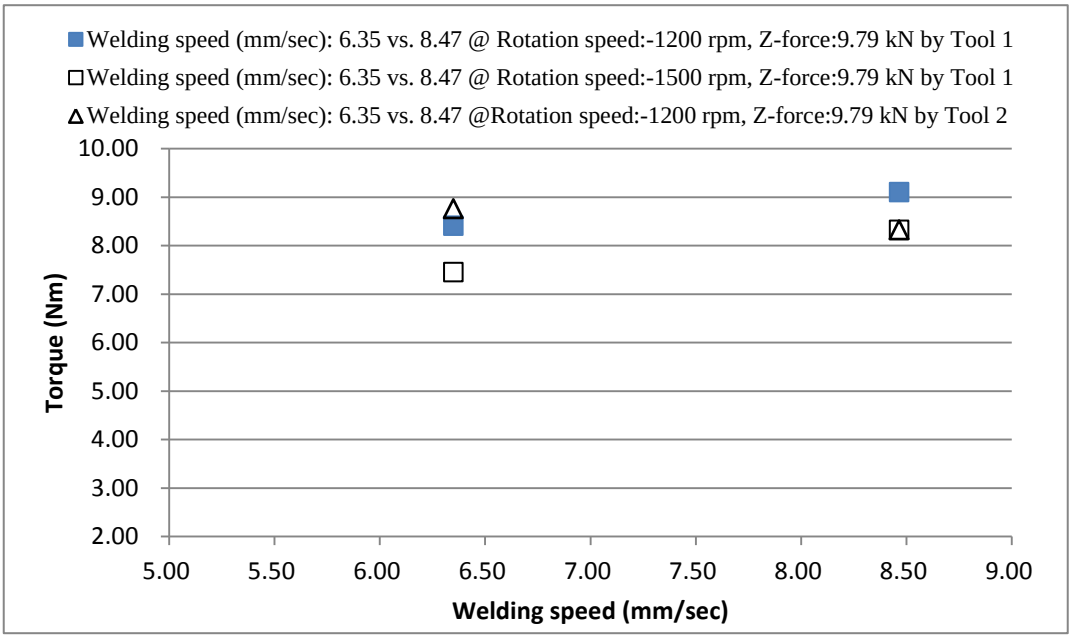

Figure 3.5 The relationship between torque and welding speed

In summary, 1) SSFSW resulted in less torque than conventional FSW. 2) Tool design with flats helped reduce torque in small degree, but not always. 3) The main welding parameter affecting SSFSW torque was rotation speed. Torque decreased with increasing rotation speed. It should be noted that torque decreased with increasing

Z-force at low rotation speed (500 rpm), but at high rotation speed (1500 rpm), Z-force affected torque little. The reason for this was not clear.

3.2.Process Response: X-force

X-force is important process response which indicates the resistance of tool in the welding direction. The effect on X-force was extensively studied.

3.2.1. **Stationary Shoulder vs. Rotational Shoulder**

Weld No.	Tools design	Z force kN	X force kN
Pin rotation speed: ±1500 rpm,Welding speed:8.47mm/sec			
#3796-3801	Stationary shoulder +Thread+3 flats (LH&RH)+Taper (Tool 3)	14.23	5.03±0.21
#3883-3886	Rotational shoulder+Thread+3 flats (RH)+Taper (Tool 4)	6.67	0.65±0.097

Table 3.8 X-force values under stationary shoulder and rotational shoulder

From Table 3.8, Z-force in SSFSW was about two times as Z-force in CFSW, in order to keep the shoulder touching the welding surface firmly. It should be noticed that the resultant X-force in SSFSW was nearly eight times as X-force in CFSW. The main reason for this could be that rotational shoulder generated more heat input on the surface material, which helped reducing surface X-force resistant. Another explanation was because of shoulder rotation in CFSW, friction force on top surface created resistance torque which was balanced to the power torque, hence it only took a little X-force to balanced forward resistance force. The effects of shoulder type on X-force can be further studied in the future with the same Z-force being used.

3.2.2. **Non-flat vs. Tri-flats**

Table 3.9 and Figure 3.6 showed the effect of pin flats on X-force.

Weld No.	Flats	X force kN
Group 1	Pin rotation speed:-1200 rpm,Welding speed:6.35 mm/sec, Z-force:9.79 kN	
#3759A	No	3.90
#3762A	Tri-flats	3.42
Group 2	Pin rotation speed:-1200 rpm,Welding speed:8.47 mm/sec, Z-force:9.79 kN	
#3760A	No	3.83
#3762B	Tri-flats	3.71
Group 3	Pin rotation speed:-1500 rpm,Welding speed:8.47 mm/sec, Z-force:9.79 kN	
#3760B	No	3.95
#3762C-3763	Tri-flats	4.04±0.035

Table 3.9 X-force values under pin with no flat and pin with tri-flat

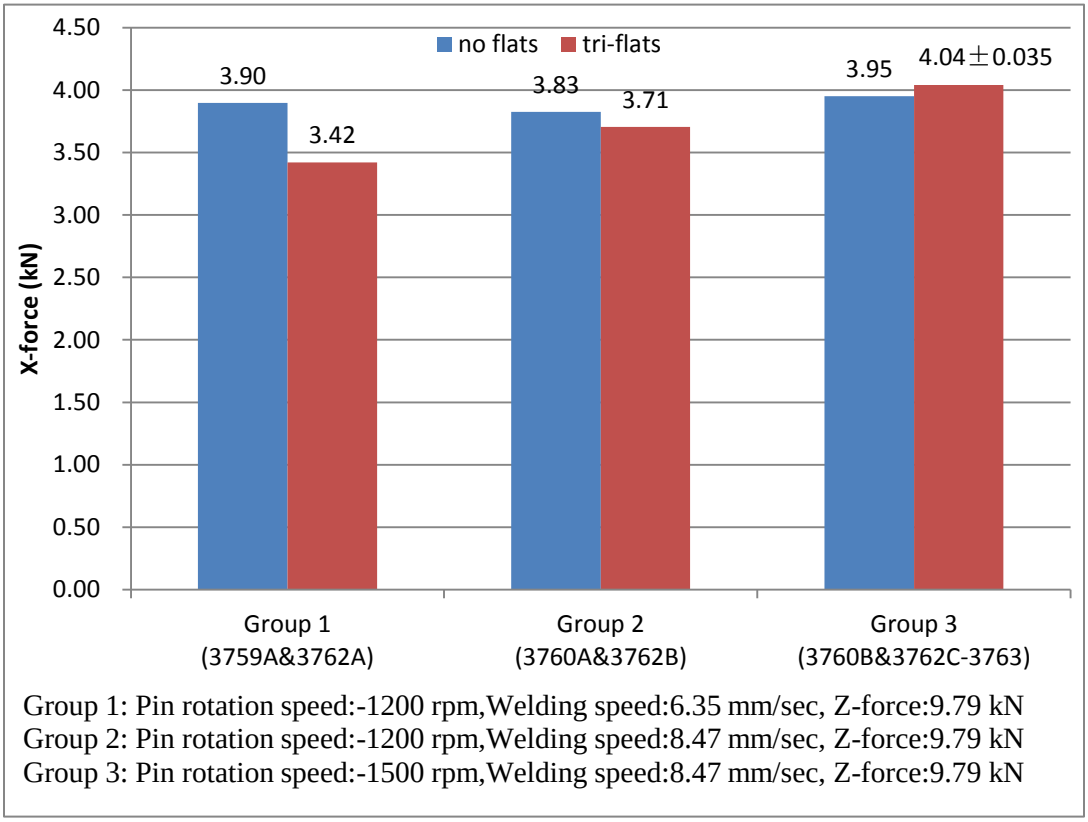

Group 1: Pin rotation speed:-1200 rpm,Welding speed:6.35 mm/sec, Z-force:9.79 kN
Group 2: Pin rotation speed:-1200 rpm,Welding speed:8.47 mm/sec, Z-force:9.79 kN
Group 3: Pin rotation speed:-1500 rpm,Welding speed:8.47 mm/sec, Z-force:9.79 kN

Figure 3.6 The relationship between X-force and presence of pin flat

X-force under tri-flat pin was slightly smaller in group 1 and group 2, but slightly bigger in group 3. The presence of tri-flats may slightly decreased material flow which would lower X-force. The presence of flat was not a major factor on X-force for SSFSW from observation.

Effect of Process Parameters

3.2.3. Effect of Rotation speed

Table 3.10 and Figure 3.7 showed the resultant X-force with respect to rotation speed.

Weld No.	Pin Design(Tool 1)	Pin rotation speed rpm	X force kN
Welding speed:6.35 mm/sec, Z-force:9.79 kN by Tool 1			
#3759A	Thread (RH)	-1200	3.90
#3759B	Thread (RH)	-1500	4.19
Welding speed:8.47 mm/sec, Z-force:9.79 kN by Tool 1			
#3760A	Thread (RH)	-1200	3.83
#3760B	Thread (RH)	-1500	3.95
#3760C	Thread (RH)	-1800	3.93
Weld No.	Pin Design (Tool 2)	Pin rotation speed rpm	X force kN
Welding speed:8.47 mm/sec, Z-force:9.79 kN by Tool 2			
#3762B	Thread+3 flats (RH)	-1200	3.71
#3762C-3763	Thread+3 flats (RH)	-1500	4.04±0.035
Weld No.	Pin Design(Tool 3)	Pin rotation speed rpm	X force kN
Welding speed:8.47 mm/sec, Z-force:14.23 kN by Tool 3			
#3796-3801	Thread+3 flats (LH&RH)	±1500	5.03±0.21
Weld No.	Pin Design(Tool 3)	Pin rotation speed rpm	X force kN
Welding speed:8.47 mm/sec, Z-force:6.67 kN by Tool 4			
#3883-3886	Thread+3 flats (RH)	-1500	0.65±0.097

Table 3.10 X-force values under different pin rotation speed

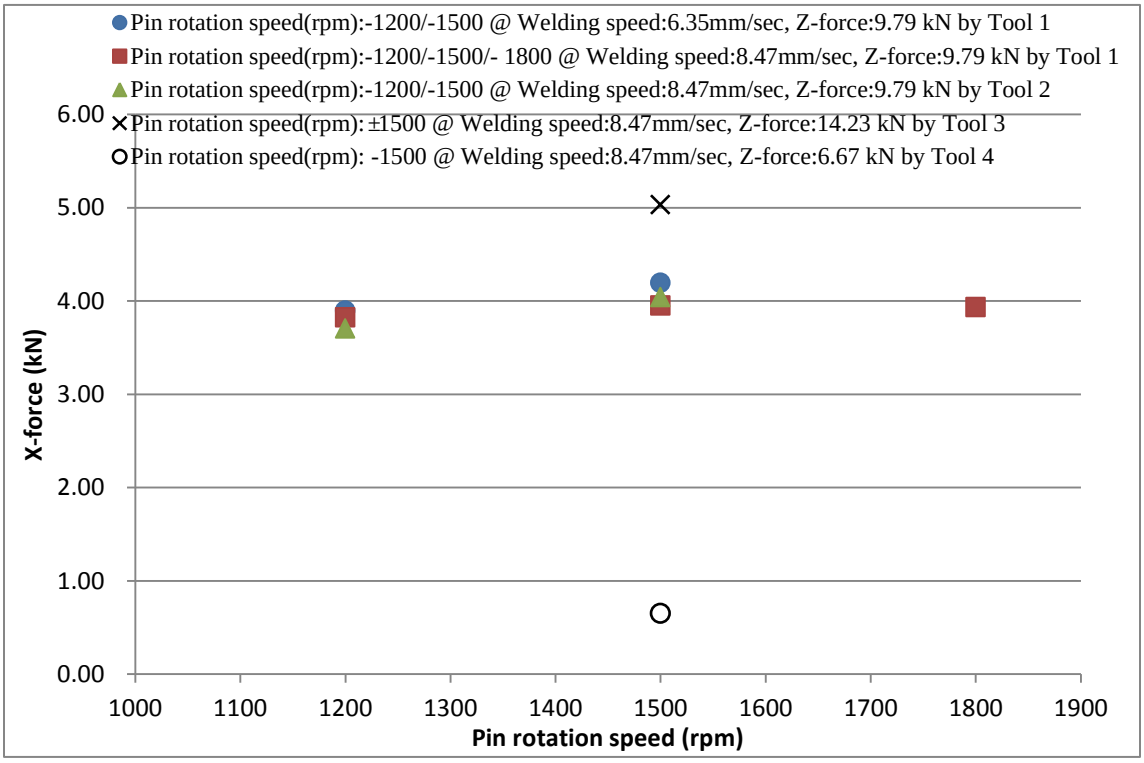

Figure 3.7 The relationship between X-force and pin rotation speed

The result showed rotation speed rarely affects X-force for SSFSW. With stationary shoulder, the resistant X axis force on the pin was much smaller compared to the resistant force on the shoulder. So increasing rotation speed only decrease the resistance force for pin. More experiments needed to be done on relationship between X-force and welding speed to verify this theory.

3.2.4. **Effect of Z-force**

Table 3.11 and Figure 3.8 showed the relationship between Z-force and X-force.

Weld No.	Pin Design (Tool 1)	Z force kN	X force kN
Welding speed: 4.23 mm/sec, Pin rotation speed: -500 rpm by Tool 1			
#3756	Thread (RH)	11.57	4.09
#3757A	Thread (RH)	10.68	3.26

#3757B	Thread (RH)	8.90	3.04
#3757C	Thread (RH)	7.12	2.60
Weld No.	Pin Design (Tool 3)	Z force kN	X force kN
Welding speed: 8.47 mm/sec, Pin rotation speed: ±1500 rpm by Tool 3			
#3795A	Thread+3 flats (RH)	17.79	6.02
#3795B	Thread+3 flats (RH)	18.68	6.20
#3796-3801	Thread+3 flats (LH&RH)	14.23	5.03±0.21
Weld No.	Pin Design (Tool 3)	Z force kN	X force kN
Welding speed: 8.47 mm/sec, Pin rotation speed: -1500 rpm by Tool 4			
#3883-3886	Thread+3 flats (RH)	6.67	0.65±0.097

Table 3.11 X-force values under different Z-force

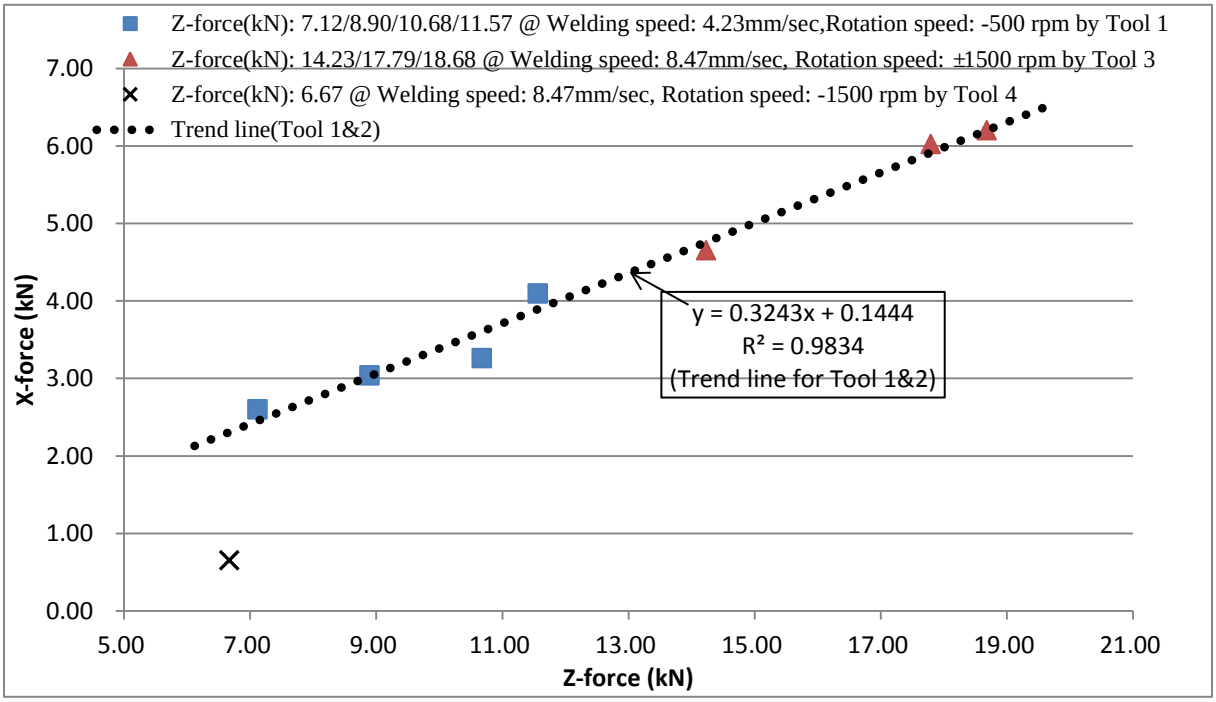

Figure 3.8 The relationship between X-force and Z-force

X-force monotonically increased with Z-force. Increasing Z-force would increase the pressure on material surface by stationary shoulder, hence increased the resistance force on shoulder, where coulomb friction should be the operative mechanism. Most part of

X-force in SSFSW was caused by the shoulder friction force. Z-force did not affect resistance force on the pin much. This indicated the majority of the X-axis force came from shoulder, not from the pin (especially not from the tiny pin). Figure 3.9 showed a more generalized relationship between Z-force and X-force, with different process condition.

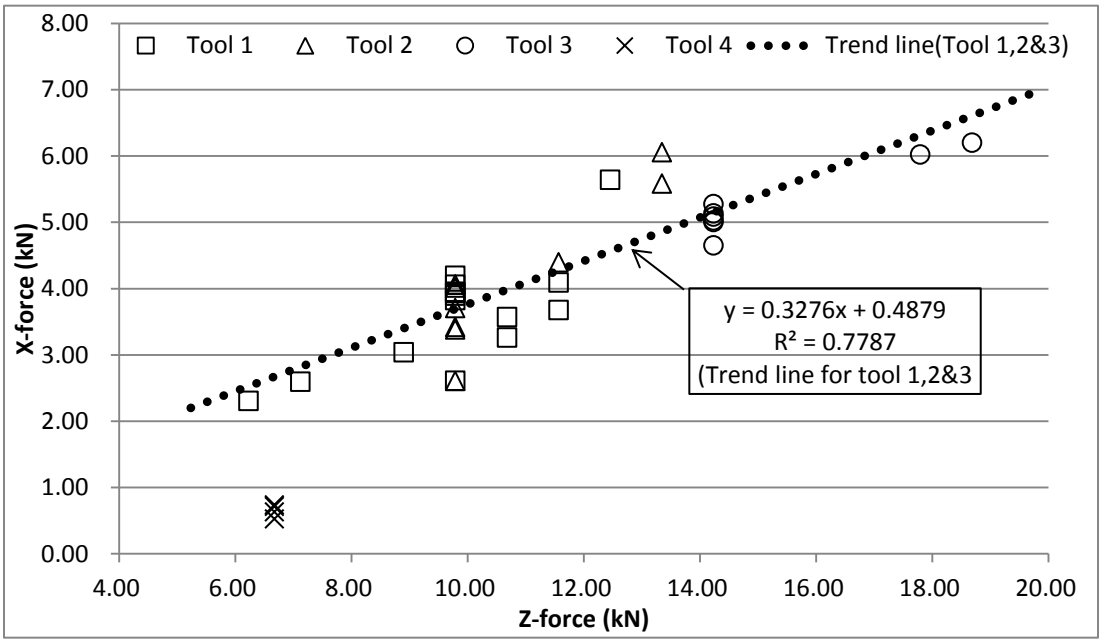

Figure 3.9 The generalized relationship between X-force and Z-force (Other control parameters may be different.)

In the more generalize figure, the linear increasing trend was also observed, which conformed the effect of Z-force on X-force. In addition, from Table 3.12, X-force of #3764 and #3794 increased instead of decreasing after pin broke, it also indicated that X-force mainly caused by stationary shoulder, not pin.

	Before pin break (kN)	After pin break (kN)	Difference from pin existed
#3764	3.38	4.88	44.38%(abs)
#3794	2.62	3.27	24.81%(abs)

Table 3.12 X-force before/after pin broken and difference

3.2.5. **Effect of Welding speed**

Table 3.13 and Figure 3.10 showed the relationship between welding speed and X-force.

Weld No.	Pin Design (Tool 1)	Welding Speed mm/sec	X force kN
Group 1	Pin rotation speed:-1200 rpm, Z-force:9.79 kN by Tool 1		
#3759A	Thread (RH)	6.35	3.90
#3760A	Thread (RH)	8.47	3.83
Group 2	Pin rotation speed:-1500 rpm, Z-force:9.79 kN by Tool 1		
#3759B	Thread (RH)	6.35	4.19
#3760B	Thread (RH)	8.47	3.95
Weld No.	Pin Design (Tool 2)	Welding Speed mm/sec	X force kN
Group 3	Pin rotation speed:-1000 rpm, Z-force:13.34 kN by Tool 2		
#3761B	Thread+3 flats (RH)	6.35	5.58
#3761C	Thread+3 flats (RH)	8.47	6.06
Group 4	Pin rotation speed:-1200 rpm, Z-force:9.79 kN by Tool 2		
#3762A	Thread+3 flats (RH)	6.35	3.42
#3762B	Thread+3 flats (RH)	8.47	3.71

Table 3.13 X-force values under different welding speed

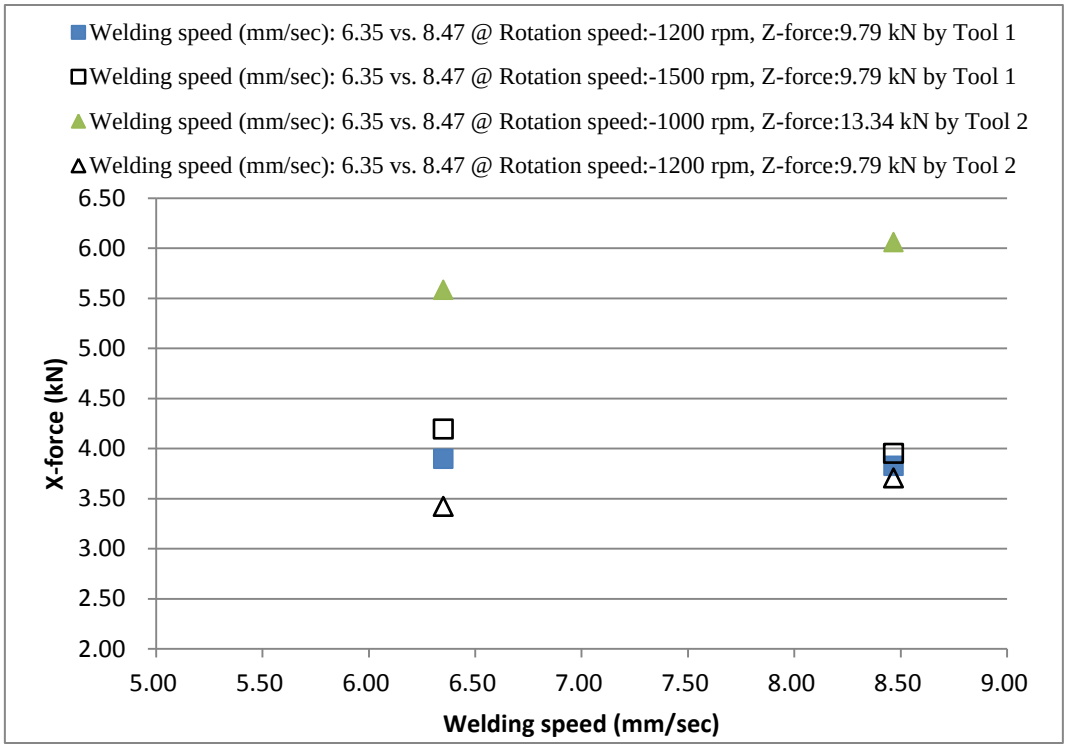

Figure 3.10 The relationship between X-force and pin rotation speed

There was no clear relationship between welding speed and X-force. One possible explanation was that heat generated on the welding surface by stationary shoulder was much less than the CFSW rotational shoulder, resistance on the shoulder was main contributor to the X-force for SSFSW, X-force was mainly associated with pressure and friction coefficient, so welding speed had little effect on X-force.

In summary, 1) SSFSW exerted higher X-force than conventional FSW. 2) Tool design with flats helped reduce X-force in small degree in most cases. 3) The main welding parameters affected SSFSW X-force was Z-force. X-force increased with increasing Z-force linearly. Observed behavior was consistent with coulomb friction mechanism.

3.3.Process Response: Power

Total welding power consisted of rotation power and travel power, which was shown in Table 3.14 . Rotation power was the product of torque and angular speed of the pin, travel power was the product of X-force and welding speed.

Weld No.	Pin design	Rotation Power (W)	Welding Power (W)	Total Power (W)
Group 1 Pin rotation speed: -1500 rpm, Welding speed:8.47 mm/sec, Z-force:9.79 kN by Tool 1				
#3760B	Thread (RH)	1306.9	33.44	1340.34
Group 2 Pin rotation speed: -1500 rpm, Welding speed:8.47 mm/sec, Z-force:9.79 kN by Tool 2				
#3762C-3763	Thread+3 flats (RH)	1169.46(avg)	34.21(avg)	1203.67(avg)
Group 3 Pin rotation speed: -1500 rpm, Welding speed:8.47 mm/sec, Z-force:17.79 kN by Tool 3				
#3795A	Thread+3 flats (RH)	1671.54	50.99	1722.53
Group 4 Pin rotation speed: -1500 rpm, Welding speed:8.47 mm/sec, Z-force:18.68 kN by Tool 3				
#3795B	Thread+3 flats (RH)	1562	52.5	1614.5
Group 5 Pin rotation speed: ±1500 rpm, Welding speed:8.47 mm/sec, Z-force:14.23 kN by Tool 3				
#3796-3801	Thread+3 flats (LH&RH)	1439.66(avg)	42.59(avg)	1482.25(avg)
Group 6 Pin rotationspeed: -1500 rpm, Welding speed:8.47 mm/sec, Z-force:6.67 kN by Tool 4				
#3883-3886	Thread+3 flats (LH)	1566.15(avg)	5.52(avg)	1571.67(avg)

Table 3.14 The components of the total welding power

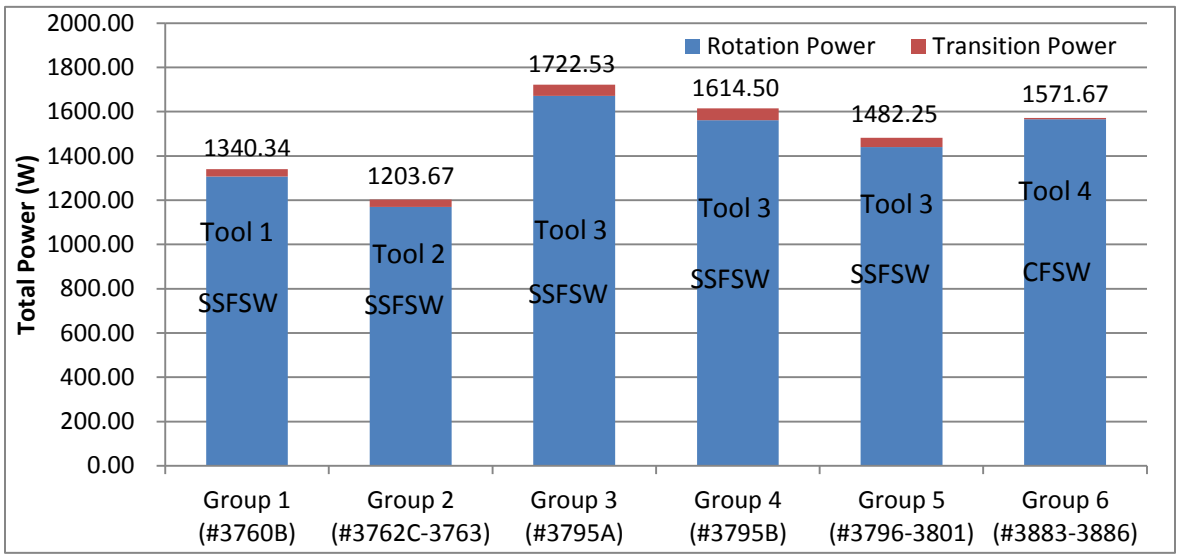

Figure 3.11 Total power by each tool

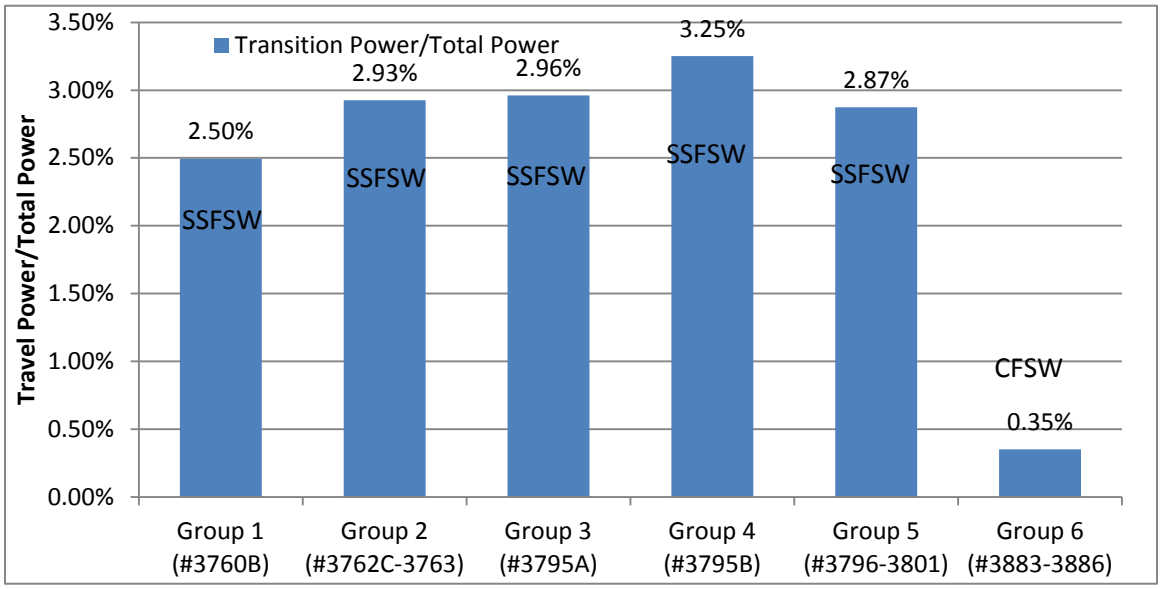

Figure 3.12 The ratio of travel power to total power

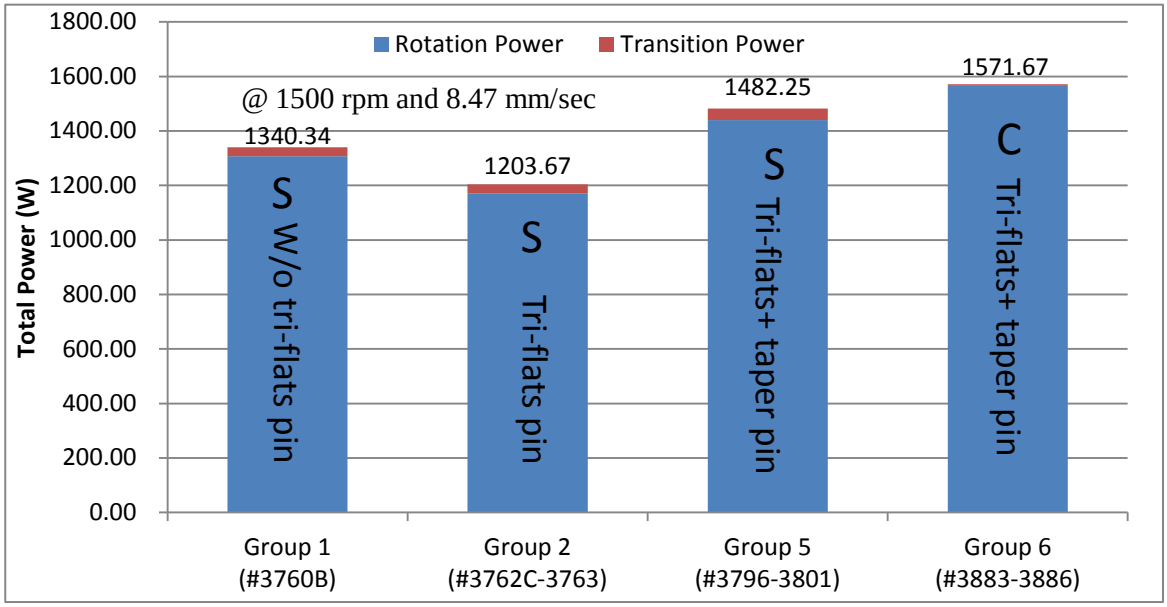

Figure 3.13 Power consumption at 1500 rpm and 8.47 mm/sec

As seen in Figure 3.11 to Figure 3.13, rotation power contributed most of the total power. The least total power was 1203.67W, which was achieved in group 2 (-1500 rpm, 8.47 mm/sec, 9.79 kN by tool 2). These implied that 1) SSFSW had less power consumption than CFSW under the similar welding control parameters. 2) SSFSW travel power

percentage was much larger than CFSW travel power percentage. 3) Under same rotation speed, welding speed and tool types, total power increased with increasing Z-force for SSFSW.

3.3.1. **The Effect of Rotation Speed**

Table 3.15 and Figure 3.14 showed the relationship between power and rotation speed for SSFSW.

Weld No.	Pin Design (Tool 1)	Rotation Speed rpm	Total Power W
@ Welding speed:6.35 mm/sec, Z-force:9.79 kN by Tool 1			
#3759A	Thread (RH)	-1200	1081.57
#3759B	Thread (RH)	-1500	1196.88
@ Welding speed:8.47 mm/sec, Z-force:9.79 kN by Tool 1			
#3760A	Thread (RH)	-1200	1175.93
#3760B	Thread (RH)	-1500	1340.34
#3760C	Thread (RH)	-1800	1075.67
Weld No.	Pin Design(Tool 2)	Rotation Speed rpm	Total Power W
@ Welding speed:8.47 mm/sec, Z-force:9.79 kN by Tool 2			
#3762B	Thread+3 flats (RH)	-1200	1076.89
#3762C-3763	Thread+3 flats (RH)	-1500	1203.67(Avg)
Weld No.	Pin Design(Tool 3)	Rotation Speed rpm	Total Power W
@ Welding speed:8.47 mm/sec, Z-force:14.23 kN by Tool 3			
#3796-3801	Thread+3 flats (LH&RH)	±1500	1482.25(Avg)
Weld No.	Pin Design(Tool 3)	Rotation Speed rpm	Total Power W
@ Welding speed:8.47 mm/sec, Z-force:6.67 kN by Tool 4			
#3883-3886	Thread+3 flats (RH)	-1500	1571.67(Avg)

Table 3.15 The relationship between power and pin rotation speed

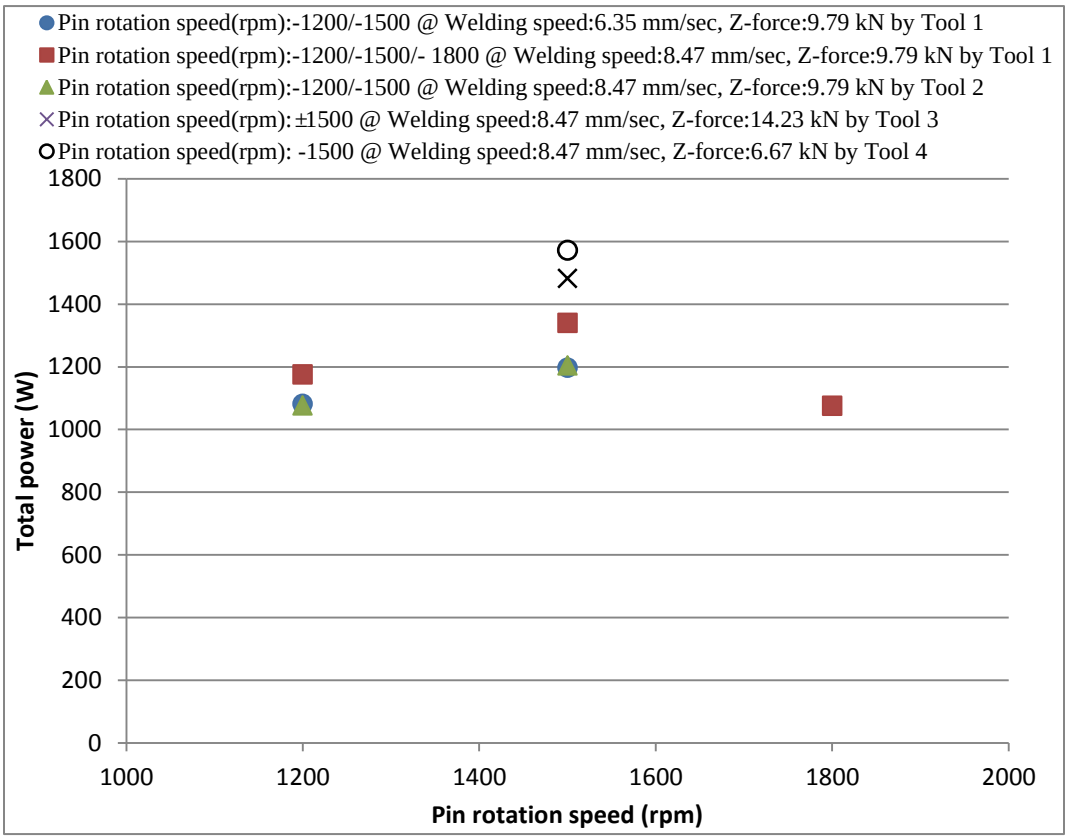

Figure 3.14 The relationship between power and pin rotation speed

From previous research by Reynolds et al, power in CFSW increased with increasing rotation speed [41]. However, for the present SSFSW in the experiments, when rotation speed was less than 1500 rpm, the total power followed this trend, when rotation speed was higher than 1500 rpm, the total power decreased with increasing rotation speed. The reason of the relationship between pin rotation speed and total power was not very clear. For the increasing trend, since the rotation power was the product of torque and angular speed of the pin, the torque declined by increasing rotation speed, and then flattened out at high rotation speed. The reason of the decline trend at high rotation speed may be due to defects. In order to verify this relationship, a more generalized power trend was

obtained by more data with different welding parameters, which was shown in Figure 3.15.

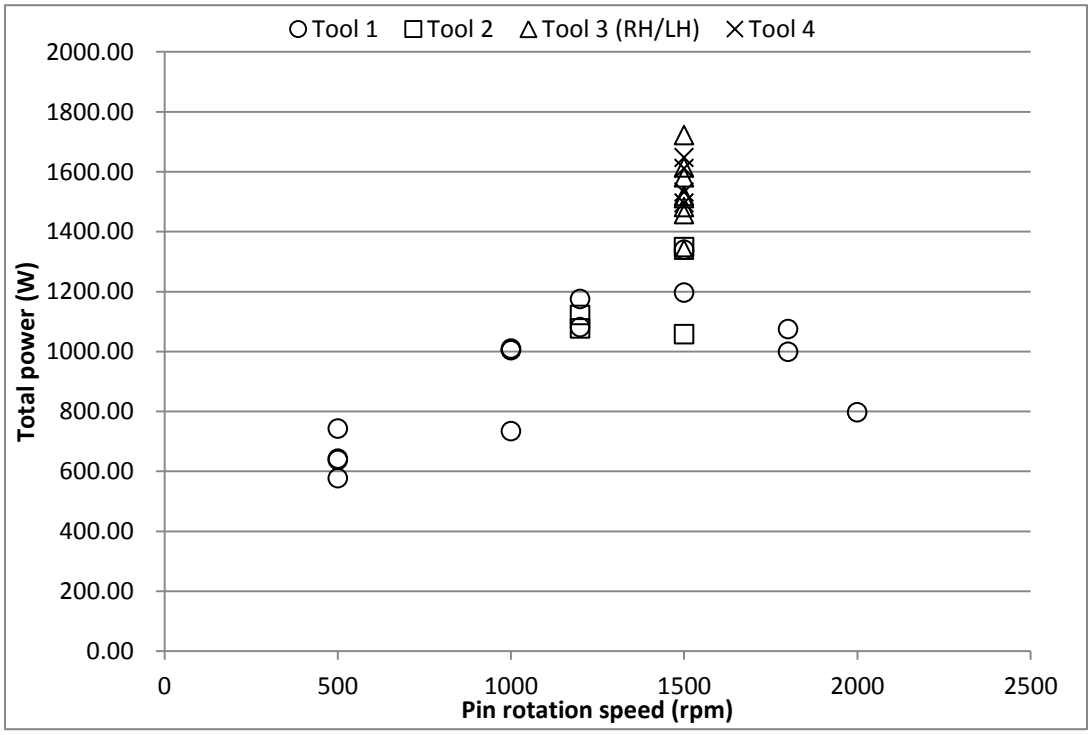

Figure 3.15 The generalized relationship between power and pin rotation speed (Other control parameters may be different.)

It was observed that total power increased with pin rotation speed at low and medium rotation speed, but decreased with rotation speed at relatively high rotation speed. For CFSW, the total power generally increased with increasing pin rotation speed, in some cases, a decline tail can be observed when rotation speed was high. The reason of the decline tail may be due to defects or melting. For SSFSW, the most probably reason was defects.

3.3.2. **The Effect of Z-force**

Table 3.16 and Figure 3.16 showed the relationship between Z-force and power in SSFSW.

Weld No.	Pin Design (Tool 1)	Z force kN	Total power W
Different Z-force @Pin rotation speed:-500 rpm, Welding speed:4.23 mm/sec, by Tool 1			
#3756	Thread (RH)	11.57	577.05
#3757A	Thread (RH)	10.68	637.93
#3757B	Thread (RH)	8.90	642.75
#3757C	Thread (RH)	7.12	743.51
Weld No.	Pin Design (Tool 3)	Z force kN	Total power W
Different Z-force @Pin rotation speed: ±1500 rpm, Welding speed: 8.47 mm/sec, by Tool 3			
#3795A	Thread+3 flats (RH)	17.79	1722.53
#3795B	Thread+3 flats (RH)	18.68	1614.50
#3796-3801	Thread+3 flats (LH&RH)	14.23	1482.25 ± 81.03
Weld No.	Pin Design (Tool 3)	Z force kN	Total power W
Different Z-force @Pin rotation speed: -1500 rpm, Welding speed: 8.47 mm/sec, by Tool 4			
#3883-3886	Thread+3 flats (RH)	6.67	1571.67 ± 69.97

Table 3.16 X-force values under different Z-force speed

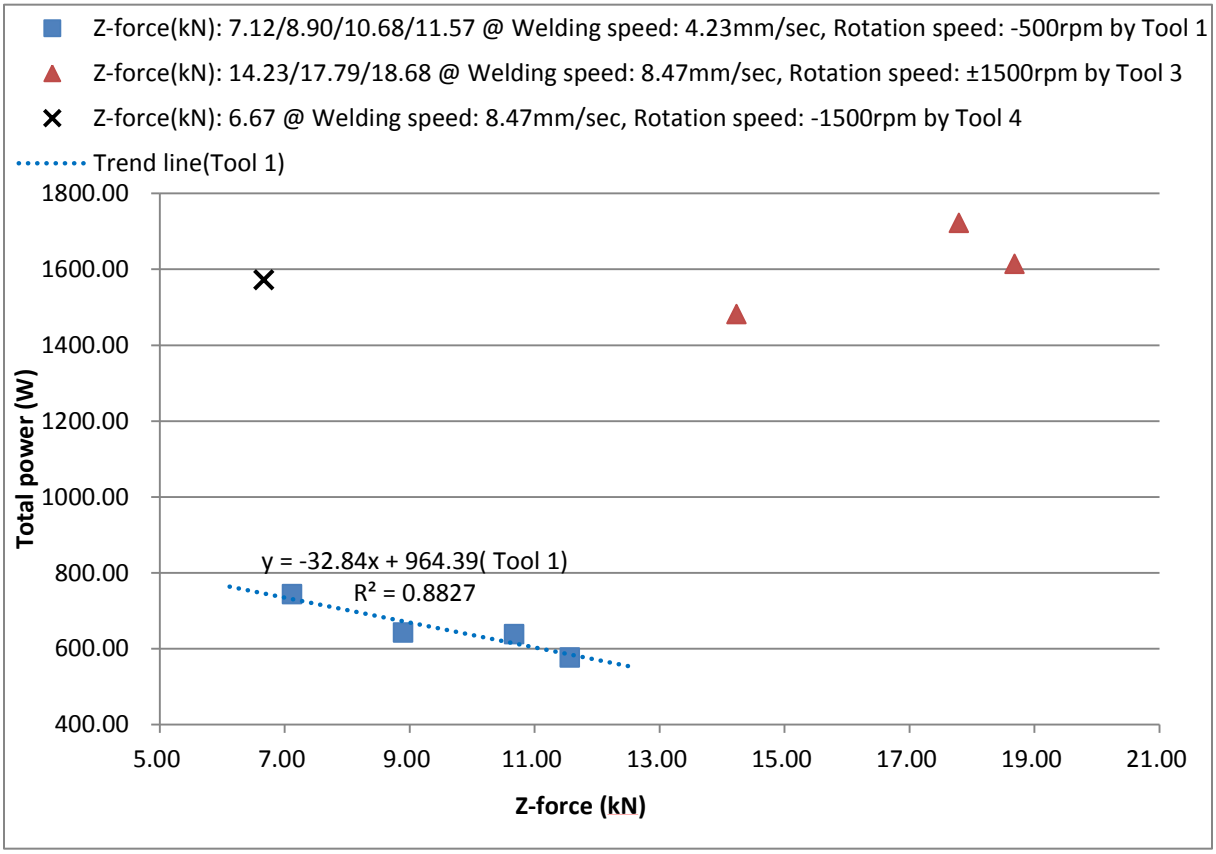

Figure 3.16 The relationship between total power and Z-force at 500 rpm and 1500 rpm

At low rotation speed, total power slightly decreased with increasing Z-force. The possible reason was that at the given low rotation speed, increasing Z-force helped increase temperature to reduce the torque. At high rotation speed, the trend of total power was not clear. The possible reason is at the given high rotation speed, temperature was higher enough to make torque reach a plateau. Another possible reason was that the lap joint weldments (3.2mm in thickness) were too thin. The result may not display the general trend. It should be noticed that the samples with lower rotation speed had the more seriously worm hole defects than the samples with high rotation speed. The decline

trend may be caused by the inadequately rotation speed. The result may not display the general trend.

Figure 3.17 showed the relationship between Z-force and travel power.

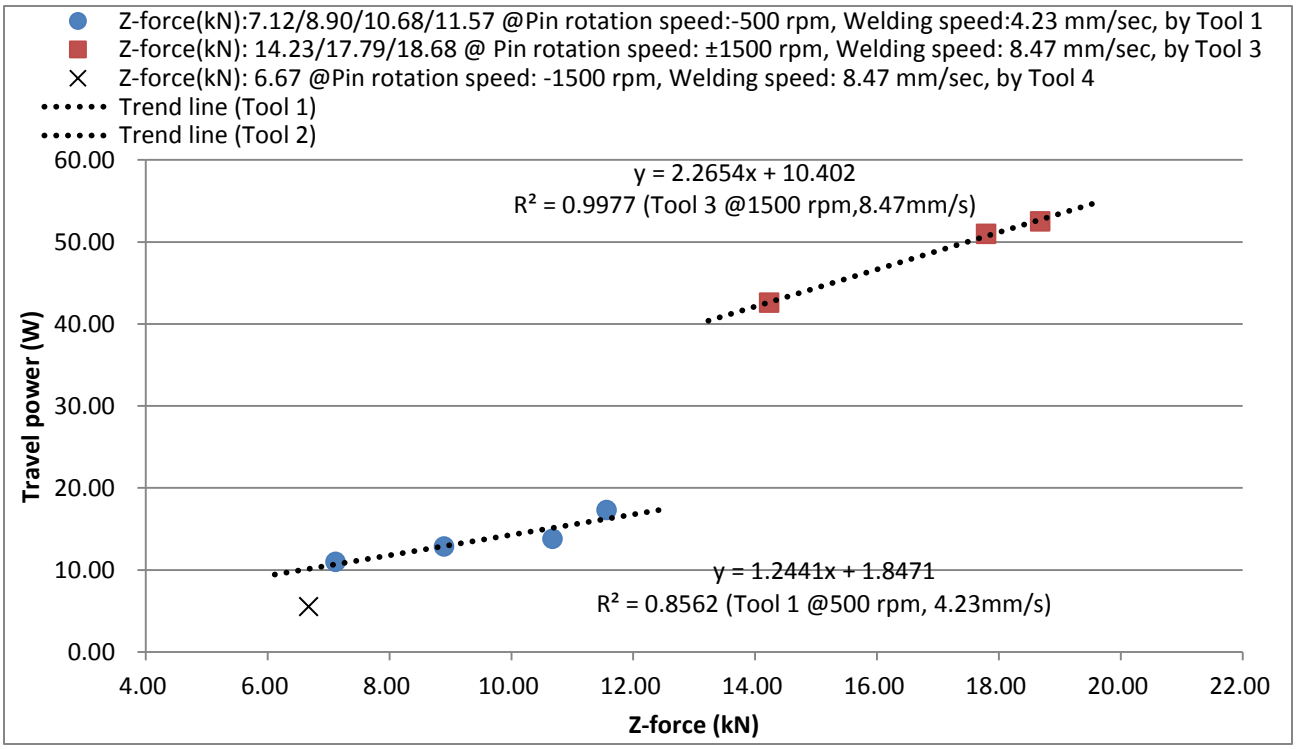

Figure 3.17 The relationship between travel power and Z-force at 4.23 mm/s and 8.47 mm/s

Travel power increased with increasing Z-force at given rotation and travel speed, since larger Z-force lead to larger friction force.

3.4.Distortion

Distortion is an important indicator of welding quality. It is caused by unrecovered plastic strain due to temperature history during FSW process[25]. Welding sheets with 1500 rpm, 8.47 mm/s by tool 3(SSFSW) and tool 4(CFSW) were chosen, since this welds were assumed to have good quality.

3.4.1. **SSFSW vs. CFSW (with same welding direction)**

The following figures showed the distortion contour picture of #3796-3797 and #3883-3884 welding sheet as welded, after post welds heat treatment (PWHT). These two weld sheets were welded in the same direction and have the same pin rotation direction. Table 3.16 to Table 3.20 showed the distortion result of #3796-3797 and #3883-3884 welding sheet. The data in grey cells was measured height value from the machine stage to the bottom surface of the weldments. Figure 3.18, Figure 3.19 and Figure 2.9 showed the distortion contour of #3796-3797 and #3883-3884 welding sheet as welded and after PWHT and their welding direction and pin rotation direction arrangement. It should be noticed that because heat treatment reduced distortion evidently, the scale bar in the post weld distortion figures was intentionally made smaller than that in as welded figures to demonstrate the clear change of distortion for the weld sheets.

3796&3797	@ Rotation speed:-1500 rpm, Welding speed:8.47 mm/sec, Z-force:14.23 kN by Tool 3								
As welded	x(mm)	0	65.31	130.63	195.94	261.26	326.57	391.88	457.20
y(mm)									
0		18.43	9.80	3.19	0.19	0.00	0.92	5.19	12.00
38.10		18.28	9.72	3.57	0.46	0.17	2.11	6.92	13.94
76.20		17.48	9.11	3.44	0.62	0.35	2.66	7.79	15.71
114.30		15.66	7.99	2.60	0.53	0.36	2.63	7.91	16.33
152.40		13.57	6.33	1.45	0.00	0.06	2.16	7.74	15.91

Table 3.17 #3796-3797 welding sheet as welded (AW) distortion result

3796&3797	@ Rotation speed:-1500 rpm, Welding speed:8.47 mm/sec, Z-force:14.23 kN by Tool 3								
PWHT	x(mm)	0	65.31	130.63	195.94	261.26	326.57	391.88	457.20
y(mm)									
0		13.05	6.81	2.07	0.10	0.00	0.62	3.83	9.08
38.10		12.76	6.61	2.36	0.28	0.16	1.64	5.27	10.57
76.20		12.17	6.18	2.18	0.34	0.24	2.02	5.92	11.98
114.30		10.64	5.24	1.68	0.34	0.32	2.02	6.05	12.37
152.40		8.96	3.89	0.72	0.00	0.05	1.57	5.79	12.05

Table 3.18 #3796-3797 welding sheet after PWHT distortion result

3883&3884	@ Rotation speed: -1500 rpm, Welding speed:8.47 mm/sec, Z-force:6.67 kN by Tool 4								
As welded	x(mm)	0	65.31	130.63	195.94	261.26	326.57	391.88	457.20
y(mm)									
0		14.56	6.64	1.49	-0.01	-0.01	1.88	7.67	16.33
38.10		16.40	8.17	2.72	0.24	0.23	2.85	8.63	17.26
76.20		17.78	9.25	3.63	1.01	0.42	3.19	9.02	17.51
114.30		17.75	9.15	3.18	0.43	0.30	2.69	8.15	16.48
152.40		17.16	8.22	2.26	0.03	-0.01	1.46	6.59	14.69

Table 3.19 #3883-3884 welding sheet as welded (AW) distortion result

3883&3884	@ Rotation speed: -1500 rpm, Welding speed:8.47 mm/sec, Z-force:6.67 kN by Tool 4								
PWHT	x(mm)	0	65.31	130.63	195.94	261.26	326.57	391.88	457.20
y(mm)									
0		9.12	3.91	0.71	-0.01	-0.01	1.10	5.05	11.29
38.10		10.49	5.19	1.67	0.17	0.16	1.83	5.78	11.85
76.20		11.70	6.01	2.23	0.58	0.25	2.02	5.91	11.46
114.30		11.93	6.07	2.06	0.32	0.23	1.64	5.12	10.55
152.40		11.76	5.43	1.27	0.00	-0.01	0.65	3.83	9.10

Table 3.20 #3883-3884 welding sheet after PWHT distortion result

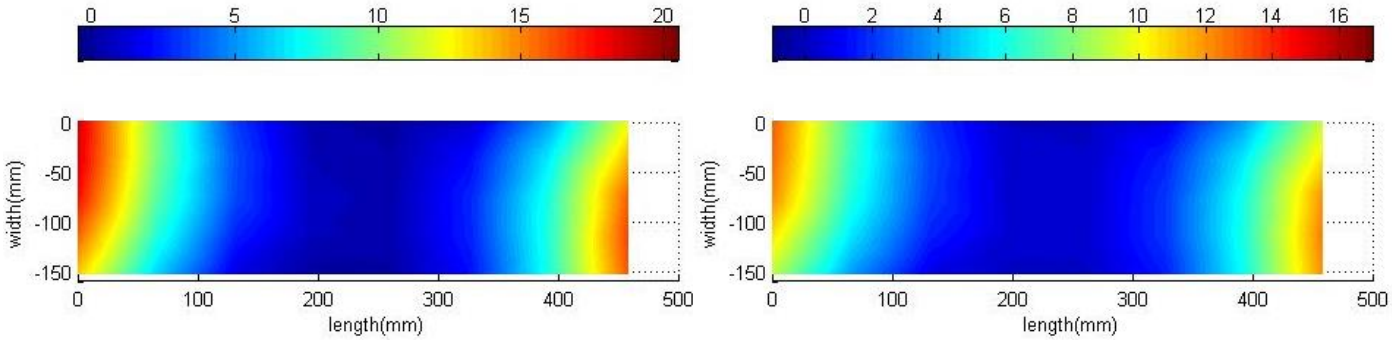

Figure 3.18 SSFSW Distortion of #3796/3797 as welded (left) and after PWHT (right)

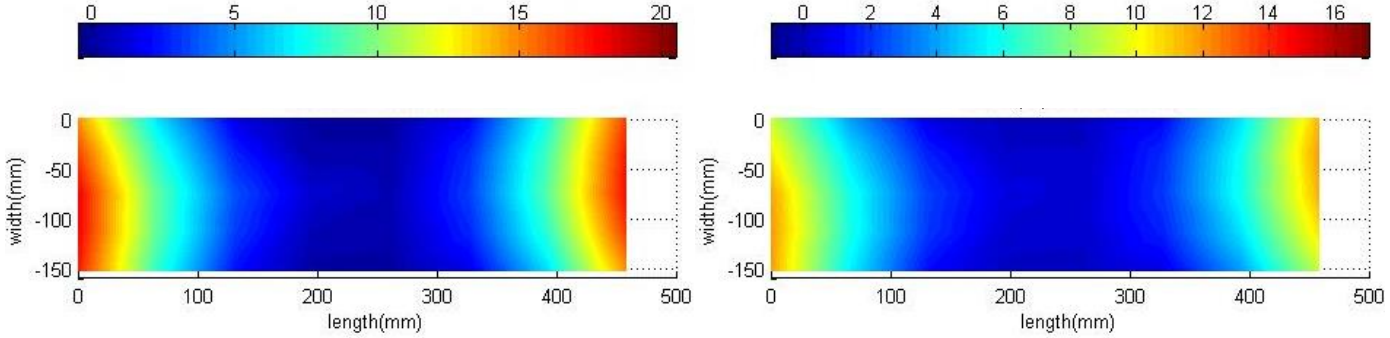

Figure 3.19 CFSW Distortion of #3883/3884 as welded (left) and after PWHT (right)

Conventional FSW was reported to have small saddle shape distortion [25]. SSFSW had similar distortion compared to conventional FSW as welded and after PWHT under same welding and pin rotation direction (See Figure 3.18 and Figure 3.19). Distortion of SSFSW was not very symmetric. In Figure 3.18, distortion at up-right and bottom-left corners was smaller than that at the rest of the sheet edge. Heat treatment helped reduce distortion for both SSFSW and convention FSW. SSFSW has similar saddle shape distortion as CFSW.

3.4.2. **SSFSW vs. CFSW (with different welding direction)**

The distortions of the welding sheets with different welding directions were showed in the following tables. In addition the contours of distortion and their welding direction and pin rotation direction arrangement were shown in the Figure 3.20, Figure 2.11 (for #3800-3801) and Figure 3.21, Figure 2.12 (for #3885-3886).

3800&3801	@ Rotation speed: 1500 rpm, Welding speed:8.47 mm/sec, Z-force:14.23 kN by Tool 3								
As welded	x(mm)	0	65.31	130.63	195.94	261.26	326.57	391.88	457.20
y(mm)									
0		17.86	9.15	3.09	0.21	0.00	0.72	4.88	12.44
-38.10		17.58	8.76	3.24	0.45	0.15	1.95	6.75	14.68
-76.20		16.68	7.99	2.72	0.25	0.33	2.82	8.02	16.13
-114.30		13.76	6.33	2.10	0.41	0.49	2.99	8.51	17.66
-152.40		11.16	4.36	0.79	0.03	0.16	2.63	8.89	17.82

Table 3.21 #3800-3801 welding sheet as welded distortion result

3800&3801	@ Rotation speed: 1500 rpm, Welding speed:8.47 mm/sec, Z-force:14.23 kN by Tool 3								
PWHT	x(mm)	0	65.31	130.63	195.94	261.26	326.57	391.88	457.20
y(mm)									
0		13.25	6.59	2.09	0.10	0.00	0.63	4.16	10.57
-38.10		13.12	6.61	2.26	0.30	0.14	1.59	5.58	12.32
-76.20		12.35	5.92	2.04	0.21	0.19	2.13	6.41	13.85
-114.30		10.79	4.85	1.61	0.39	0.48	2.39	6.71	13.99
-152.40		8.81	3.21	0.50	0.03	0.12	1.91	6.68	13.83

Table 3.22 #3800-3801 welding sheet after PWHT distortion result

3885&3886	@ Rotation speed: -1500 rpm, Welding speed:8.47 mm/sec, Z-force:6.67 kN by Tool 4								
As welded	x(mm)	0	65.31	130.63	195.94	261.26	326.57	391.88	457.20
y(mm)									
0		17.74	8.47	2.36	0.03	0.00	1.54	7.17	16.09
-38.10		18.57	9.41	3.30	0.33	0.21	2.72	8.56	17.36
-76.20		18.83	9.74	3.73	1.19	0.49	3.47	9.43	18.20
-114.30		17.84	8.87	3.10	0.45	0.42	3.16	9.05	17.80
-152.40		15.95	7.36	1.84	0.00	0.01	2.08	8.09	16.50

Table 3.23 #3885-3886 welding sheet as welded distortion result

3885&3886	@ Rotation speed: -1500 rpm, Welding speed:8.47 mm/sec, Z-force:6.67 kN by Tool 4								
PWHT	x(mm)	0	65.31	130.63	195.94	261.26	326.57	391.88	457.20
y(mm)									
0		10.43	4.68	1.16	0.02	-0.01	0.94	4.84	11.38
-38.10		11.30	5.71	1.97	0.19	0.21	1.93	5.93	12.29
-76.20		12.27	6.38	2.19	0.81	0.38	2.42	6.56	12.74
-114.30		12.07	5.70	1.79	0.29	0.37	2.23	6.31	12.31
-152.40		11.18	4.73	0.85	0.00	0.02	1.40	5.60	11.41

Table 3.24 #3885-3886 welding sheet after PWHT distortion result

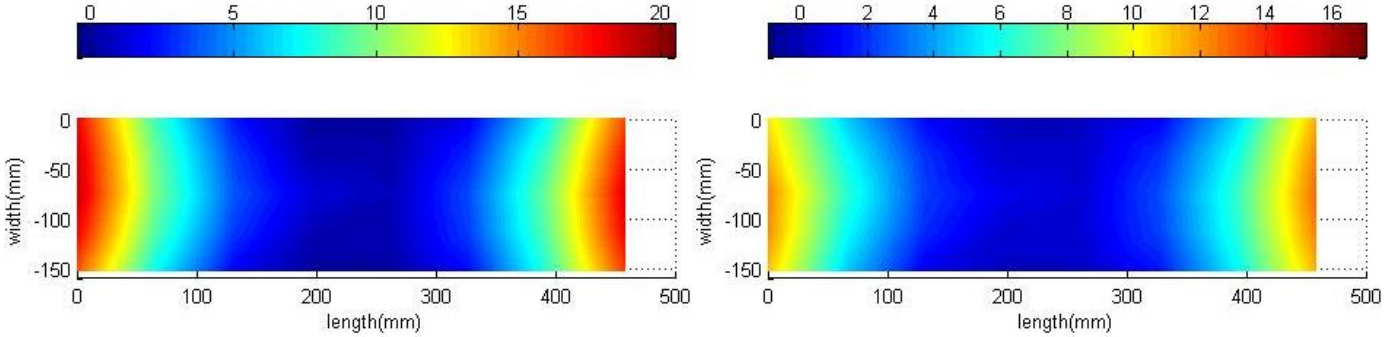

Figure 3.20 SSFSW Distortion of #3800/3801 as welded (left) and after PWHT (right)

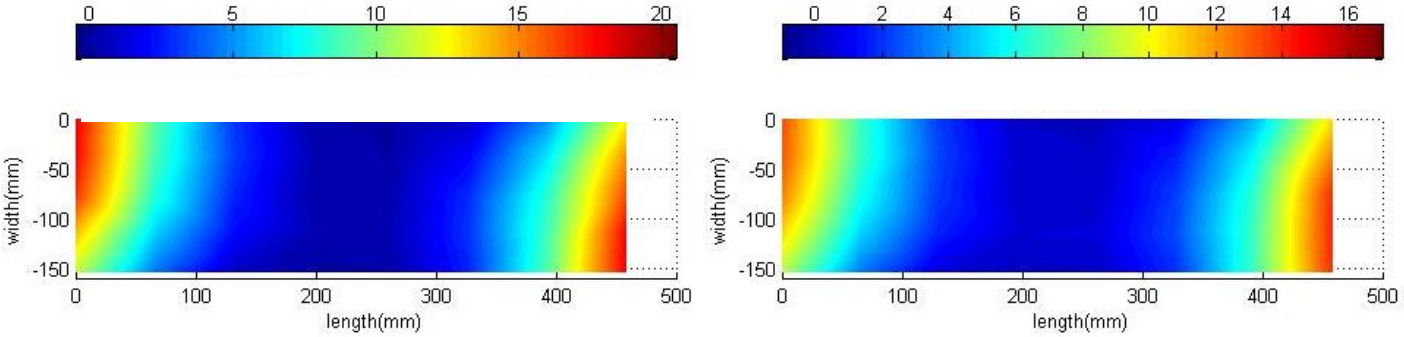

Figure 3.21 CFSW Distortion of #3885/3886 as welded (left) and after PWHT (right)

Again, SSFSW didn't show much difference in distortion over conventional FSW as welded and after PWHT. SSFSW had similar saddle shape distortion as CFSW. Welding direction did not affect the distortion too much.

3.4.3. **Effects of Opposite Pin Rotation Direction(LH/RH)**

Figure 2.10 and Figure 3.22 showed the welding direction and pin rotation direction arrangement and the distortion contour of welding sheets as welded and after PWHT.

3798&3799	@ Rotation speed: ±1500 rpm, Welding speed:8.47 mm/sec, Z-force:14.23 kN by Tool 3								
As welded	x(mm)	0	65.31	130.63	195.94	261.26	326.57	391.88	457.20
y(mm)									
0		18.21	10.12	3.46	0.22	0.01	1.11	6.36	14.96
-38.10		17.71	9.75	3.73	0.50	0.21	2.37	8.01	17.09
-76.20		16.11	8.57	3.20	0.39	0.32	3.37	9.60	19.70
-114.30		13.70	6.95	2.18	0.39	0.57	3.64	10.10	20.49
-152.40		11.31	4.64	0.76	0.01	0.24	3.34	10.36	20.37

Table 3.25 #3798-3799 welding sheet as welded distortion result

3798&3799	@ Rotation speed: ±1500 rpm, Welding speed:8.47 mm/sec, Z-force:14.23 kN by Tool 3								
PWHT	x(mm)	0	65.31	130.63	195.94	261.26	326.57	391.88	457.20
y(mm)									
0		13.48	7.29	2.20	0.11	0.00	0.78	4.88	11.70
-38.10		13.11	7.20	2.65	0.36	0.19	1.94	6.50	13.94
-76.20		12.15	6.49	2.39	0.28	0.27	2.71	7.74	16.08
-114.30		10.41	5.10	1.66	0.36	0.54	2.98	8.10	16.43
-152.40		8.53	3.49	0.61	0.03	0.23	2.68	8.27	16.51

Table 3.26 #3798-3799 welding sheet after PWHT distortion result

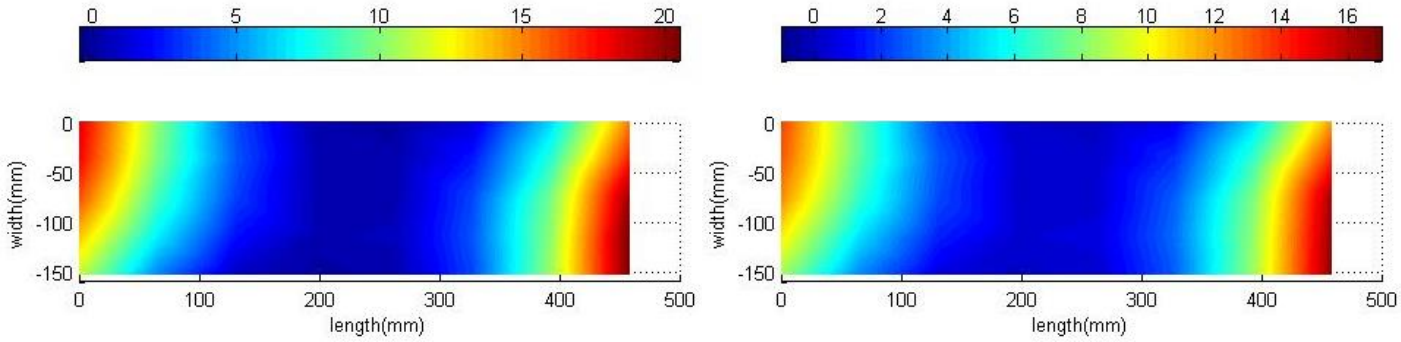

Figure 3.22 SSFSW Distortion of #3798/3799 as welded (left) and after PWHT (right)

Distortion of weldments with opposite rotation direction tended to have slightly larger distortion in SSFSW than that in CFSW.

3.4.4. **Heat Treatment Effects on Distortion**

Heat treatment reduced the distortion of both the SSFSW and conventional FSW weldments. Figure 3.23 showed average distortion fitting radius on each welding sheet as welded and after PWHT.

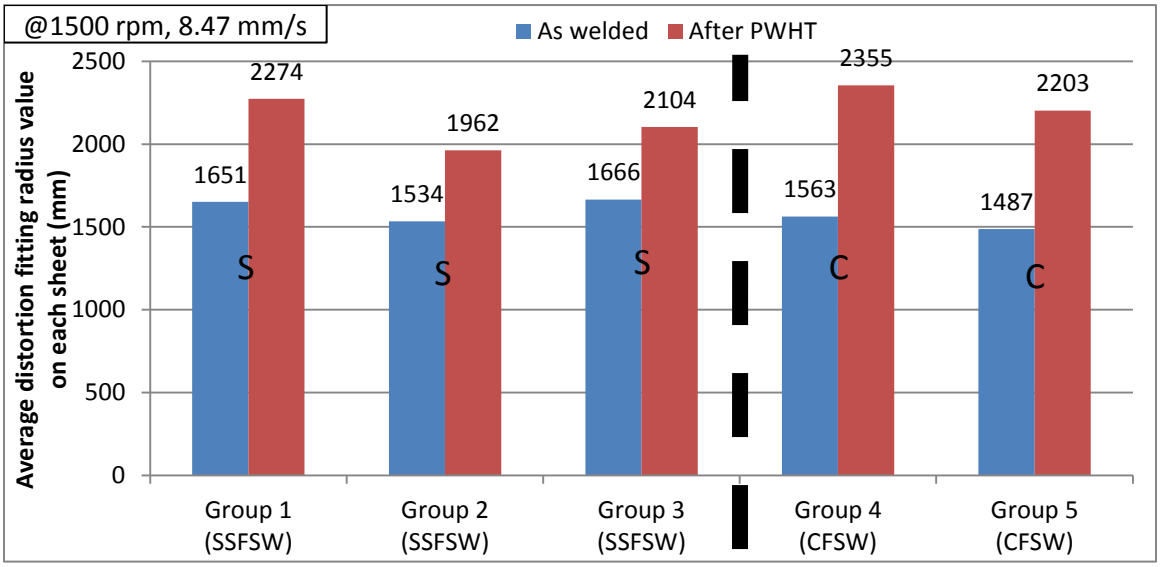

Group 1: Both welds with same welding and rotation direction (#3796-3797)
Group 2: Both welds with same welding direction but different pin rotation direction (#3798-3799)
Group 3: Both welds with opposite welding direction but same pin rotation direction (#3800-3801)
Group 4: Both welds with same welding and rotation direction (#3883-3884)
Group 5: Both welds with opposite welding direction but same pin rotation direction (#3885-3886)

Figure 3.23 Average distortion fitting radius on each welding sheet (as welded and after PWHT)

Heat treatment reduced distortion significantly. PWHT reduced the distortion of CFSW welding sheet slightly more than SSFSW. Same welding and rotation direction arrangement resulted in lower distortion after PWHT than the other arrangements for the present study. Distortion of weldments with same welding direction but different rotation direction arrangement tended to have larger distortion for SSFSW for the present study.

In all, both welding direction and tool rotation direction arrangements had influence on distortion.

3.5. Welding Surface

Welding surface photo for welding sheet under different welding parameters and tool properties are showed in the following figures.

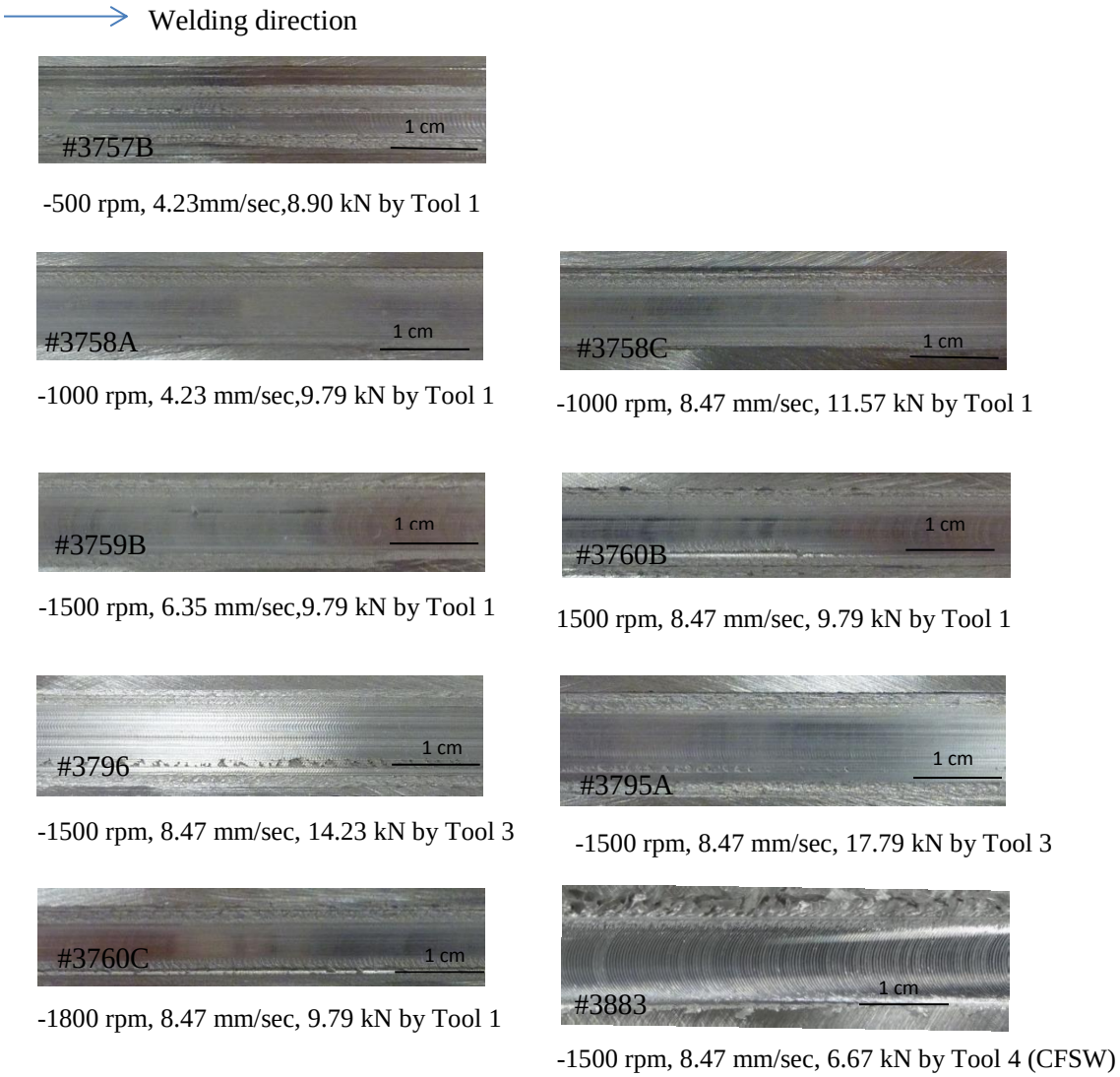

Figure 3.24 Welding Surface at different welding parameters and welding tools: #3757(A,B,C), #3759B, #3760B, #3796, #3795A, #3760C, #3883.

The results showed SSFSW can achieve relatively smooth welding surface with little or no flash compared to CFSW (Here CFSW was not with its optimized control parameters). When rotation speed was below 1000 rpm, welding surface quality for SSFSW increased with rotation speed, and reached the best surface quality at 1000 rpm (see #3757B vs. #3758A). Surface quality was slight lower when rotation speed was 1500 rpm (see #3759B). When rotation speed increased to 1800 rpm, continuous surface void can be clearly observed. (see #3760C). Welding surface quality decreased with welding speed (see#3759B vs. #3760B). Increasing Z-force helped increase surface quality (#3795A vs #3796). Comparing #3760B and #3796, the welding surface changed from having continuous surface void to having intermittent surface voids when Z-force increases from 9.79 kN to 14.23kN. The welding surface voids were reduced when Z-force reached to 17.79 kN (See #3795A). Increasing Z-force helped keep the rotating pin contacting the welding surface firmly, hence reduced the surface lack of fill (voids) [43]. SSFSW required larger downward force compared to Conventional FSW for the present shoulder design.

3.6. Cross Section Observation

3.6.1. **Effects of Welding Parameters**

Figure 3.25 to Figure 3.29 showed the Metallographic pictures at cross section of AA7075-T6 for SSFSW under different welding parameters. It should be noticed that

because of the limited numbers of experiments, both defect-free and defective welding cross section were shown and discussed here. For SSFSW, WNZ displayed fine and equiaxed grain. The microstructure image revealed relatively non-symmetric weld nugget area. Sharp boundary can be observed on advancing side, while on retreating side, rather blurry boundary was observed. The typical "onion–ring" pattern was observed at advancing side SSFSW. The shape of the onion-ring was studied to be associated with extrusion of cylindrical sheets of material during FSW process [42]. However its mechanism is not understood well yet. Cavity defects of different degree can be observed at advancing side.

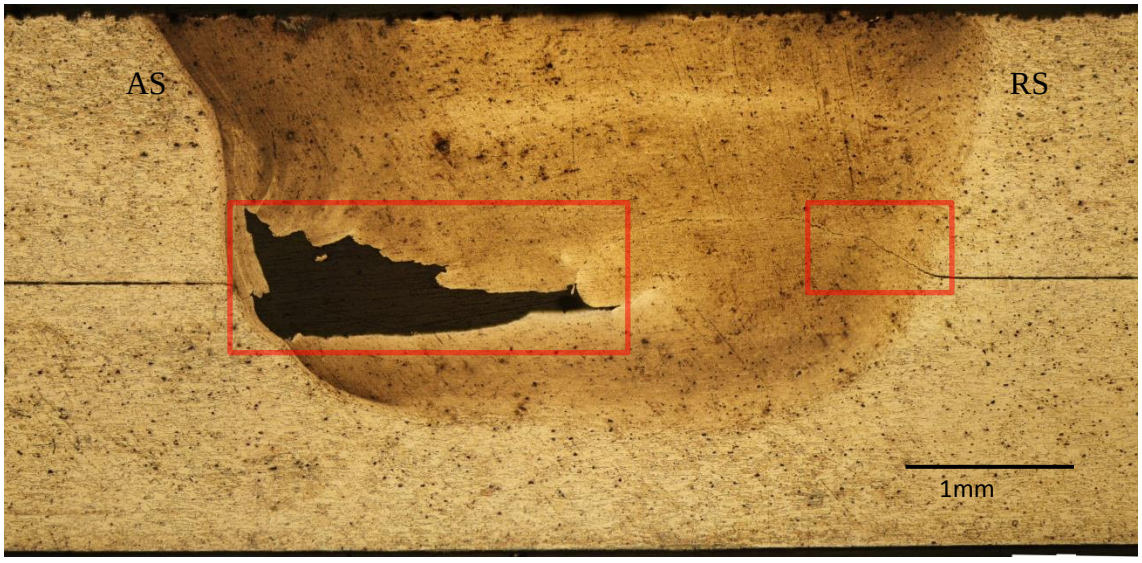

Figure 3.25 Metallographic picture of SSFSW #3757A welding sheet cross section at -500 rpm ,4.23 mm/sec, 10.68 kN tool 1(RH)

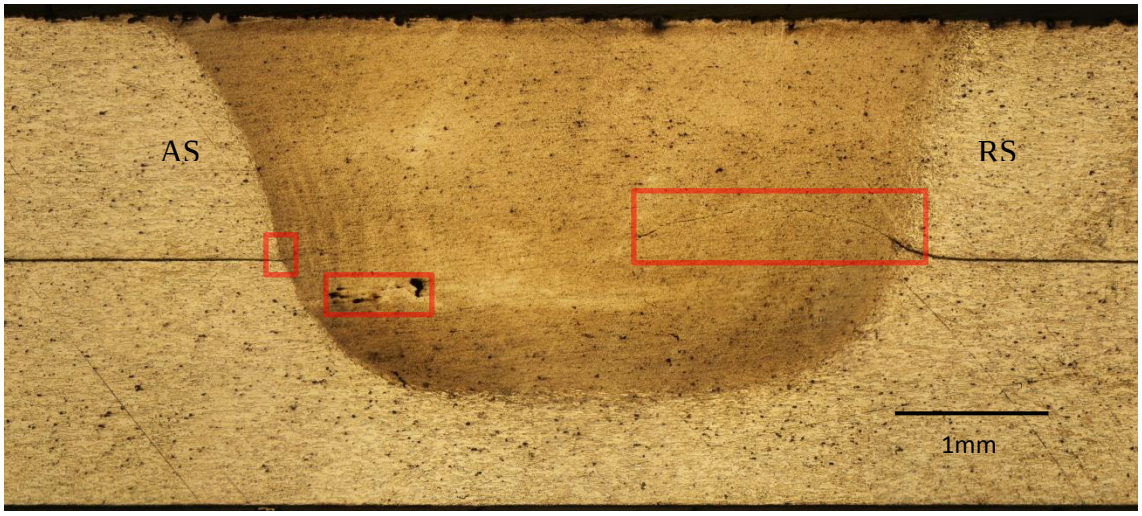

Figure 3.26 Metallographic picture of SSFSW #3758A welding sheet cross section at -1000 rpm, 4.23 mm/sec, 9.79 kN tool 1(RH)

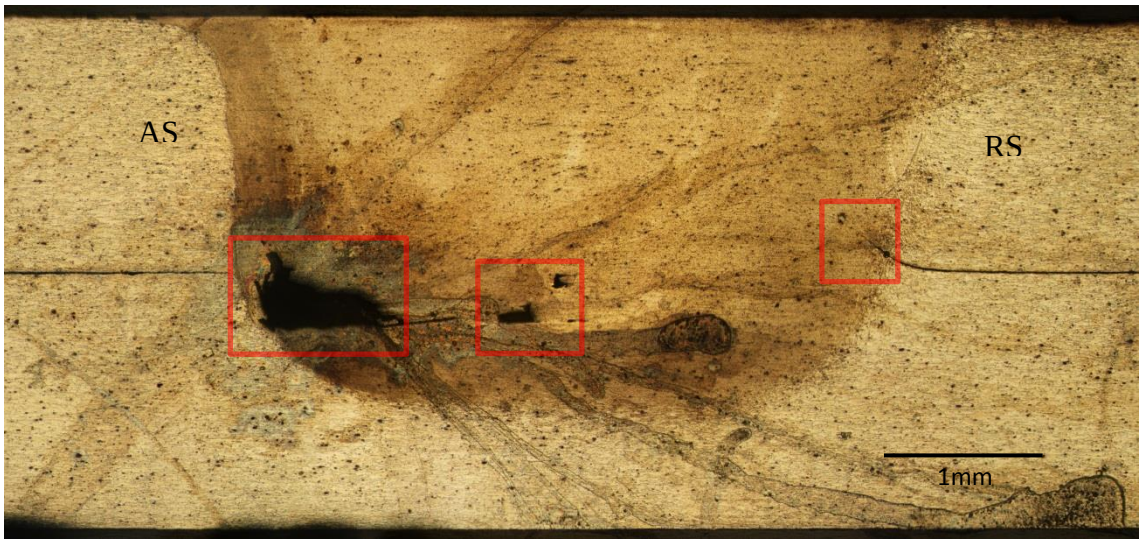

Figure 3.27 Metallographic picture of SSFSW #3760A welding sheet cross section at -1200 rpm, 8.47 mm/sec, 9.79 kN tool 1(RH)

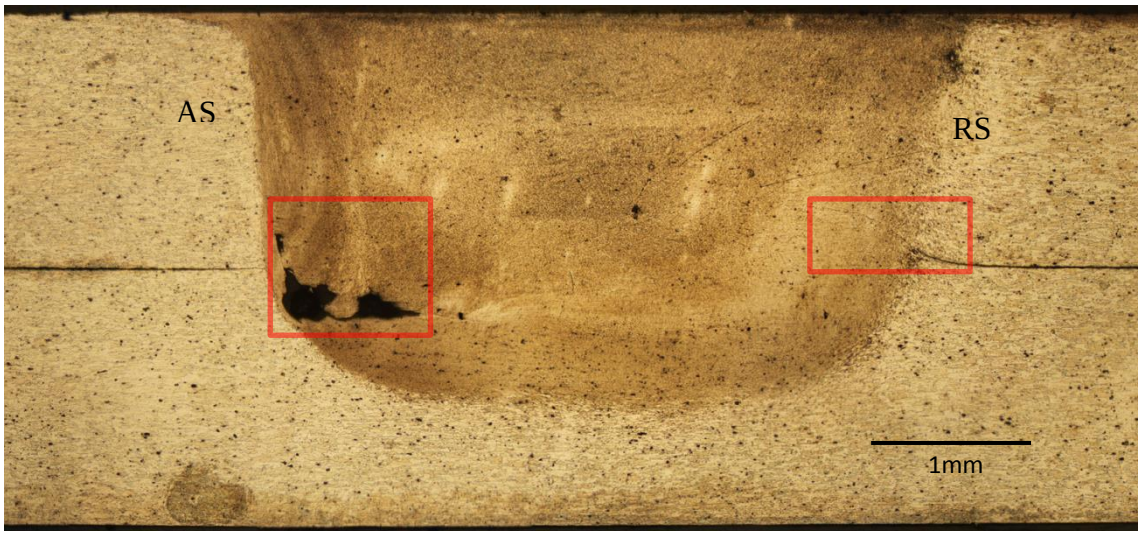

Figure 3.28 Metallographic picture of SSFSW #3760B welding sheet cross section at -1500 rpm, 8.47 mm/sec, 9.79 kN tool 1(RH)

Figure 3.29 Metallographic picture of SSFSW #3760C welding sheet cross section at -1800 rpm, 8.47 mm/sec, 9.79 kN tool 1(RH)

When rotation speed was below 1000 rpm, it was observed that the cross section quality at cross section increased with rotation speed. The welding quality was optimum when rotation speed reached 1000 rpm. When rotation speed was higher than 1000 rpm, further increase of rotation speed lead to more severe defect. Decreasing welding speed

tend to increase welding quality. And the welding quality was optimum when welding speed was 4.23 mm/sec. This was because less welding speed generated larger heat input, hence improved the grain reformation. The “S” shape line, which formed in result of break-up of the oxide layer, was clearly observed at lower welding speed, because of the lower heat input in FSW process[43]. The weld with best cross section feature and the least defects was at -1000 rpm, 4.23 mm/sec, 9.79 kN.

Both weldments under -1500 rpm, 8.47 mm/s and -1000 rpm, 4.23 mm/sec had smaller defects than weldments under other control parameters. However, since welds under -1500 rpm, 8.47 mm/s had much higher welding efficiency, it was chosen in later study, where flat design was introduced to reduce the defects.

3.6.2. **Effects of Tool Property**

Figure 3.26 to Figure 3.34 showed the Metallographic pictures at cross section under different design tools.

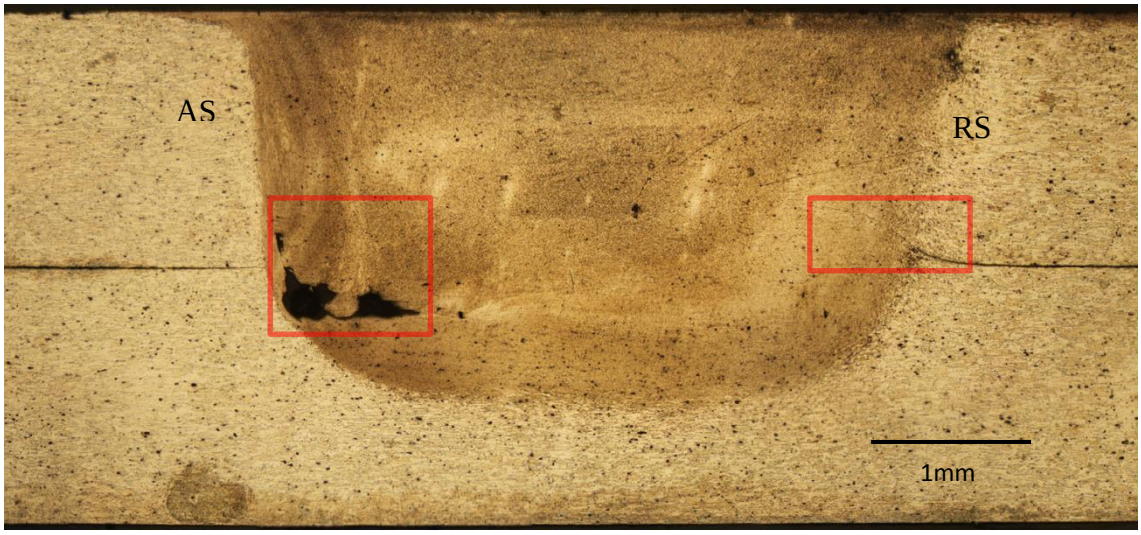

Figure 3.30 Metallographic picture of SSFSW #3760B welding sheet cross section at -1500 rpm, 8.47 mm/sec, 9.79 kN tool 1(RH)

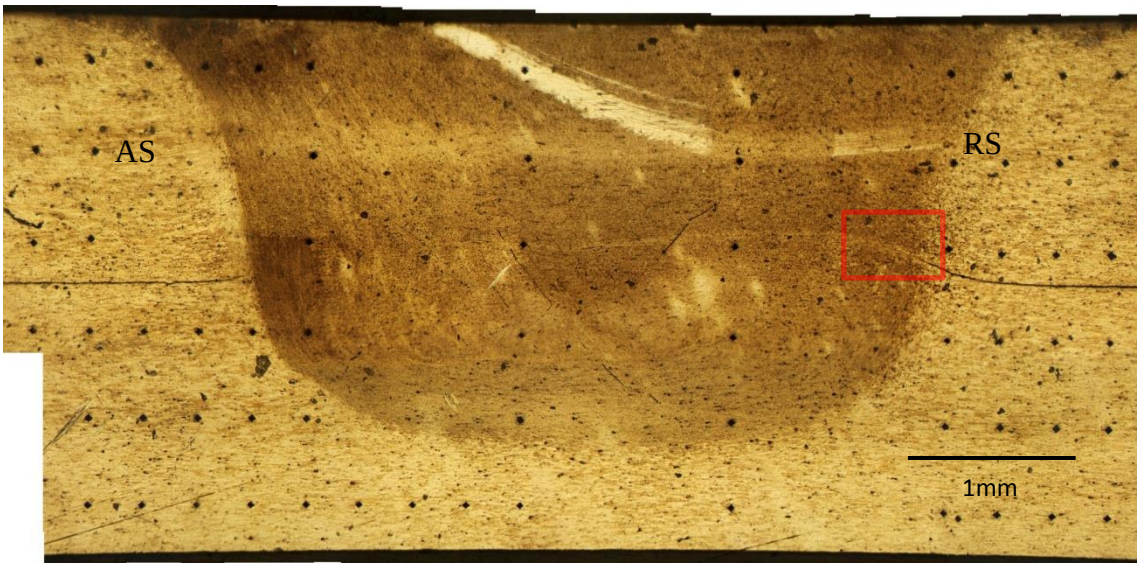

Figure 3.31 Metallographic picture of SSFSW #3763 welding sheet cross section at -1500 rpm, 8.47 mm/sec, 9.79 kN tool 2(RH)

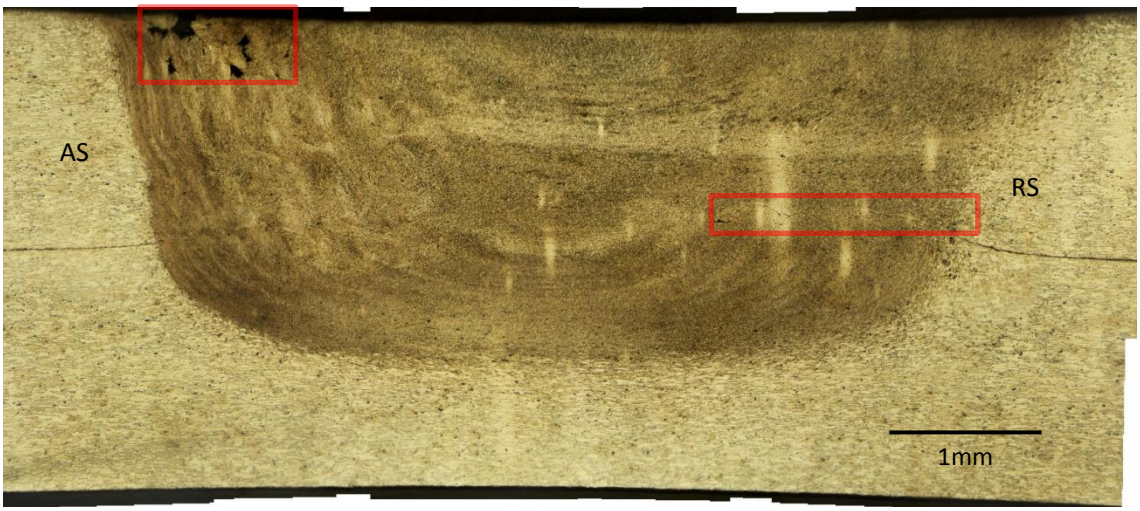

Figure 3.32 Metallographic picture of SSFSW 3797 welding sheet cross section at -1500 rpm, 8.47 mm/sec, 14.23 kN tool 3(RH)

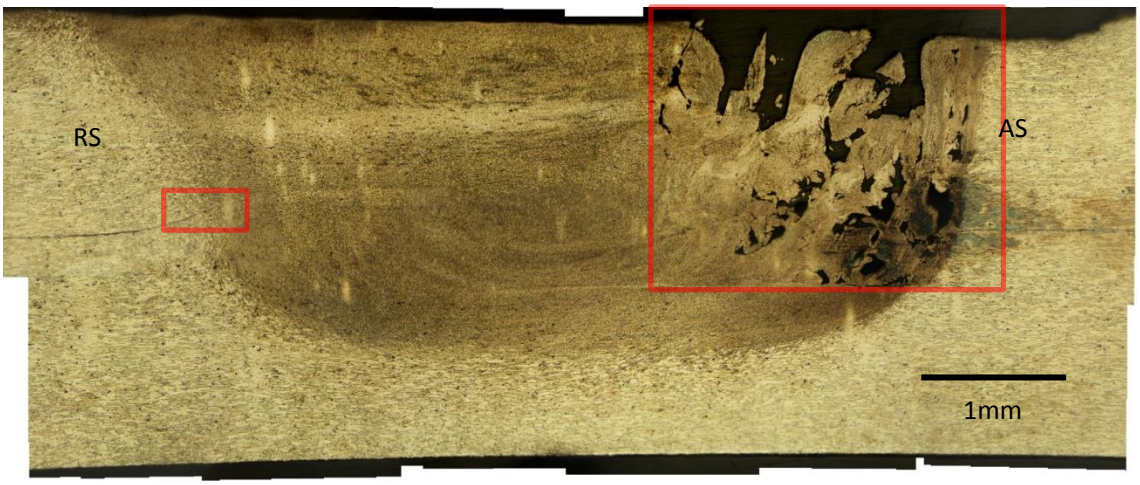

Figure 3.33 Metallographic picture of SSFSW #3799 welding sheet cross section at 1500 rpm, 8.47 mm/sec, 14.23 kN tool 3(LH)

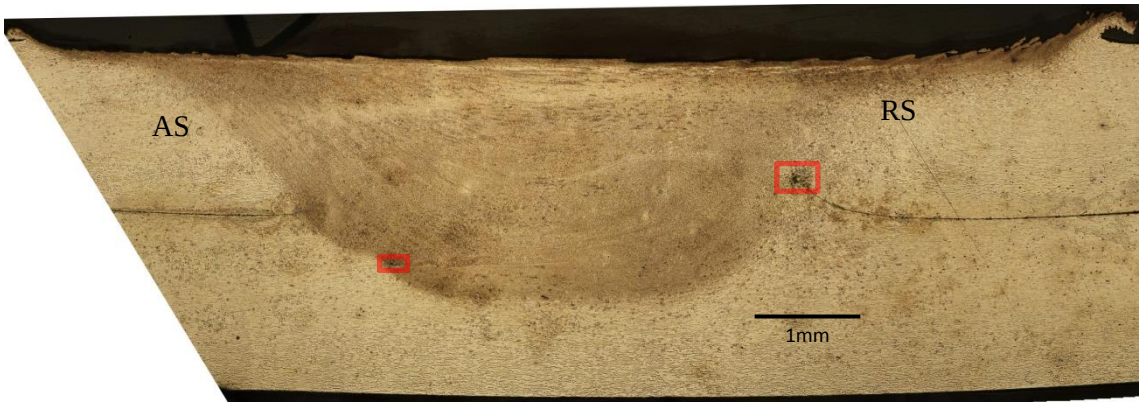

Figure 3.34 Metallographic picture of CFSW #3884 welding sheet cross section at -1500 rpm, 8.47 mm/sec, 6.67 kN tool 4(RH)

Welding quality at cross section was better when flat pin was adopted. Also, bigger pin size resulted in bigger welding nugget area. Reynolds et al reported this relationship between nugget size and pin size. They found that the nugget area was slightly larger than the pin diameter.

There were more wormholes in #3799(LH) than that in #3797(RH), which was not expected. (The tool for RH and LH was checked for uniformity, see Appendix D.) This poor welding quality of #3799(LH) lead to poor tensile strength, which was shown in later section.

Rotational shoulder exerted more heat on sheet surface, hence the area of deformation was near the surface for CFSW. It should be noticed that the typical flash was produced by CFSW. The top widths of welds in SSFSW were smaller than the top widths of welds in CFSW, owing to the little heat input by stationary shoulder. The boundary slope of CFSW WNZ was gentler than SSFSW's, which was affected by rotation shoulder.

3.7. Grain Size

Generally, the grain size mainly depends on its experience temperature and its duration time (Heat/energy input) under the same thermal boundary condition. The actual transient temperature is hard to measure. It is related to rotation speed, welding speed and advance per revolution, specific weld energy and weld power. Any factor alone is not able to

represent temperature well. Among these factors, the total power seem to reflect the maximum temperature the best [18] . Duration time is a function of welding speed. Also, for a given weld, heat-up and cool-down rate depends mostly on welding speed. The microscopic pictures of grains were shown in Appendix C. Table 3.27 and Figure 3.35 showed the relationship between grain size and total power.

Weld No	Welding Speed mm/sec	Total Power W	Grain Size μm
#3757A	4.23	637.93	1.1±0.11
#3758A	4.23	1004.84	1.2±0.13
#3760A	8.47	1175.93	1.3±0.04
#3760B	8.47	1340.34	1.5±0.11
#3798	8.47	1519.86	2.2±0.13

Table 3.27 Grain size under different total power in SSFSW

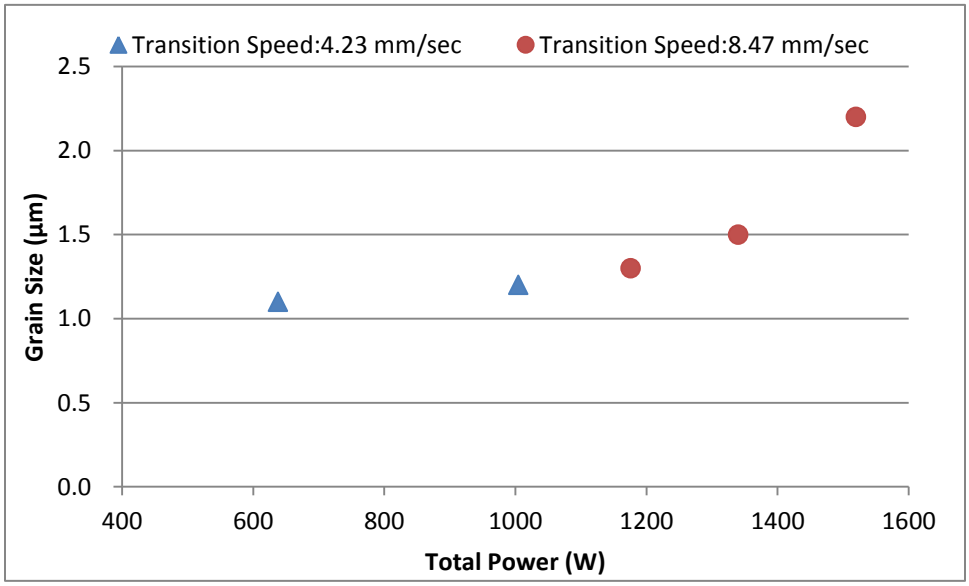

Figure 3.35 Relationship between total power and grain size.

Grain size was measured in the center of welding nugget (It is hard to see the grain clearly with optic microscope, further digital magnification on computer is needed). Grain size increased with increasing total power under two set of welding speeds. And

grain size increased more rapidly when total power and welding speed are high.

3.8.Microhardness

The Vickers hardness of the welding sheets was measured for SSFSW with 9.79 kN and 14.23 kN downward force and CFSW with 6.67 KN downward force. All three sample have little or no defect. Hardness of 7075-T6 base material from material data information is 175HV [10]. The experimental hardness of base material was 167.5 HV as received and 178.7 after T6 heat weld treatment (PWHT). Hardness contour maps and mid-thickness region hardness at cross section are presented in Figure 3.37 to Figure 3.39, and their welding condition was listed in Table 3.28.

Welding No.	Tool Type	Welding length	Pin rotation speed rpm	Welding speed mm/sec	Z-force kN
#3763	Thread+3 flats (RH) (Tool 2 SSFSW)	576.6mm (22.7in)	-1500	8.47	9.79
#3764(pin break)	Thread+3 flats (RH) (Tool 2 SSFSW)	208.3mm (8.2in)	-1500	8.47	9.79
#3796	Thread+3 flats (RH) (Tool 3 SSFSW)	431.8mm (17in)	-1500	8.47	14.23
#3797	Thread+3 flats (RH) (Tool 3 SSFSW)	431.8mm (17in)	-1500	8.47	14.23
#3883	Thread+3 flats (RH) (Tool 4 CFSW)	431.8mm (17in)	-1500	8.47	6.67
#3884	Thread+3 flats (RH) (Tool 4 CFSW)	431.8mm (17in)	-1500	8.47	6.67

Table 3.28 Tool type and welding parameters of welding sample in microhardness test

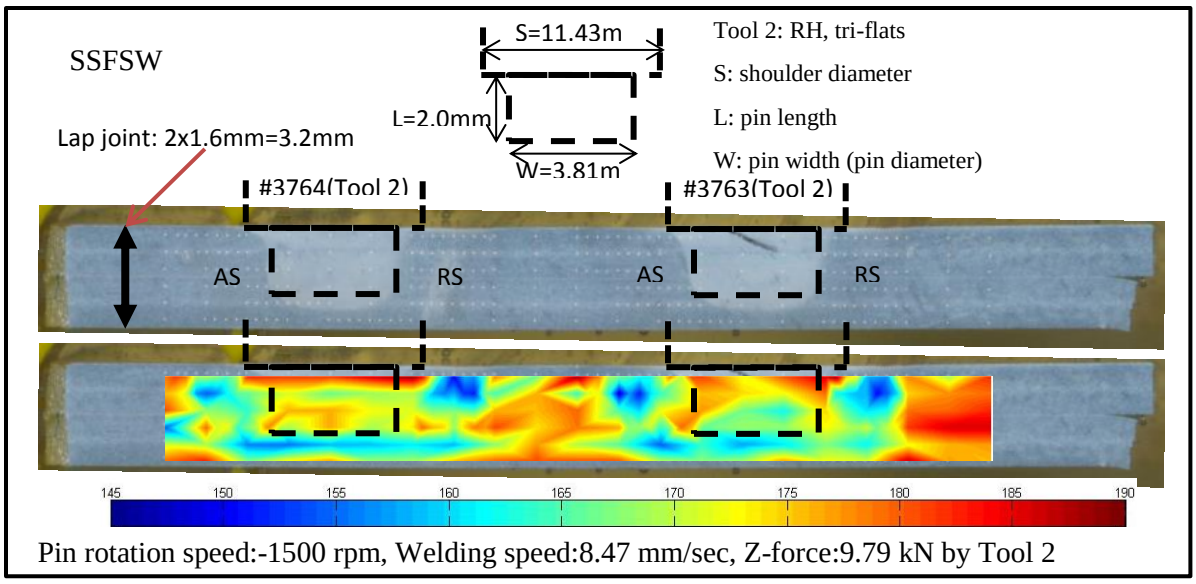

Figure 3.36 #3763-3764 contour map of microhardness distribution with tool welding location

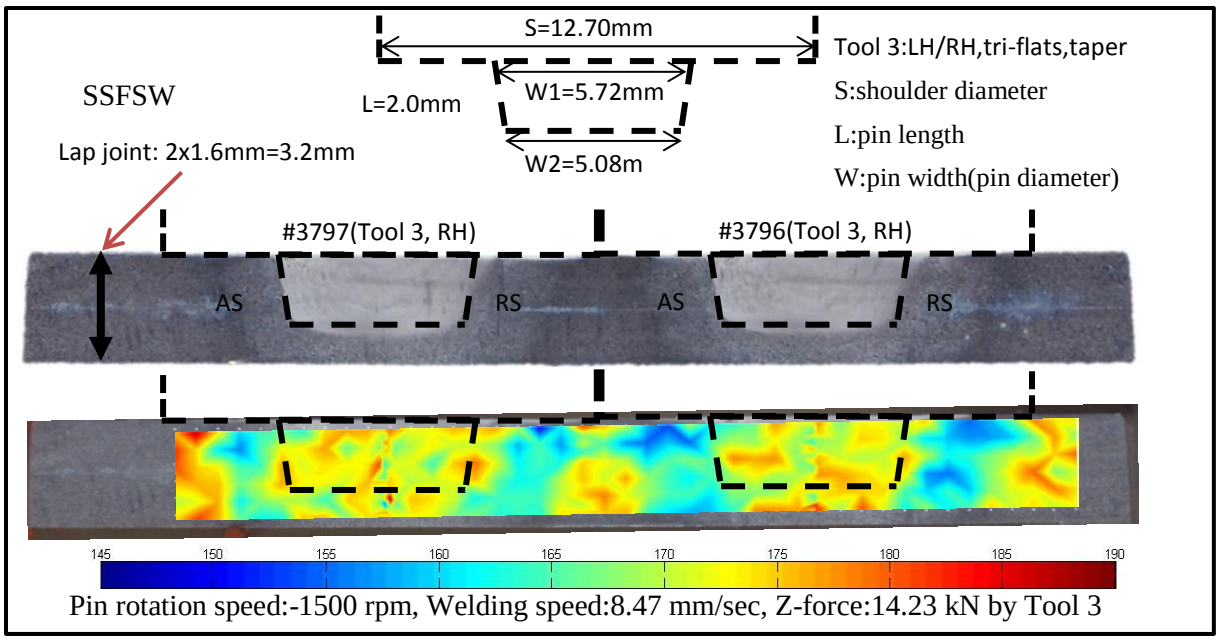

Figure 3.37 #3883-3884 contour map of microhardness distribution with tool welding location

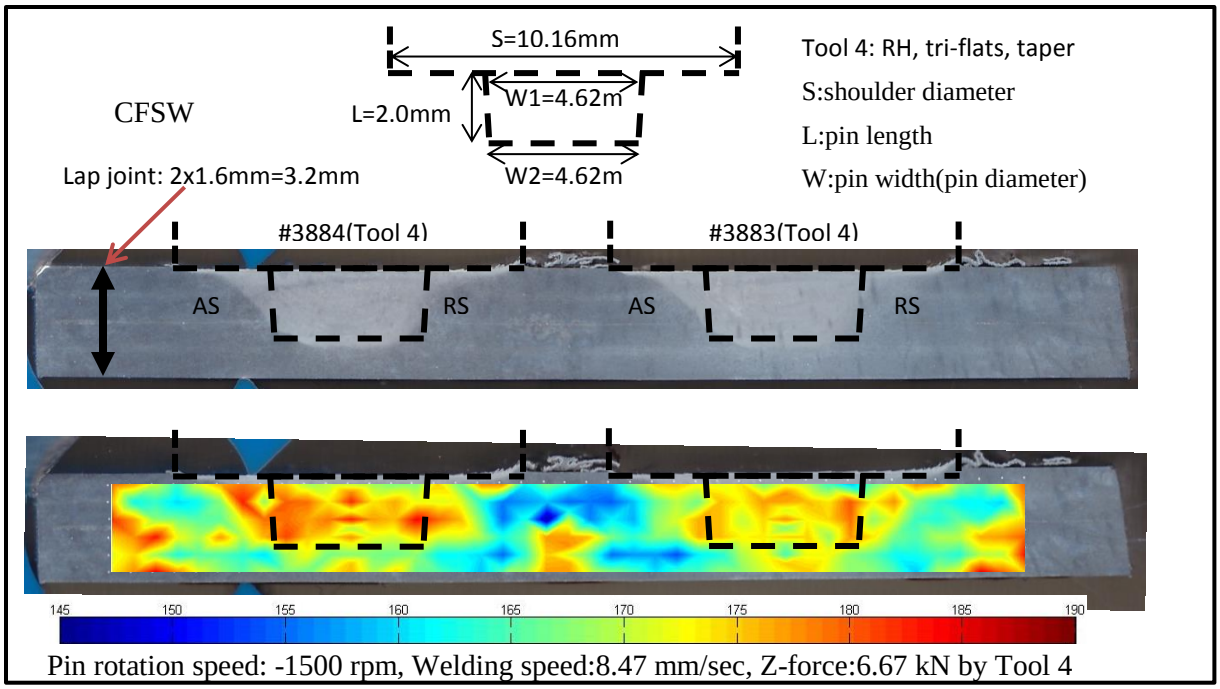

Figure 3.38 #3763-3764 contour map of microhardness distribution with tool welding location

The typical "W" shape was observed for all three samples. The pin location was overlapping at WNZ, where it had high HV. SSFSW showed similar hardness distribution compared to conventional FSW, however, the lowest HV was from CFSW sample. It was indicated that stationary shoulder can helped improve hardness. The lowest hardness was 145 HV (86% base material hardness as received) which was happened at HAZ between two welding pass for CFSW. Highest hardness was 183HV (109% base material hardness as received), which happened in WNZ for CFSW. Hardness at BM also reached above 180HV for both CFSW and SSFSW. The hardness difference between the HAZ and WNZ was associated to the temperature and welding speed [18]. The change of hardness was more homogeneous for SSFSW. This was caused by the uniform heat input of SSFSW.

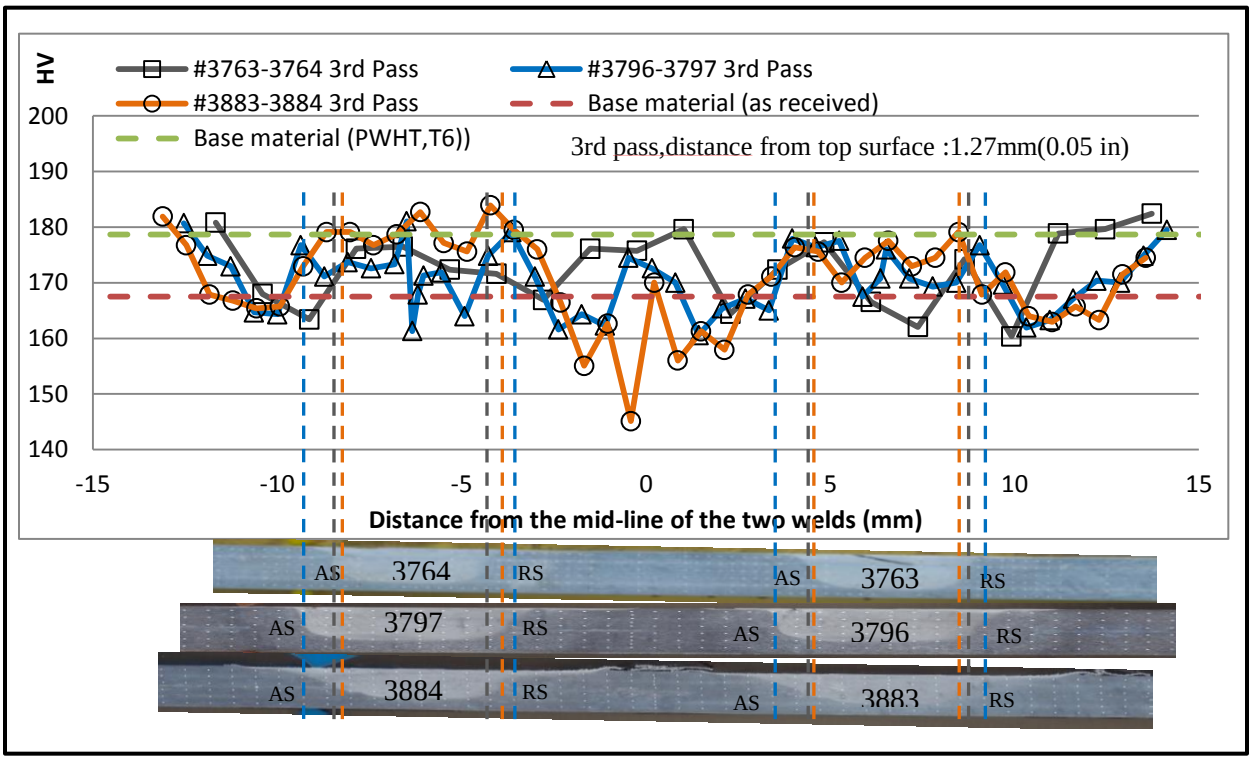

Figure 3.39 Microhardness distribution at cross section.

Near the surface of #3763-3764 (Z-force was 14.23 kN), there was thin layer area where the hardness was relatively high. This area was referred as shoulder-affected zone (SAZ) in some literature. The non-rotational shoulder had higher cool rate near surface that result in finer grain and higher mirohardness [34]. However, for #3796-3797 (Z-force was 9.79 kN), the different of hardness at SAZ from that at WNZ wasn't obvious.

For CFSW (#3883-3884), hardness at WNZ and base material was higher, and hardness at HAZ was lower. It was curious that #3883's lowest hardness happened at advancing side, #3884's lowest hardness happened at retreating side. This may due to the additive thermal effect by rotating shoulder at HAZ between two welding pass.

3.9.Tensile

7xxx alloy is designed to have high strength, so its strength after welding process is very important. Base material's yield stress is 503 MPa, ultimate stress is 572 MPa, and elongation at break is 11% [10]. Literature from conventional FSW suggested high ductility formed in WNZ, and welding speed and rotation speed are the main factors for ductility. The tested welding sheets were chosen with rotation speed at 1500 rpm, for they have relatively fewer defects from observation. The longitudinal tensile test was performed after PWHT to achieve better results. The displacement vs. stress was shown in Figure 3.40.

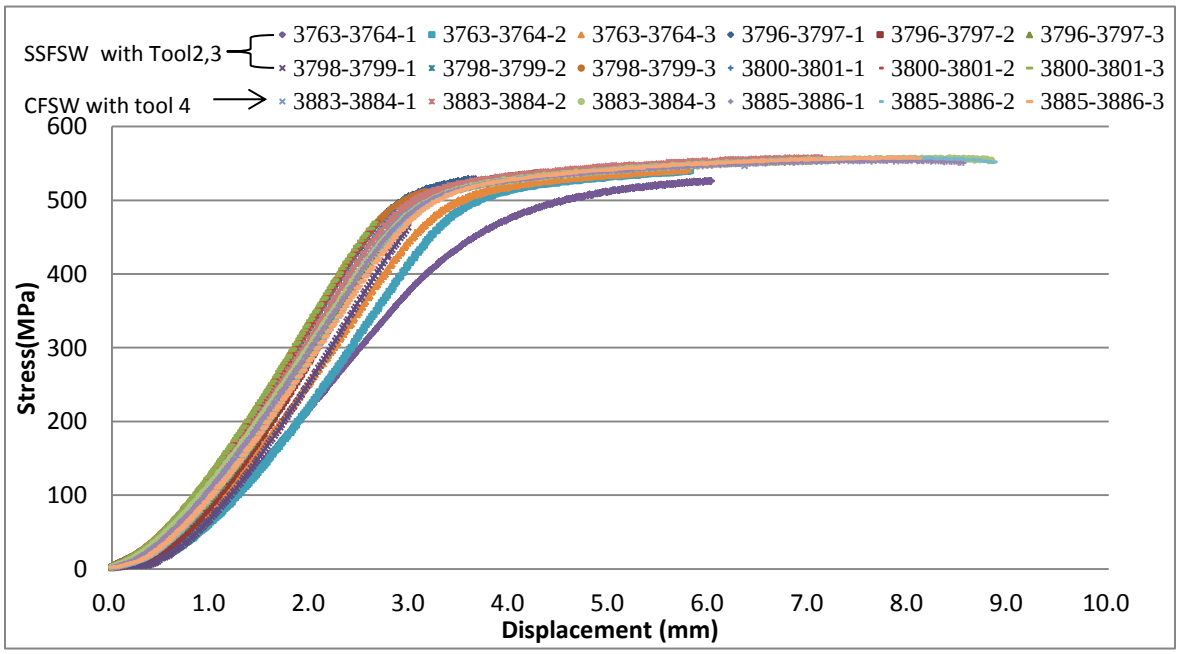

Figure 3.40 Displacement vs. stress curve for every tested welding sample

Similar Stress vs. Displacement trend of sample with few or no defects was observed, which indicated that with proper tool design and welding parameters, SSFSW can deliver

a quite similar strength. Also, it is observed that some samples failed before their plastic deformation. Sample with median UTS value for each weldment was chosen to depict a more clear relationship in Figure 3.41.

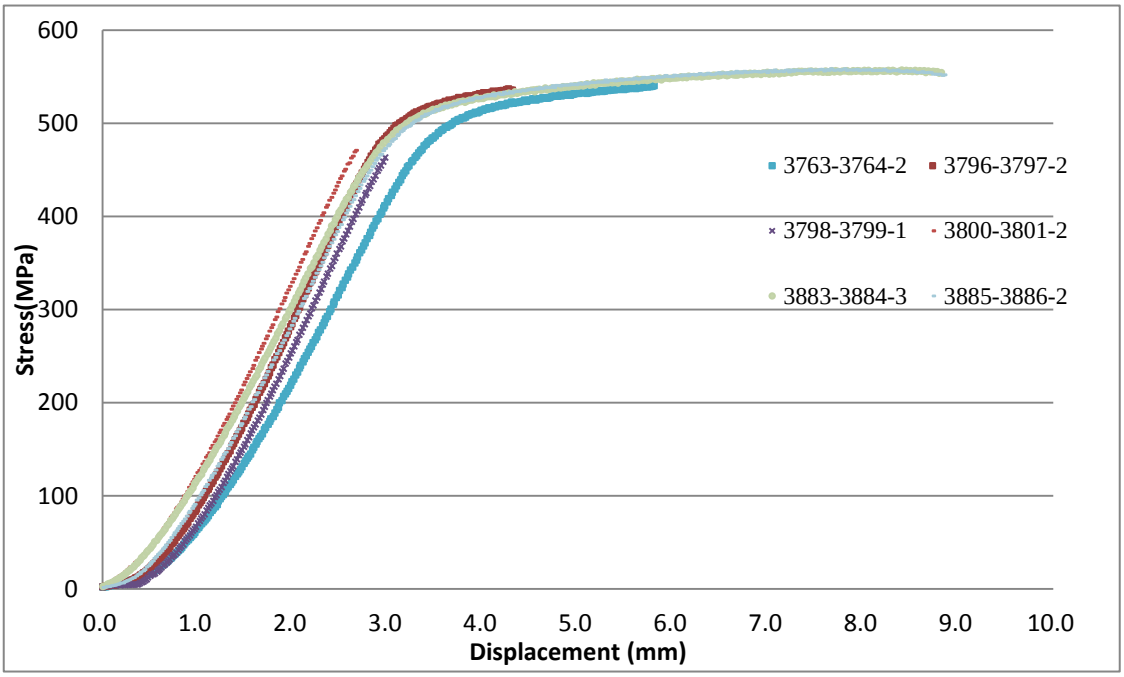

Figure 3.41 Average elongation vs. stress curve of welding samples.

The shape of #3798-3799 and #3800-3801 Stress vs. Displacement curve showed brittle like behavior with no necking, which indicated sudden failure caused by large defects. For #3885-3886, all its samples failed outside the welding area, their yield stress and displacement were the highest and closest to parental material. #3763-3764 and #3796-3797 has high yield stress, but relatively low displacement. Table 3.29 and Figure 3.42 showed the ultimate stress and fraction location of each sample.

Specimen No	Ultmate Load (kN)	Ultmate Stress (MPa)	Fracture Location
SSFSW3763-3764-1	21.36	526.21	outside the welding (in the grab area)
SSFSW3763-3764-2	21.95	540.58	#3764 Adv side bottom sheet
SSFSW3763-3764-3	22.03	542.57	#3764 Adv side bottom sheet
SSFSW3763-3764(Avg)	21.78±0.36	536.45±8.93	Same welding direction, Tool 2(RH)
SSFSW3796-3797-1	21.46	528.63	#3797 Adv side bottom sheet
SSFSW3796-3797-2	21.81	537.13	#3797 Adv side bottom sheet
SSFSW3796-3797-3	22.18	546.35	#3797 Adv side bottom sheet
SSFSW3796-3797(Avg)	21.82±0.36	537.37±8.86	Same welding direction, Tool 3(RH)
SSFSW3798-3799-1	18.8	463.15	#3799 Adv side both sheets
SSFSW3798-3799-2	17.22	424.11	#3799 Adv side both sheets
SSFSW3798-3799-3	20.77	511.61	#3799 Adv side both sheets
SSFSW3798-3799(Avg)	18.93±1.78	466.29±43.83	Same welding direction, Tool 3(RH/LH)
SSFSW3800-3801-1	19.63	483.53	#3800 Adv side both sheets
SSFSW3800-3801-2	19.12	470.84	#3800 Adv side both sheets
SSFSW3800-3801-3	19.1	470.29	#3801 Adv side both sheets
SSFSW3800-3801(Avg)	19.28±0.30	474.89±7.49	Opposite welding direction, Tool 3(RH)
CFSW3883-3884-1	22.41	551.97	#3884 Adv side bottom sheet
CFSW3883-3884-2	22.65	557.84	#3884 Adv side bottom sheet
CFSW3883-3884-3	22.62	557.21	#3883 Ret side bottom sheet
CFSW3883-3884(Avg)	22.56±0.13	555.67±3.22	Same welding direction,Tool 4(RH)
CFSW3885-3886-1	22.52	554.78	outside the welding
CFSW3885-3886-2	22.67	558.28	outside the welding
CFSW3885-3886-3	22.68	558.64	outside the welding
CFSW3885-3886(Avg)	22.62±0.086	557.23±2.13	Opposite welding direction,Tool 4(RH)

Table 3.29 Ultimate stress, ultimate load and fracture location.

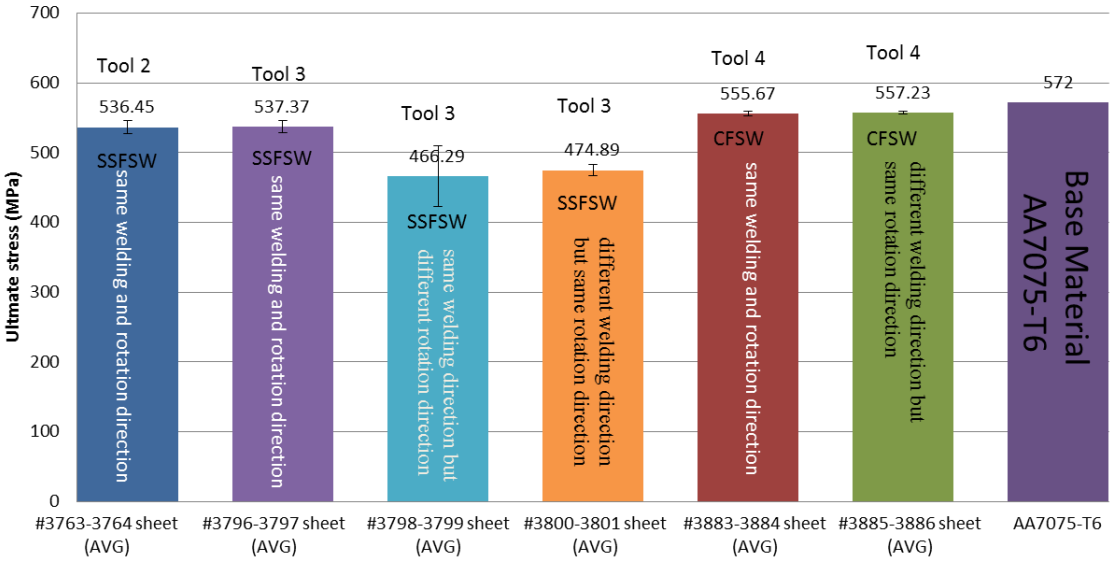

SSFSW:

#3763-3764: Both welds with same welding and rotation direction by Tool 2(RH)

#3796-3797: Both welds with same welding and rotation direction by Tool 3(RH)

#3798-3799: Both welds with same welding direction but different rotation direction by Tool 3(LH/RH)

#3800-3801:Both welds with different welding direction but same rotation direction by Tool 3 (LH)

CFSW:

#3883-3884: Both welds with same welding and rotation direction by Tool 4(RH)

#3885-3886:Both welds with different welding direction but same rotation direction by Tool 4(RH)

Base Material:AA7075-T6

Figure 3.42 Bar chart of average ultimate stress.

It was found that for double pass SSFSW: 1) for the same welding direction, same pin rotation direction result in better strength (#3796-3797 vs. #3798-3799 vs. #3800-3801), The reason was that the #3798-3799(same welding direction but different rotation direction) and #3800-3801(different welding direction but same rotation direction) had big defects. 2) Under the similar welding arrangement, if there was no defect in the SSFSW sample, it would most likely to have similar strength as CFSW.

From Table 3.29 and appendix F, when two welds (in one sheet) Adv sides were both in the middle of the welding pass(#3798-3799 and #3800-3801), the tensile sample would most likely fail between the two nugget at HAZ zone. When the Advancing side and Ret side were both in the middle of the two welding passes in one sheet, the tensile sample would most likely failed at Advancing side(located outside the both welds). The reason for this could be the overlapping of advancing side and retreating side helped to even the difference of material displacement at each side. Besides, welding sheet interface curved gently on the retreating side, but curve abruptly on the advancing side [22]. Both #3798-3799 and #3800-3801 failed between the welding pass, which verified the strength be affected by material flow during welding process. Another possible reason was that the cavity defects happened at the Advancing side (See Figure 3.43 and Appendix F) Ultimate stress of AA7075-T6 parent material is 572 MPa. Overall, double-pass SSFSW was able to achieve high material strength (81% - 93%). For conventional FSW, UTS almost regains the parent material UTS (97%).

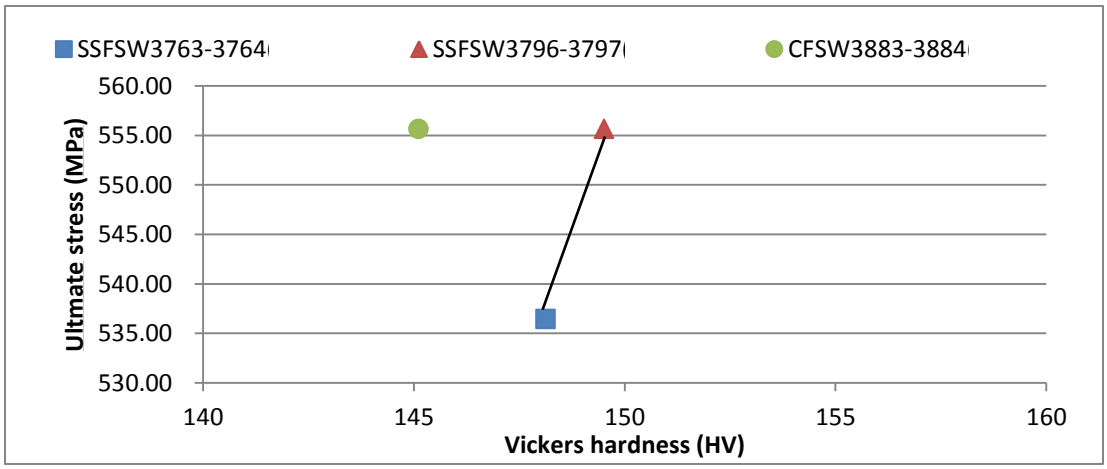

Figure 3.43 The relationship between minimum mirohardness and average ultimate stress.

The figure above was the minimum mirohardness on tested sheets. Ultimate stress usually positively associates with mirohardness. It was observed that UTS increase with increasing minimum hardness.

3.10. Fracture Characteristics

The photo of fracture pictures for all tensile test samples were shown in Appendix C. Most of the samples failed near HAZ zone at the advancing side, some at retreating side. Two samples failed between two parallel welding pass, and two failed at base material area. The failure tended to happen at the defect area.

The fracture characteristic of SSFSW with -1500 rpm, 8.47 mm/sec ,9.79 kN by tool 2 was investigated. Scanned photo after tensile test were shown in Figure 3.44. It was observed that failure happened at the bottom-left of WNZ at advancing size. Fracture micrographic photos for #3764 and #3763 were shown in Figure 3.45and Figure 3.46

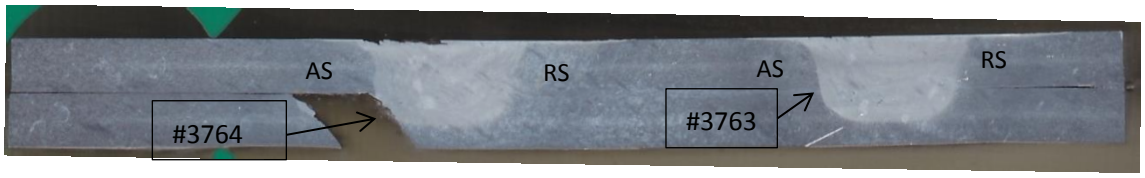

Figure 3.44 #3763-3764 facture cross section scanned picture

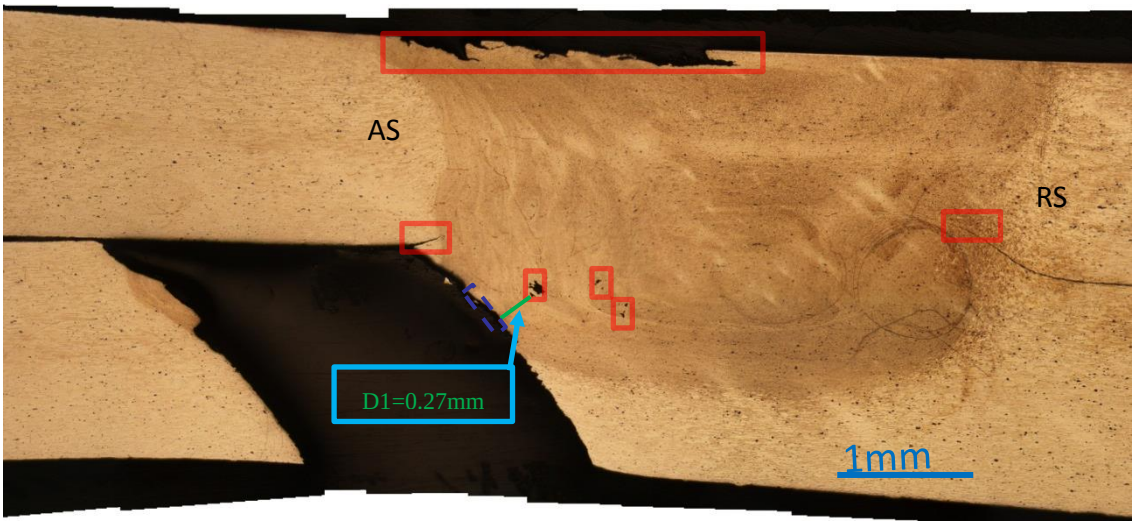

Figure 3.45 Metallographic #3764 facture after tensile test

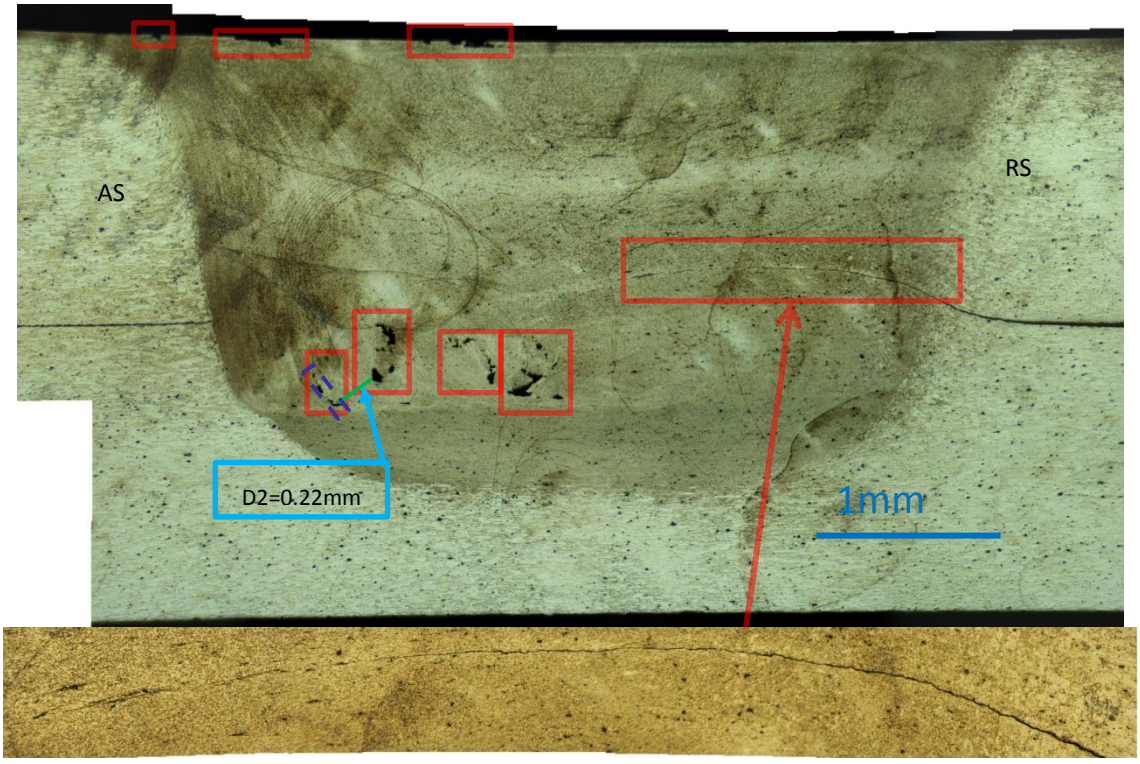

Figure 3.46 #3763 on the fractured sample after tensile test

Comparing feature in #3763 and #3764, it can be inferred that their defect happened in similar area. The wormhole defects were enlarged after tensile test. So

interface wormhole defect at fracture could be the main reason for the failure. The interface defect was marked in red frame in #3763 and the wormhole defect can be seen in SEM fracture section below.

3.11. Fracture SEM

Scanning electron microscopy (SEM) was performed on #3763-3764 welding sheet to study AA7075 SSFSW fractography. Figure 3.47 showed the location of fracture, which was at advancing side of #3764. Figure 3.48-Figure 3.53 are the SEM fracture photos of #3764 sample from 1200x to 10000x. Figure 3.44 showed the SEM photo for base material in #3763-3764.

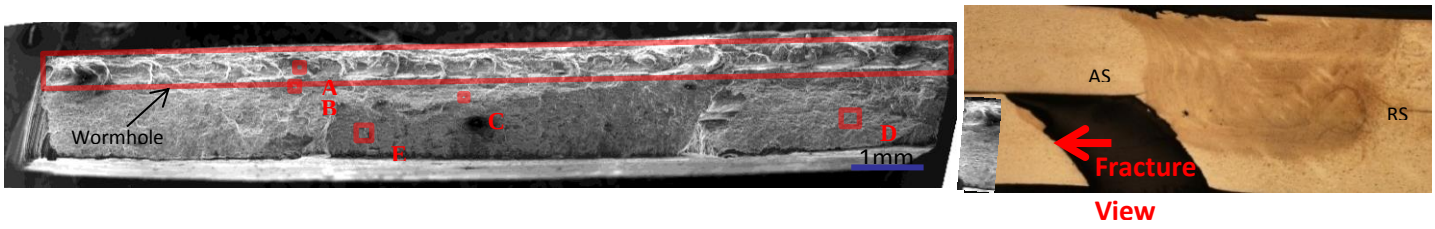

Figure 3.47 Panoramagram of fracture surface #3764

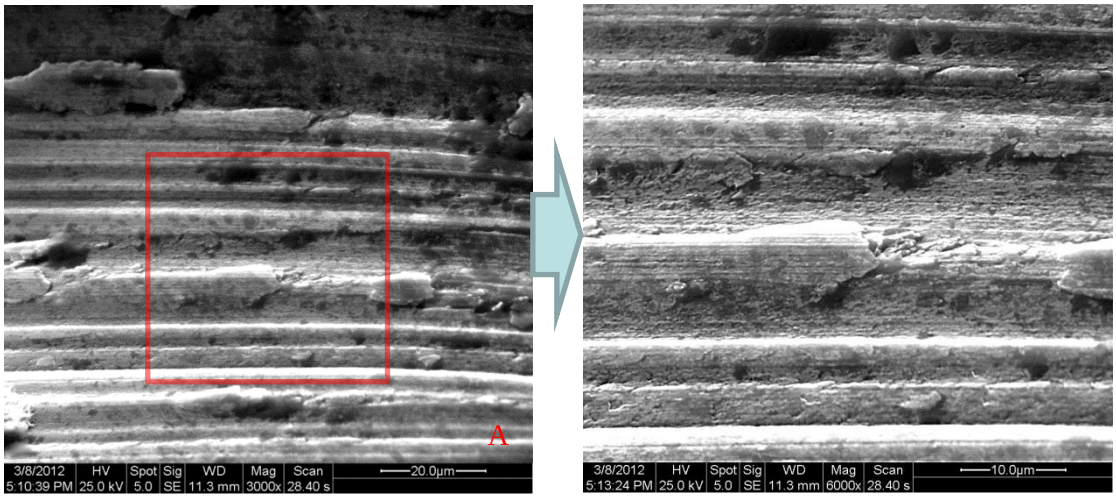

Figure 3.48 #3764 fracture surface structure at wormhole area in WNZ

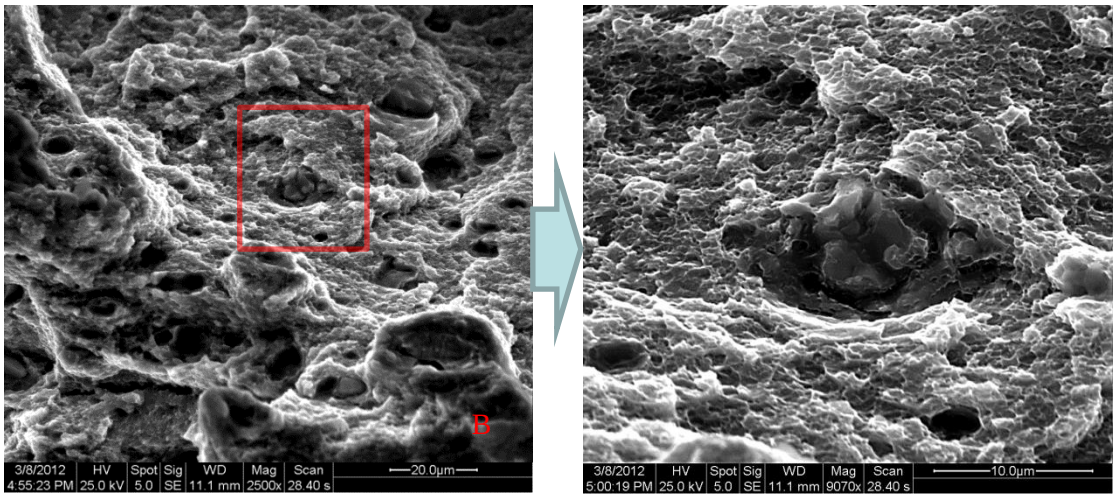

Figure 3.49 #3764 fracture surface structure just below the worm hole defects in WNZ

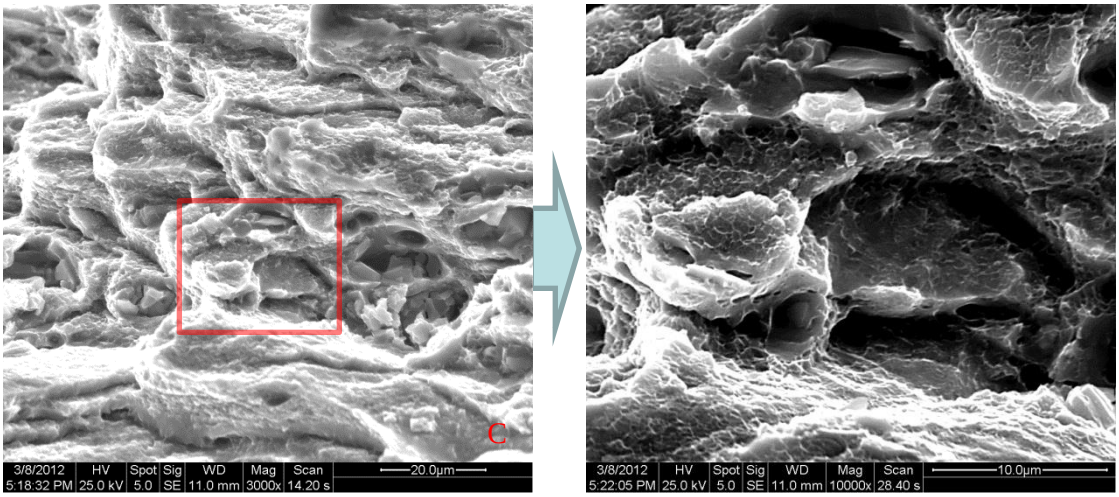

Figure 3.50 #3764 fracture surface structure in TMAZ or HAZ zone

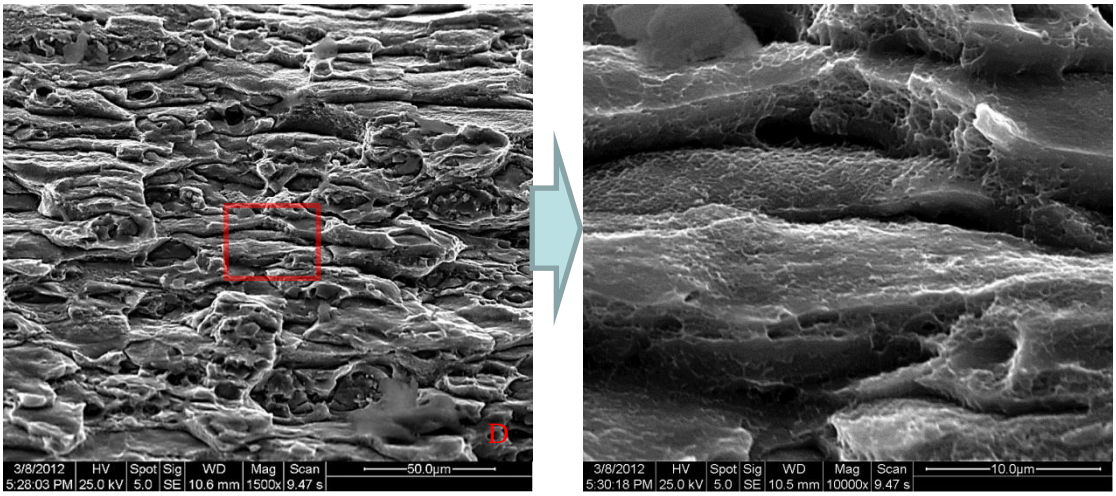

Figure 3.51 #3764 fracture surface structure away from the wormhole

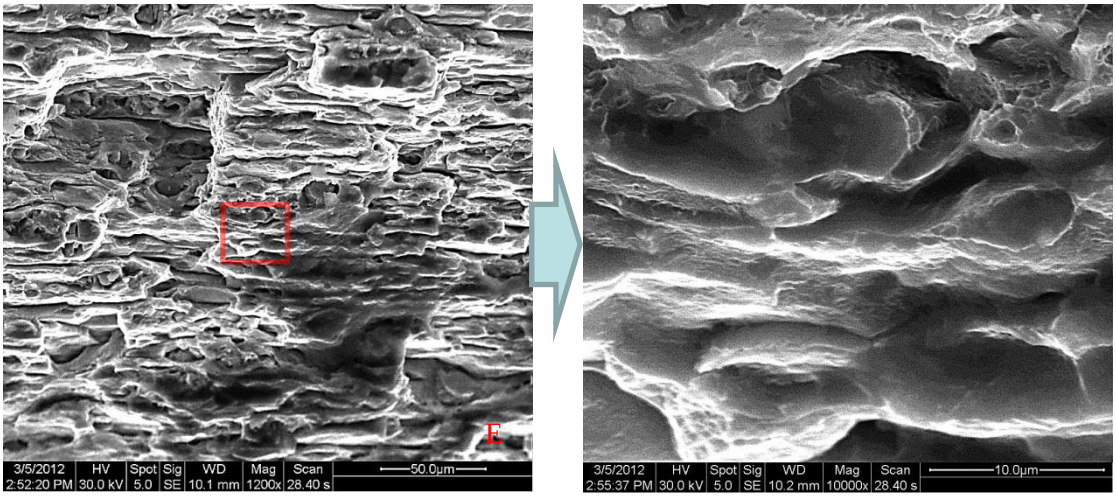

Figure 3.52 #3764 fracture surface structure further away from the worm hole, near the edge

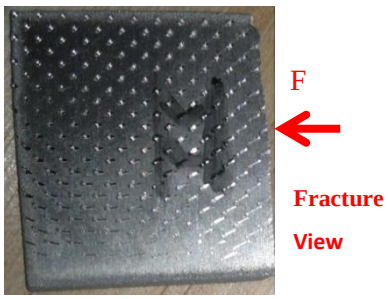

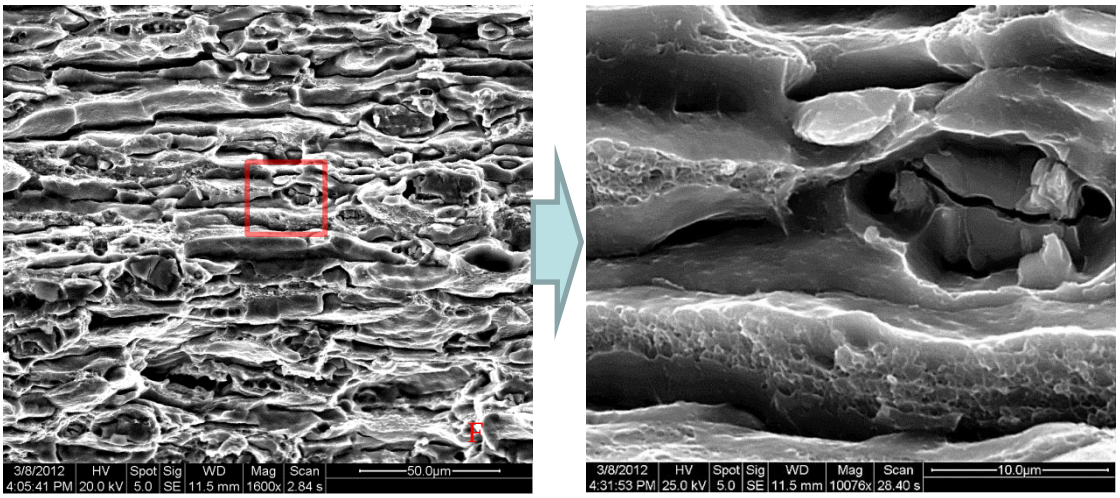

Figure 3.53 #3764 fracture surface structure of base material

The fracture surfaces at wormhole area (A) displayed distinguishing parallel strip shape from shear force by FSW process. This wormhole caused material surface rather smooth

and less cohesive to surrounding material, hence they were more easy to break under tensile test. Literature explained that wormhole defects tended to form close to the pin at advancing side for there was a stagnant or reversal flow zone at the advancing side close to the pin during FSW process [7]. The surface at WNZ (B) was observed to have microvoid. This was most likely the start of the crack. Besides, the microvoid in nugget zone reduced the strength of the material and produce unstable shear fracture. See Picture (C), some area at TMAZ transition zone displayed cup and-cone like structure, which suggested ductile fracture during tensile failure. Other area at TMAZ displayed shear dimples that were formed under shear stress after the initial crack. From HAZ to Base material, shear dimples were observed more obviously. (See D, E, F) The materials at different location (D, E) of HAZ exhibited very similar morphology. Base material (F) had some large dimples as well as shear dimples, which showed it has more ductile feature than material TMAZ and HAZ.

3.12. Summary

Process Responses

- Torque mainly decreased with increasing pin rotation speed. Welding speed, tool tri-flats feature and shoulder type had little effect on torque.

- X-force showed strong positive correlation with Z-force for a stationary shoulder. Most part of X-force in SSFSW was caused by the shoulder friction. Rotation speed, welding speed and tool tri-flats feature have little effect on X-force.
- Because of a non-rotation shoulder, SSFSW may apply wider downward force range than CFSW and still obtain good joint.
- SSFSW had slight less torque than CFSW, while SSFSW exerted more than twice X-force as Conventional FSW.
- Rotation power contributes most of the total power. SSFSW travel power percentage was larger than CFSW travel power percentage.
- Total power increased with pin rotation speed at low and medium rotation speed, but decreased with rotation speed at relatively high rotation speed for the present experiments.
- Travel power increased with increasing Z-force at given rotation and travel speed.

Distortion

- Saddle shape was observed for distortion distribution in SSFSW.
- Welding direction and tool rotation direction arrangements affected distortion.
- PWHT helped to reduce distortion significantly.

Welding surface

- SSFSW was able to produce fine welding surface with little or no flash. Its surface quality depends on welding control parameter.

- The best SSFSW welding surface quality was achieved at -1000 rpm ,4.23 mm/s, 9.79 kN and -1500 rpm,6.35 mm/s,9.79 kN, for the present experiments

Metallography

- For AA7075 in SSFSW, WNZ displayed fine and equiaxed grain.
- The boundary slope of CFSW WNZ was gentler than SSFSW's, which was affected by rotation shoulder.
- Most cavity defects happened at Advancing side.

Grain Size

- Grain size increased with increasing total power.

Microhardness

- The typical "W" shape was observed for SSFSW hardness distribution.
- SSFSW showed similar hardness distribution compared to conventional FSW, however, the lowest Vickers Hardness was observed from CFSW sample.

Tensile Properties

- SSFSW can deliver a quite similar Ultimate stress as CFSW.
- The parallel welding pass with same rotation and welding direction resulted in higher tensile strength, due to lack of defects, for the present study.
- When two Adv side HAZ of the welds are overlay, there was a bigger chance that the tensile bar will fail at the overlay area.

Facture Characteristics

- Material failed at the largest cavity near the edge of WNZ at advancing side.
- BM (Base material) showed more ductile feature than other parts of the weld.

CHAPTER 4 CONCLUSION & RECOMMENDATION

This thesis extensively investigated the properties of Stationary Shoulder Friction Stir Welding process on AA7075-T6 parallel lap joint. Experimental results showed torque mainly decreased with increasing rotation speed. X-force mainly increases with increasing Z-force, where coulomb friction should be the operative mechanism. PWHT (T6) helped to reduce distortion obviously. Distortion test showed that SSFSW had similar distortion compared to conventional FSW. Metallographic Cross section observation showed SSFSW can produce fine and equiaxed grain. Grain size increased with increasing total power. Microhardness test demonstrated sample in SSFSW process has similar microhardness distribution as CFSW. SSFSW sample with fewer defects had relative high tensile strength, maximum ultimate stress (UTS) of 537.37 MPa. Fracture study showed that cavity happened near the edge of WNZ at advancing side of material.

Further studies need to be conducted to find better welding condition or heat treatment in order to get defects free welds with smaller distortion.

1) Test more control parameter combinations to find out the defects free SSFSW welds.
2) Change or revise the tool design to reduce or eliminate the defects.

3) Try other PWHT method to help reduce distortion further.

4) Conduct more SSFSW experiments with temperature measurement to investigate the unclear reason of general trend of relationship between the control parameters and respond parameters.

REFERENCES

[1] Thomas W. M., Nicholas E. D., Needham J. C., Murch M. G., Templesmith P., and Dawes C. J., 1991, GB Patent application no. 9125978.8, December.

[2] Rhodes C. G., Mahoney M. W., Bingel W. H., Spurling R. A., and Bampton C. C., 1997, "Effects of friction stir welding on microstructure of 7075 aluminum," Scripta Materialia, **36**(1), pp. 69–75.

[3] Bussu G., and Irving P. E., 2003, "The role of residual stress and heat affected zone properties on fatigue crack propagation in friction stir welded 2024-T351 aluminium joints," International Journal of Fatigue, **25**(1), pp. 77–88.

[4] Jata K. V., Sankaran K. K., and Ruschau J. J., 2000, "Friction-stir welding effects on microstructure and fatigue of aluminum alloy 7050-T7451," Metallurgical and Materials Transactions A, **31**(9), pp. 2181–2192.

[5] Mishra R. S., and Mahoney M. W., 2007, Friction Stir Welding and Processing, ASM International.

[6] Indira Rani M., Marpu R. N., and ACS K., 2006, "A study of process parameters of friction stir welded AA 6061 aluminum alloy in O and T6 conditions," Journal of Engineering and Applied Sciences, **6**.

[7] Nandan R., DebRoy T., and Bhadeshia H. K. D. H., 2008, "Recent advances in friction-stir welding – Process, weldment structure and properties," Progress in Materials Science, **53**(6), pp. 980–1023.

[8] Davies P. S., Wynne B. P., Rainforth W. M., Thomas M. J., and Threadgill P. L., 2011, "Development of Microstructure and Crystallographic Texture during Stationary Shoulder Friction Stir Welding of Ti-6Al-4V," Metall and Mat Trans A, **42**(8), pp. 2278–2289.

[9] "Info, Aluminum" [Online]. Available: http://www.metalreference.com/INFO_Aluminum.html. [Accessed: 27-Jan-2013].

[10] “ASM Material Data Sheet” [Online]. Available: http://asm.matweb.com/search/SpecificMaterial.asp?bassnum=MA7075T6. [Accessed: 18-Jan-2013].

[11] “Heat Treatment of Aluminum Alloys” [Online]. Available: http://www.mlevel3.com/BCIT/heat%20treat.htm. [Accessed: 18-Mar-2013].

[12] De Backer J., Christiansson A.-K., Oqueka J. M., and Bolmsjö G., 2012, “Investigation of path compensation methods for robotic friction stir welding,” Industrial Robot: An International Journal, **39**(6), pp. 7–7.

[13] Fujii H., Cui L., Maeda M., and Nogi K., 2006, “Effect of tool shape on mechanical properties and microstructure of friction stir welded aluminum alloys,” Materials Science and Engineering: A, **419**(1–2), pp. 25–31.

[14] Arora A., Nandan R., Reynolds A. P., and DebRoy T., 2009, “Torque, power requirement and stir zone geometry in friction stir welding through modeling and experiments,” Scripta Materialia, **60**(1), pp. 13–16.

[15] Long T., Tang W., and Reynolds A. P., 2007, “Process response parameter relationships in aluminium alloy friction stir welds,” Science & Technology of Welding & Joining, **12**(4), pp. 311–317.

[16] Mahoney M. W., Rhodes C. G., Flintoff J. G., Bingel W. H., and Spurling R. A., 1998, “Properties of friction-stir-welded 7075 T651 aluminum,” Metall and Mat Trans A, **29**(7), pp. 1955–1964.

[17] Hansen V., Karlsen O. B., Langsrud Y., and Gjønnes J., 2004, “Precipitates, zones and transitions during aging of Al-Zn-Mg-Zr 7000 series alloy,” Materials science and technology, **20**(2), pp. 185–193.

[18] Reynolds A. P., Tang W., Khandkar Z., Khan J. A., and Lindner K., 2005, “Relationships between weld parameters, hardness distribution and temperature history in alloy 7050 friction stir welds,” Science & Technology of Welding & Joining, **10**(2), pp. 190–199.

[19] Su J.-Q., Nelson T. W., and Sterling C. J., 2005, “Microstructure evolution during FSW/FSP of high strength aluminum alloys,” Materials Science and Engineering: A, **405**(1), pp. 277–286.

[20] Guerra M., Schmidt C., McClure J. ., Murr L. ., and Nunes A. ., 2002, “Flow patterns during friction stir welding,” Materials Characterization, **49**(2), pp. 95–101.

[21] Colligan, 1999, “Material flow behavior during friction stir welding of aluminum,” Welding Journal, **78**, p. 229.

[22] L. CEDERQVIST, and A. P. REYNOLDS, 2001, “Factors Affecting the Properties of Friction Stir Welded Aluminum Lap Joints,” **80 (12)**.

[23] Xunhong W., and Kuaishe W., 2006, “Microstructure and properties of friction stir butt-welded AZ31 magnesium alloy,” Materials Science and Engineering: A, **431**(1–2), pp. 114–117.

[24] J. -Q Su T. W. N., “Microstructural investigation of friction stir welded 7050-T651 aluminium,” Acta Materialia, (3), pp. 713–729.

[25] Shi Q.-Y., Silvanus J., Liu Y., Yan D.-Y., and Li H.-K., 2008, “Experimental study on distortion of Al-6013 plate after friction stir welding,” Science and Technology of Welding and Joining, **13**(5), pp. 472–478.

[26] Li T., Shi Q. Y., and Li H.-K., 2007, “Residual stresses simulation for friction stir welded joint,” Science and Technology of Welding & Joining, **12**(8), pp. 664–670.

[27] Schmidt H., Hattel J., and Wert J., 2003, “An analytical model for the heat generation in friction stir welding,” Modelling and Simulation in Materials Science and Engineering, **12**(1), p. 143.

[28] Richards D. G., Prangnell P. B., Withers P. J., Williams S. W., Nagy T., and Morgan S., 2010, “Efficacy of active cooling for controlling residual stresses in friction stir welds,” Science and Technology of Welding & Joining, **15**(2), pp. 156–165.

[29] Nelson T. W., Steel R. J., and Arbegast W. J., 2003, “In situ thermal studies and post-weld mechanical properties of friction stir welds in age hardenable aluminium alloys,” Science and Technology of Welding & Joining, **8**(4), pp. 283–288.

[30] Threadgill, 1997, Friction stir welds in aluminium alloys - preliminary microstructural assessment.

[31] Hassan K., Prangnell P. B., Norman A. F., Price D. A., and Williams S. W., 2003, "Effect of welding parameters on nugget zone microstructure and properties in high strength aluminium alloy friction stir welds," Science and Technology of Welding & Joining, **8**(4), pp. 257–268.

[32] Denquin A., Allehaux D., Campagnac M.-H., Lapasset G., and Office National d'Etudes et de Recherches Aerospatiales (ONERA) 92-Chatillon (France);, 2002, "Microstructural evolution and strength mismatch within a friction stir welded 6056 aluminium alloy," OFFICE NATIONAL D ETUDES ET DE RECHERCHES AEROSPATIALES ONERA-PUBLICATIONS-TP, (20).

[33] Ahmed M. M. Z., Wynne B. P., Rainforth W. M., and Threadgill P. L., 2011, "Through-thickness crystallographic texture of stationary shoulder friction stir welded aluminium," Scripta Materialia, **64**(1), pp. 45–48.

[34] Liu H. J., Li J. Q., and Duan W. J., "Friction stir welding characteristics of 2219-T6 aluminum alloy assisted by external non-rotational shoulder," Int J Adv Manuf Technol, pp. 1–10.

[35] Li J. Q., and Liu H. J., 2013, "Effects of tool rotation speed on microstructures and mechanical properties of AA2219-T6 welded by the external non-rotational shoulder assisted friction stir welding," Materials & Design, **43**, pp. 299–306.

[36] Martin J. P., Stanhope C., and Gascoyne S., 2011, "Novel techniques for cor-ner joints using friction stir welding," Friction Stir Welding and Processing VI. Hoboken, NJ, USA, pp. 179–186.

[37] Richter-Trummer V., Suzano E., Beltrão M., Roos A., Dos Santos J. F., and De Castro P. M. S. T., 2012, "Influence of the FSW clamping force on the final distortion and residual stress field," Materials Science and Engineering: A, **538**, pp. 81–88.

[38] Annual Book of ASTM Standards, American Society for Testing and Materials, Pennsylvania.

[39] Reynolds A. P., 2008, "Flow visualization and simulation in FSW," Scripta Materialia, **58**(5), pp. 338–342.

[40] Steuwer A., Hattingh D. G., James M. N., Singh U., and Buslaps T., 2012, "Residual stresses, microstructure and tensile properties in Ti‐6Al‐4V friction stir welds," Science and Technology of Welding & Joining, **17**(7), pp. 525–533.

[41] Venkateswaran P., and Reynolds A. P., 2012, “Factors affecting the properties of Friction Stir Welds between aluminum and magnesium alloys,” Materials Science and Engineering: A.

[42] Krishnan K. N., 2002, “On the formation of onion rings in friction stir welds,” Materials Science and Engineering: A, **327**(2), pp. 246–251.

[43] Hwang R. Y., and Chou C. P., 1997, “The study on microstructural and mechanical properties of weld heat affected zone of 7075-T651 aluminum alloy,” Scripta Materialia, **38(**2), pp. 215–221.

Appendix A Cross Section Scan Photos

The corresponding parameters please see the Table 3.1

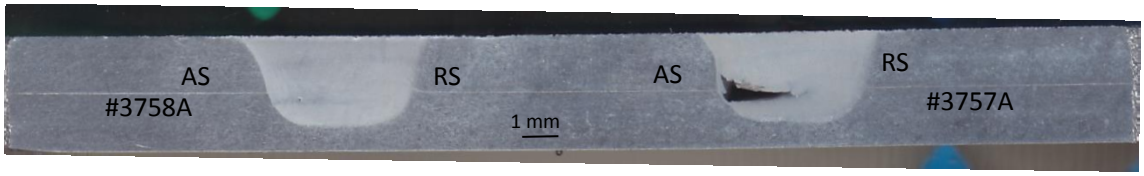

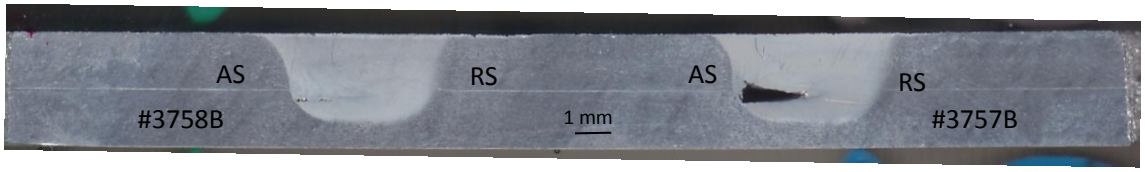

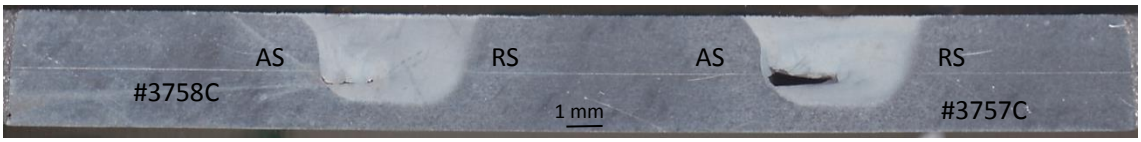

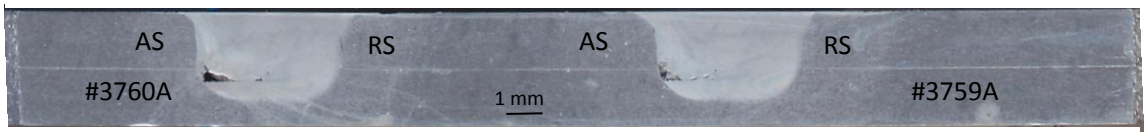

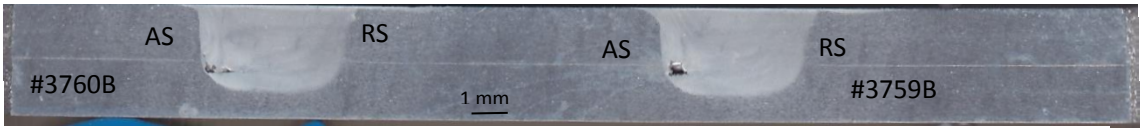

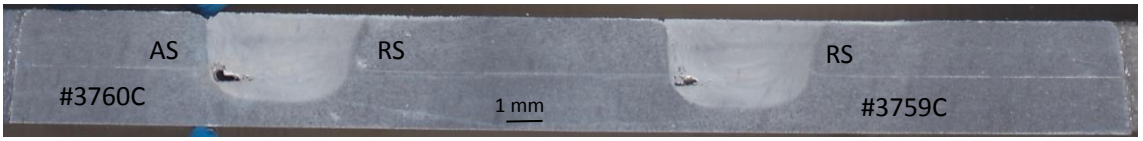

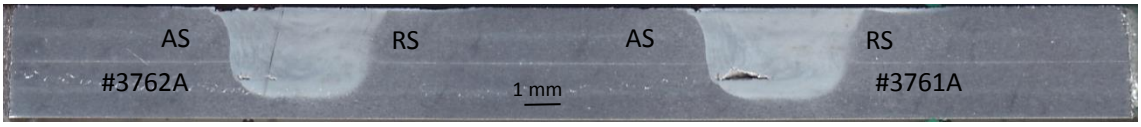
AS
RS
AS
RS
#3762A
1 mm
#3761A

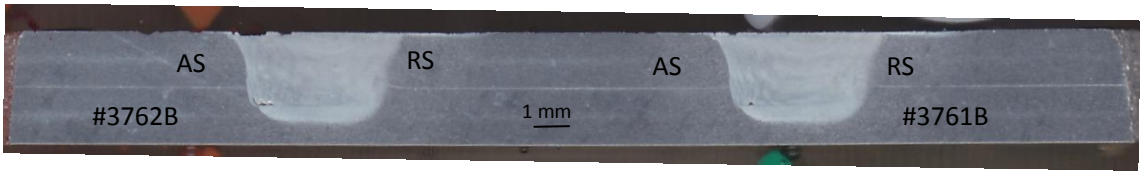
AS
RS
AS
RS
#3762B
1 mm
#3761B

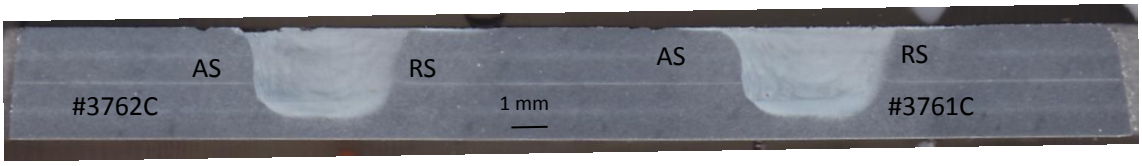
AS
RS
AS
RS
#3762C
1 mm
#3761C

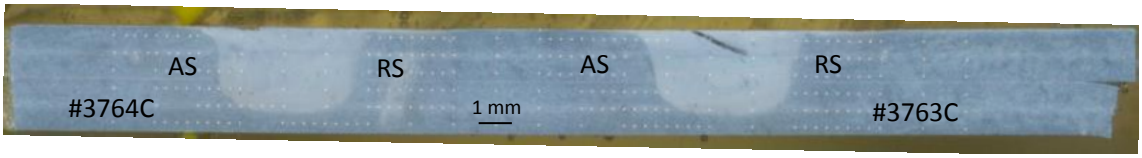
AS
RS
AS
RS
#3764C
1 mm
#3763C

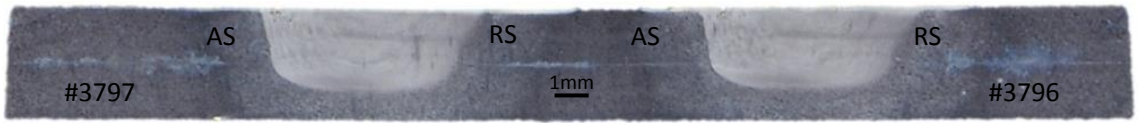
AS
RS
AS
RS
#3797
1mm
#3796

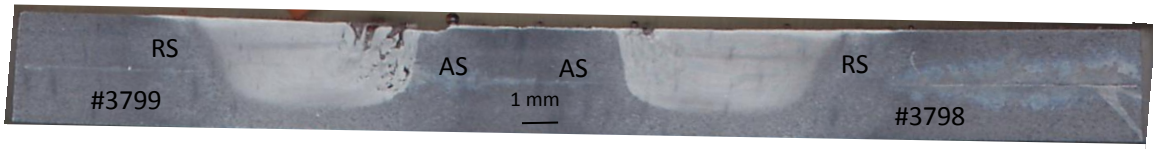
RS
AS
AS
RS
#3799
1 mm
#3798

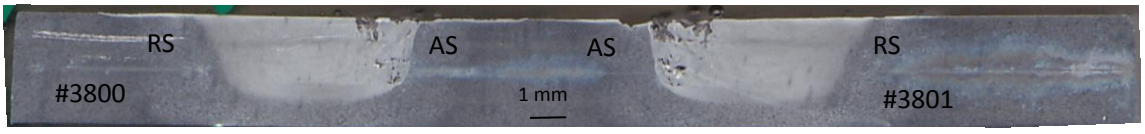
RS
AS
AS
RS
#3800
1 mm
#3801

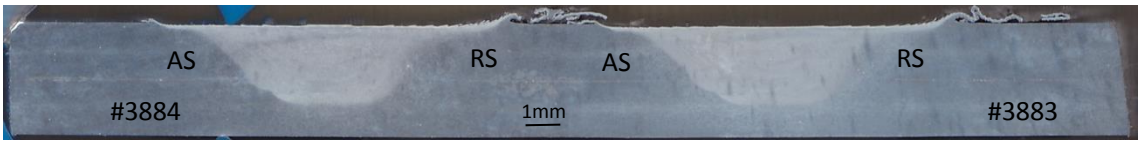
AS
RS
AS
RS
#3884
1mm
#3883

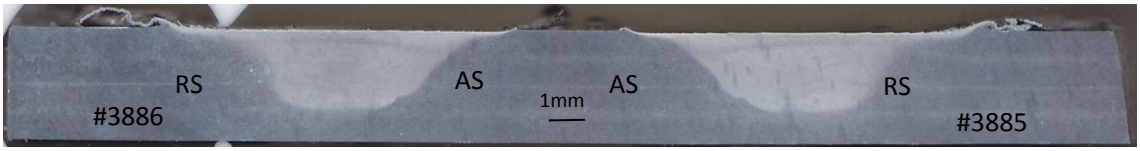
RS
AS
AS
RS
#3886
1mm
#3885

Appendix B Cross Section Observation (not displayed in the context)

The corresponding parameters please see the Table 3.1

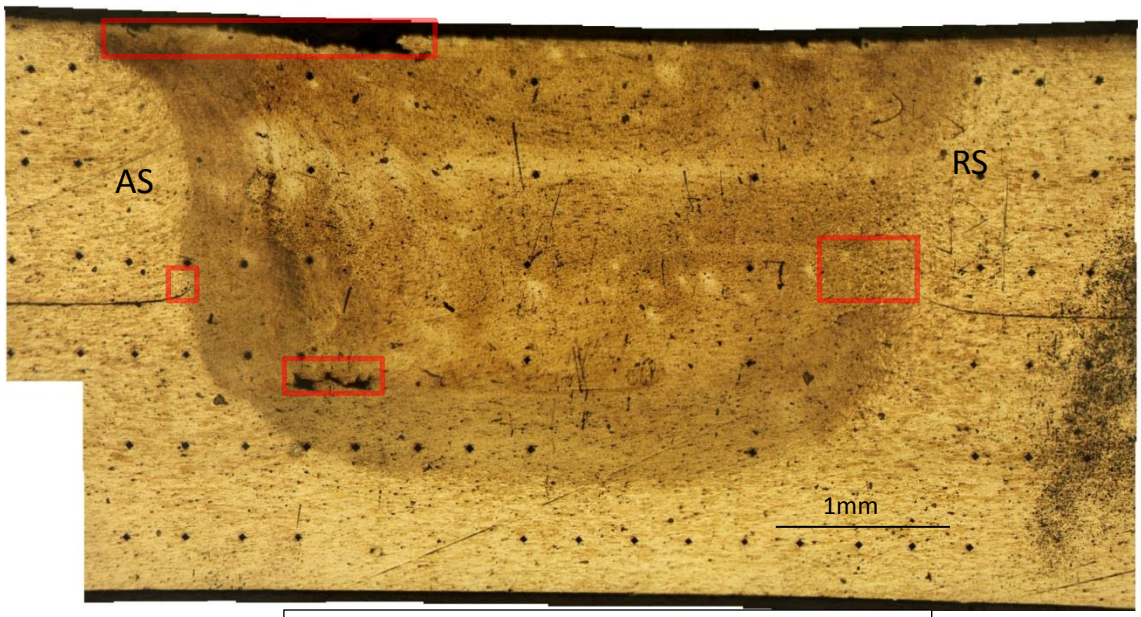

#3764 Nugget area (after hardness test) by tool 2(RH)

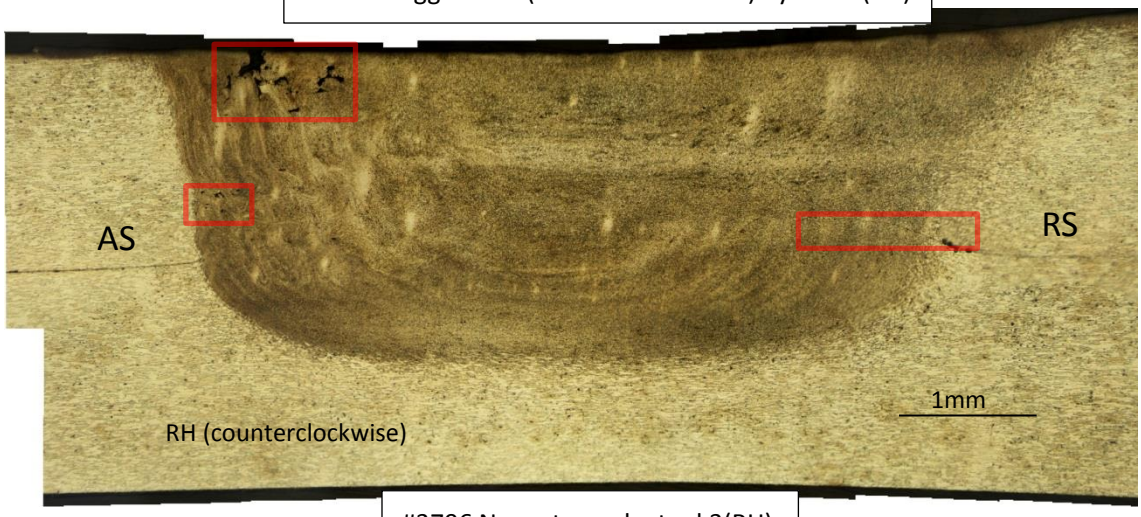

#3796 Nugget area by tool 3(RH)

#3798 Nugget area by tool 3(RH)

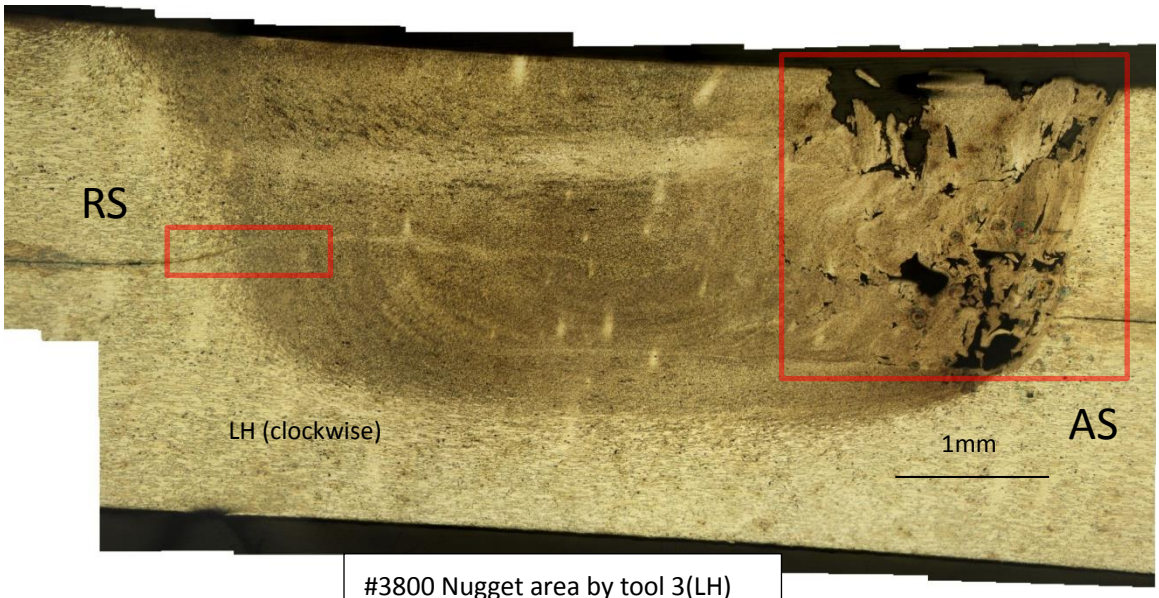

#3800 Nugget area by tool 3(LH)

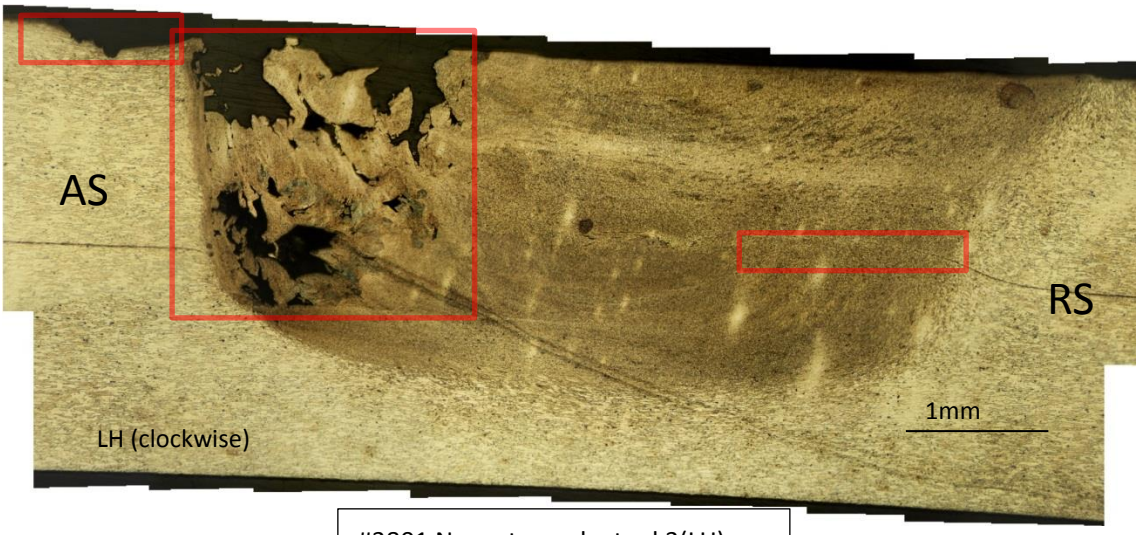

#3801 Nugget area by tool 3(LH)

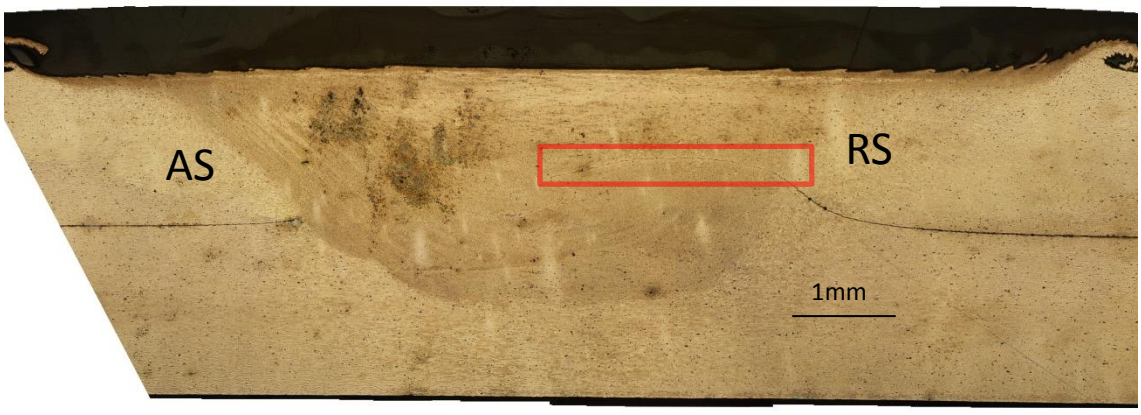

#3883 Nugget area by tool 4(RH)

#3885 Nugget area by tool 4(RH)

#3886 Nugget area by tool 4(RH)

Appendix C Grain Observation at Nugget Center

The corresponding parameters please see the Table 3.1

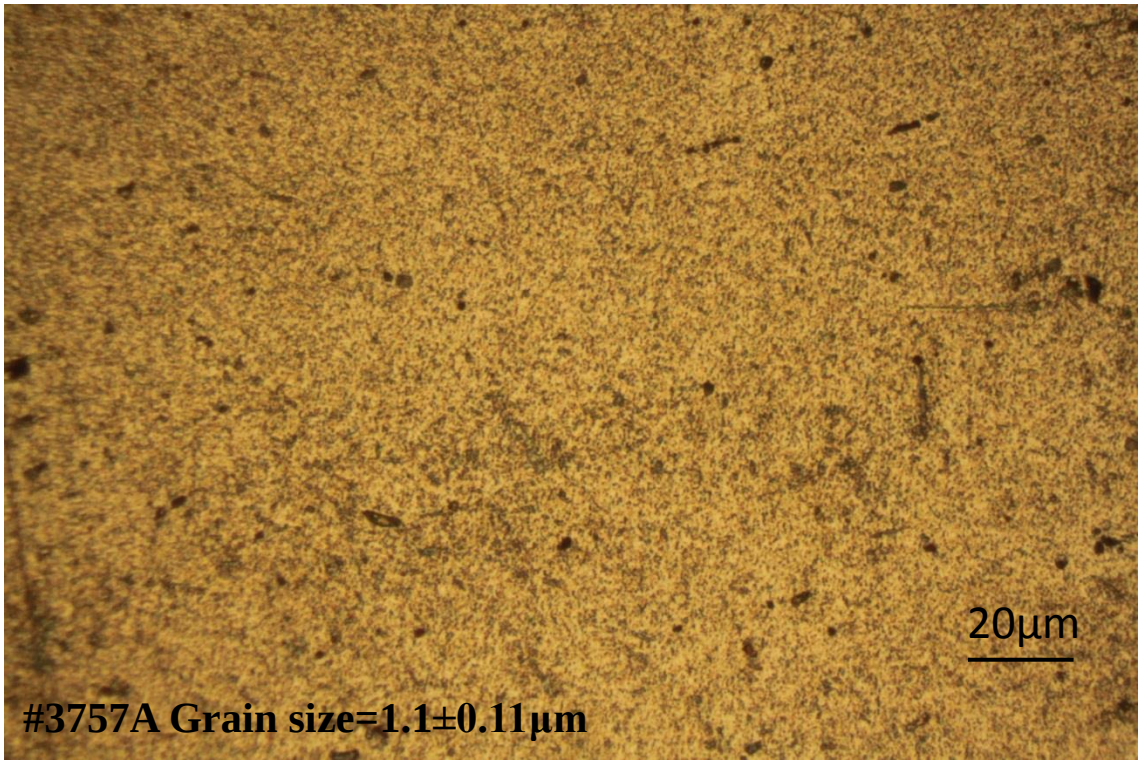

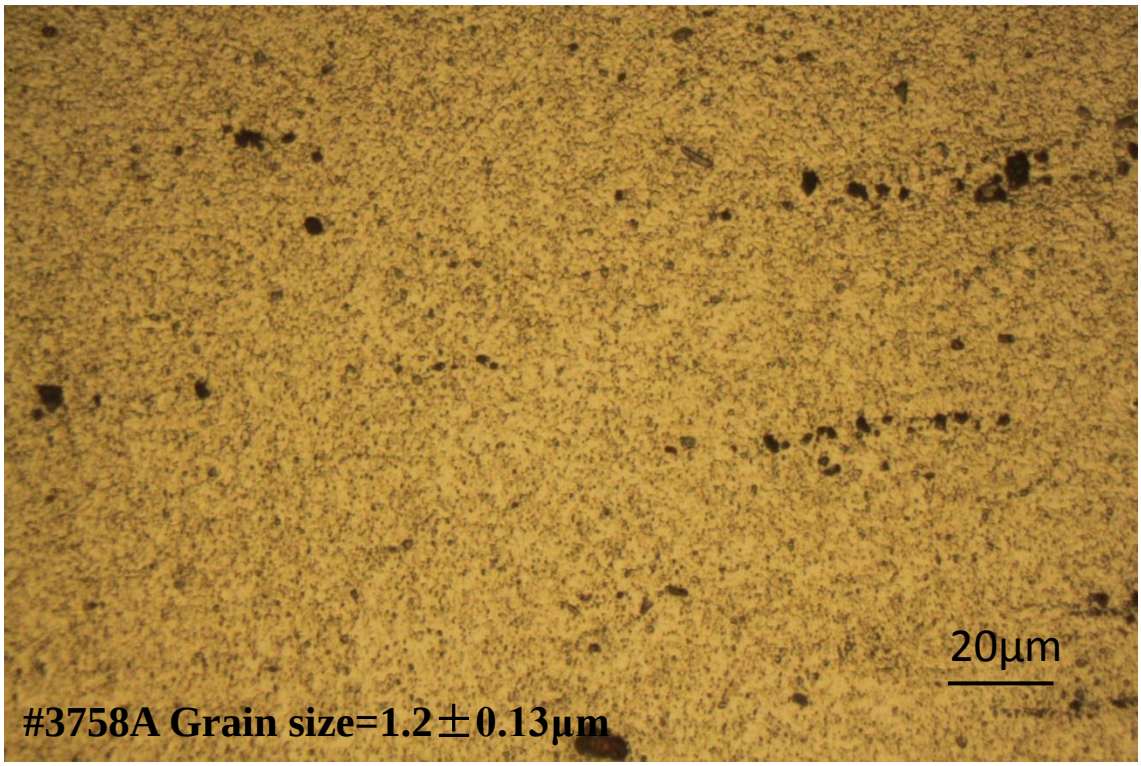
20μm
#3758A Grain size=1.2±0.13μm

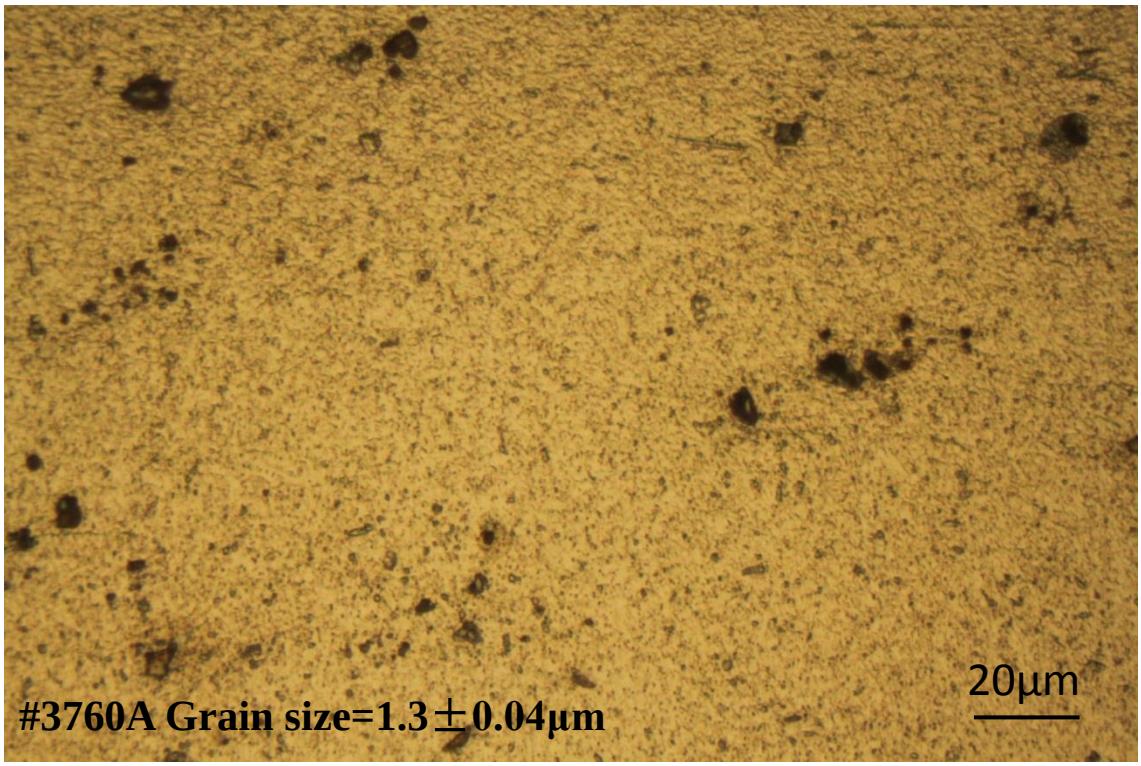
20μm
#3760A Grain size=1.3±0.04μm

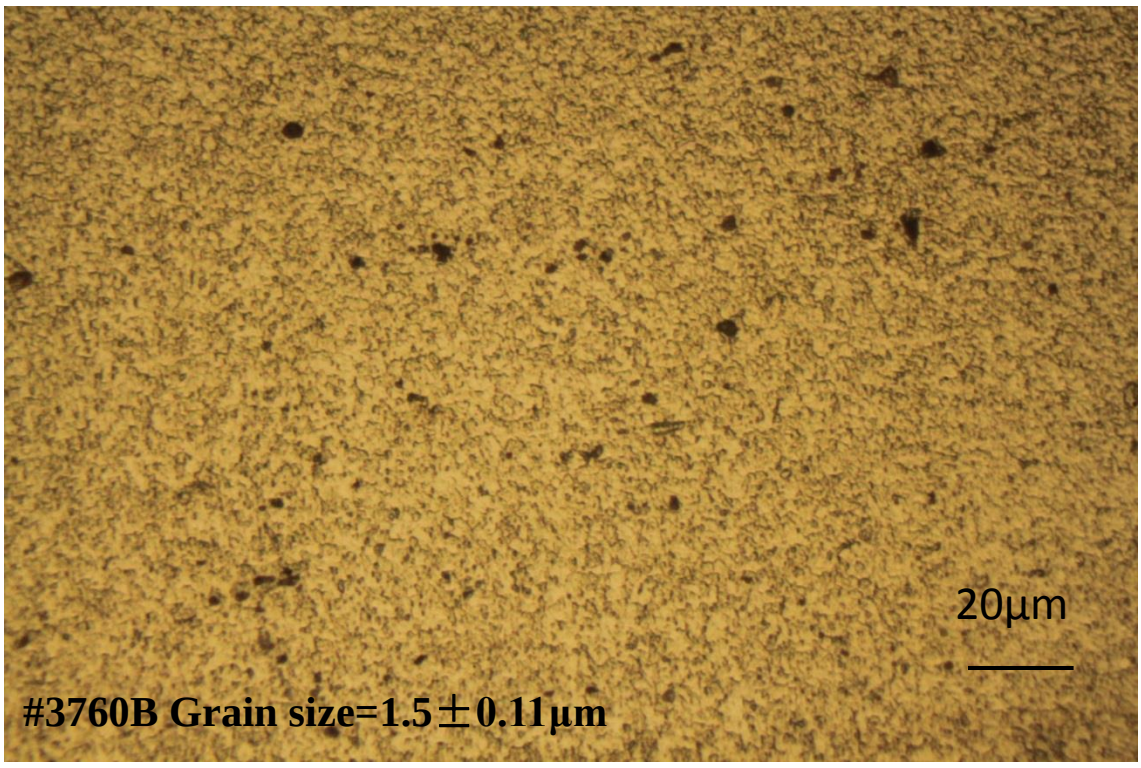

#3760B Grain size=1.5±0.11μm

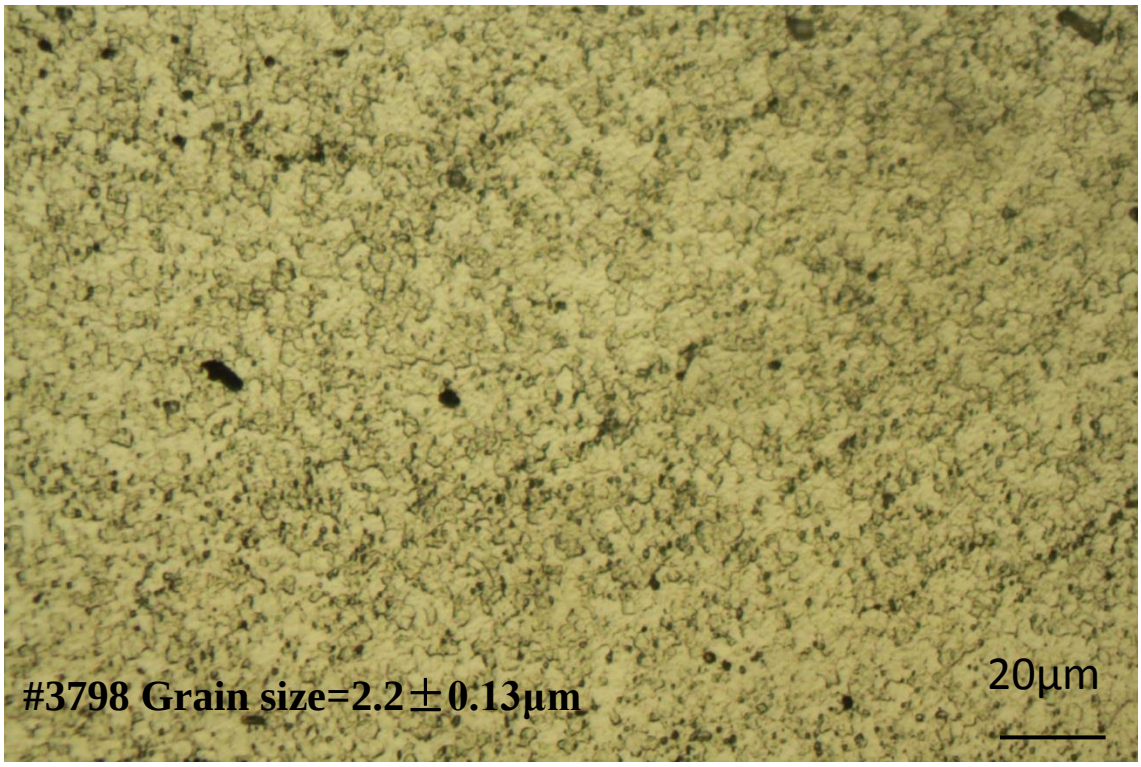

#3798 Grain size=2.2±0.13μm

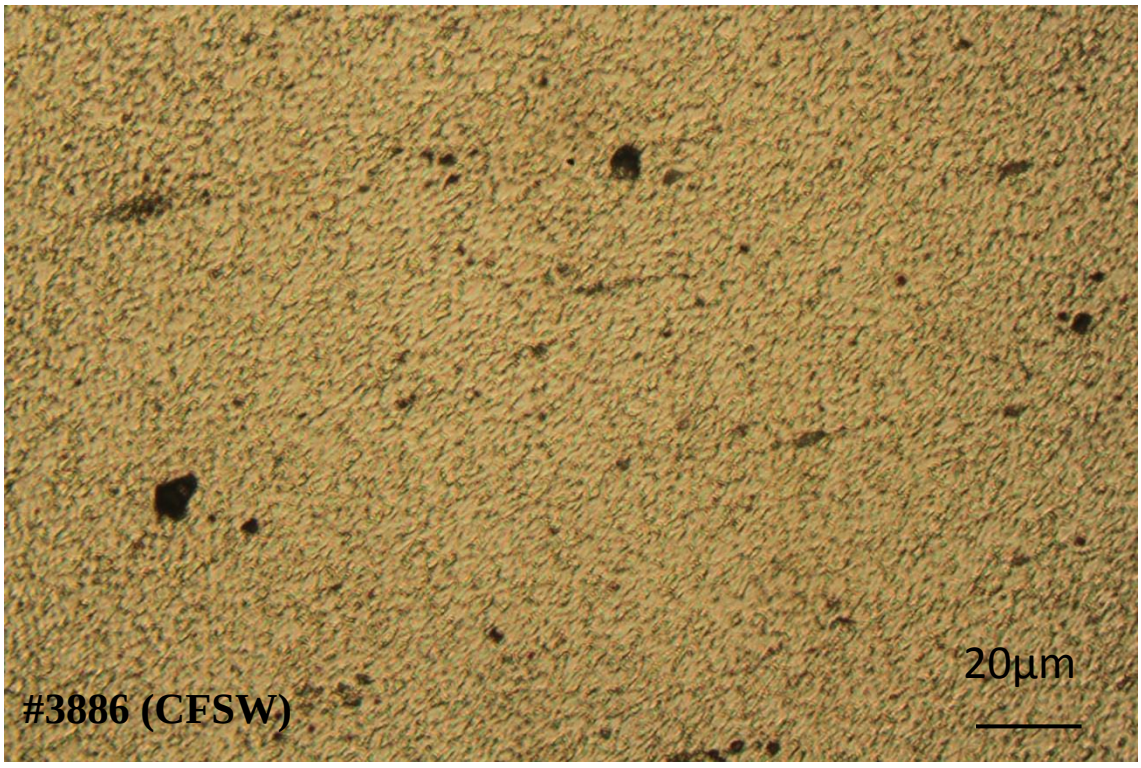
#3886 (CFSW)
20µm

Appendix D Comparison between Tool 3 RH&LH

Tool 3	LH(mm)	RH(mm)
d1	2.00	1.99
d2	2.54	2.52
d3	32.16	32.16
d4	90.82	87.16
d5	25.37	25.37
d6	7.14	7.10
θ1	18.5^{o}	18.4^{o}
Flats	3 flats	3 flats
thread number	≤ 2	≤ 2
taper(θ2)	7.8^{o}	6^{o}
θ3	8.9^{o}	8.5^{o}
θ4	58.8^{o}	57.8^{o}
θ5	58^{o}	60^{o}
d7	5.09	5.06
d8	5.65	5.63
d9	0.61	0.64
d10-1	0.34	0.39
d10-1: depth from adjacent peak to the flat surface 1		
d10-2	0.31	0.41
d10-2: depth from adjacent peak to the flat surface 2		
d10-3	0.31	0.4
d10-3: depth from adjacent peak to the flat surface 3		

Appendix E Microhardness Distribution at Cross Section

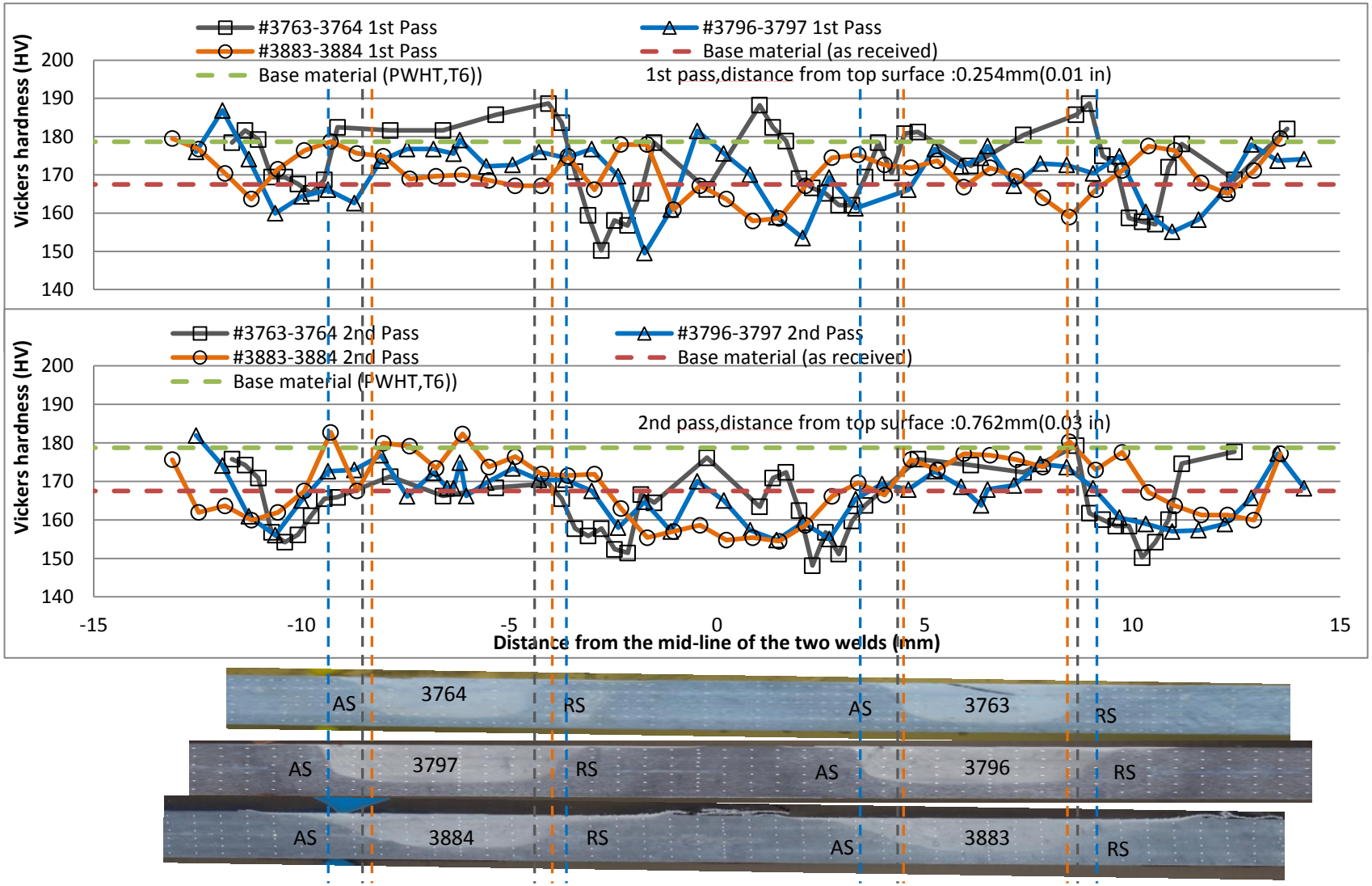

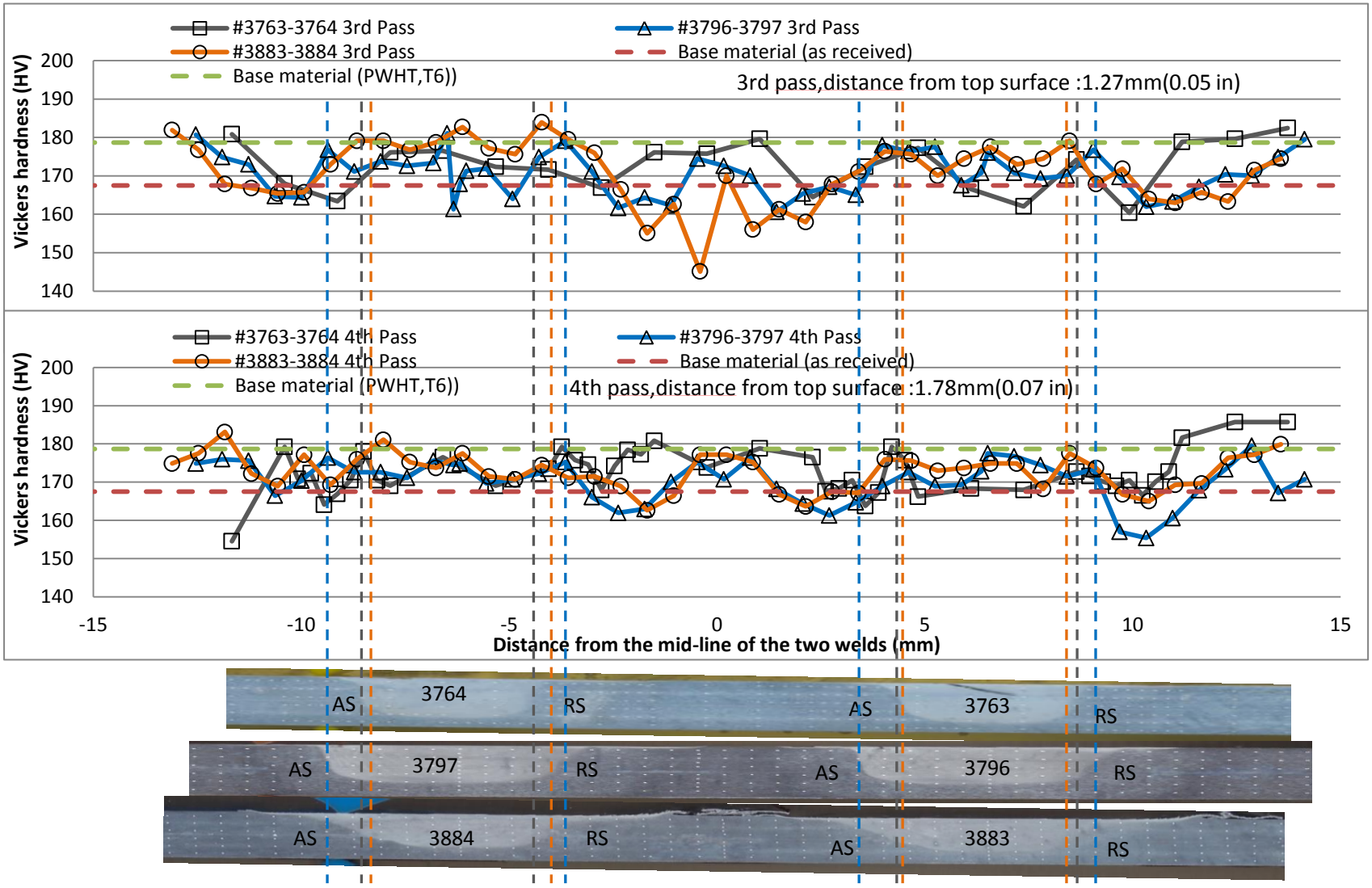
#3763-3764 3rd Pass
#3796-3797 3rd Pass
#3883-3884 3rd Pass
Base material (as received)
Base material (PWHT,T6))
3rd pass,distance from top surface :1.27mm(0.05 in)
Vickers hardness (HV)
200
190
180
170
160
150
140
#3763-3764 4th Pass
#3796-3797 4th Pass
#3883-3884 4th Pass
Base material (as received)
Base material (PWHT,T6))
4th pass,distance from top surface :1.78mm(0.07 in)
-15
-10
-5
0
5
10
15
Distance from the mid-line of the two welds (mm)
AS
3764
RS
AS
3763
RS
AS
3797
RS
AS
3796
RS
AS
3884
RS
AS
3883
RS

#3763-3764: The 6th pass of indentation is outside the nugget.
#3796-3797: The 6th pass of indentation is outside the nugget, the 5th pass of indentation is along the bottom nugget boundary.
#3883-3884: The 6th pass of indentation is outside the nugget, the 5th pass of indentation is along the bottom nugget boundary.

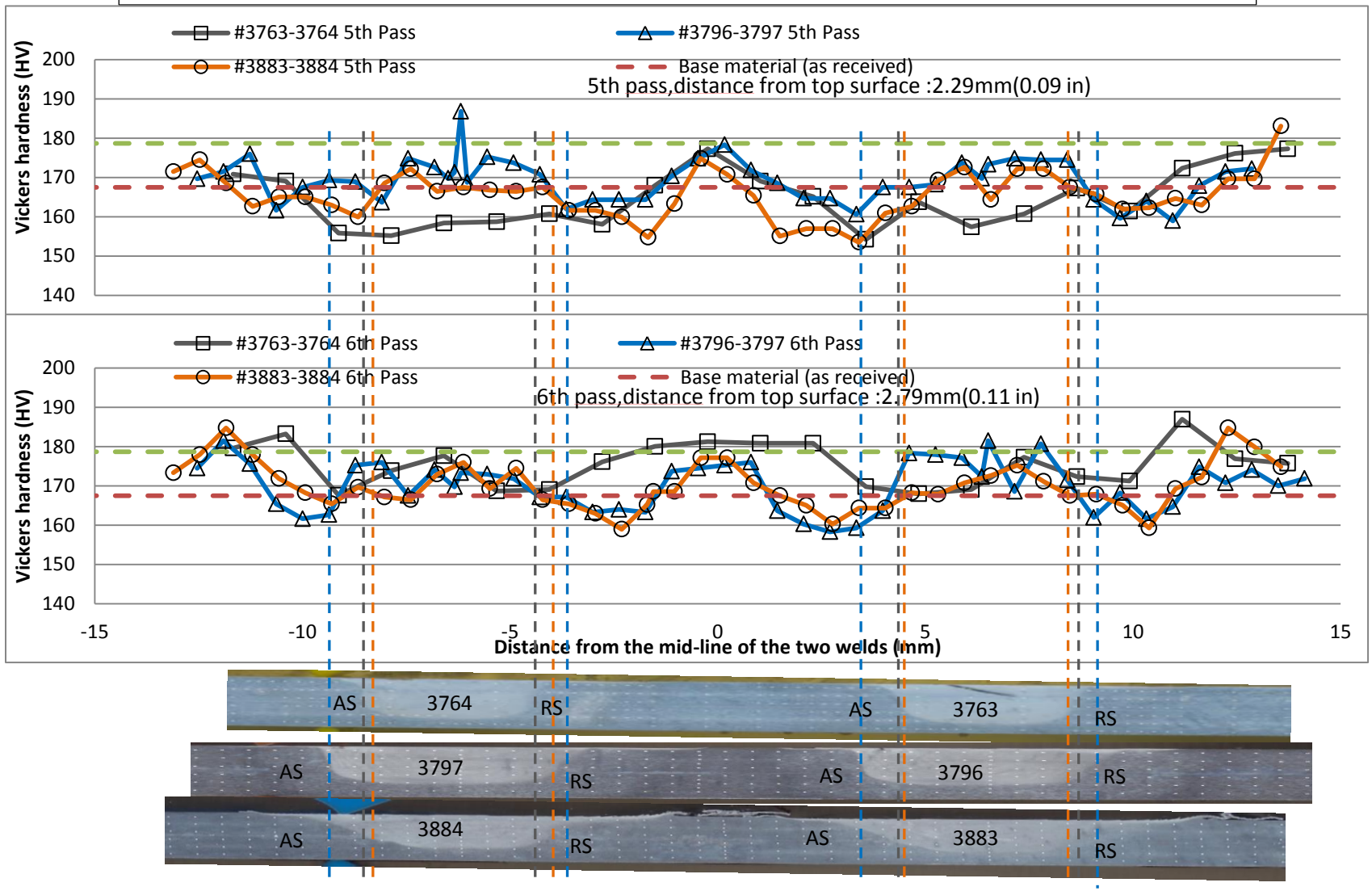

Appendix F Tensile Test Fracture Photos

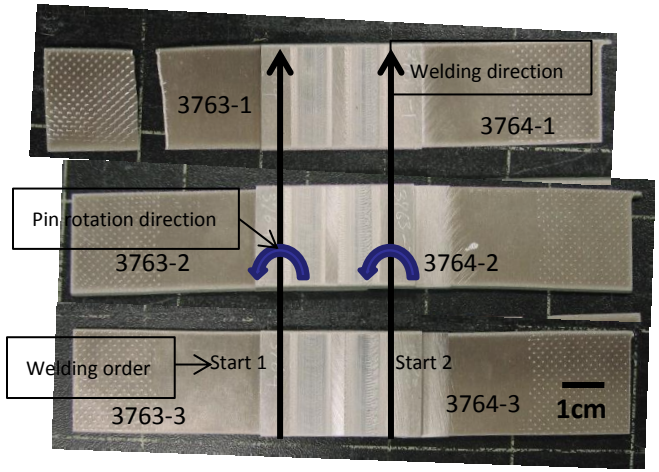

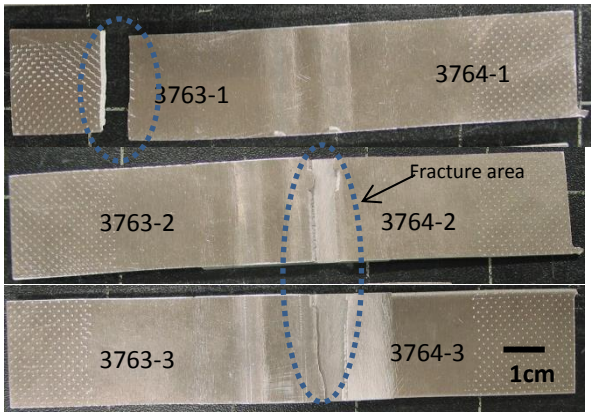

Top view 3763-3764 fractured tensile bars Bottom view

Pin rotation speed:-1500RPM, Welding speed:8.47mm/sec, Z-force:9.79kN by Tool 2

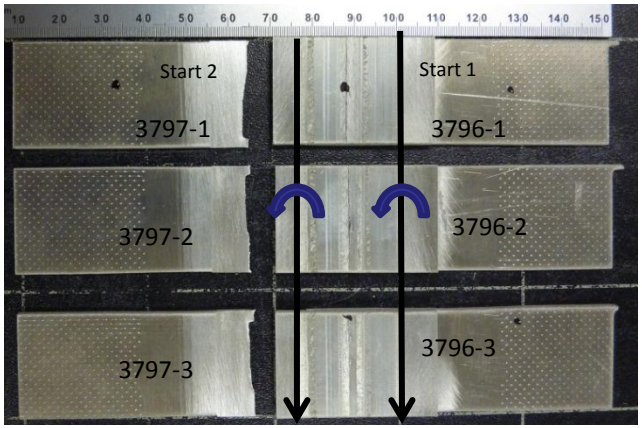

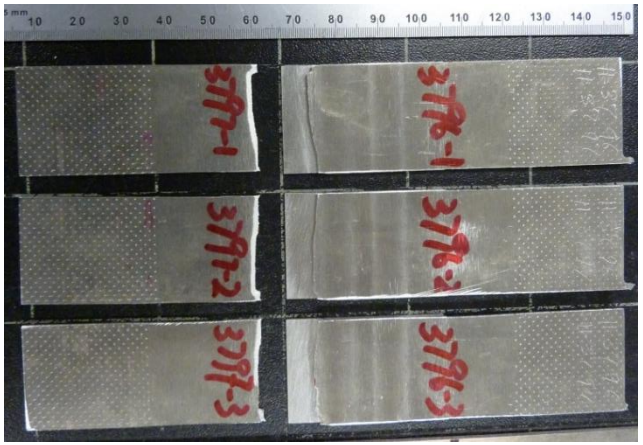

Top view 3796-3797 fractured tensile bars Bottom view

Pin rotation speed:-1500RPM, Welding speed:8.47mm/sec, Z-force:14.23kN by Tool 3

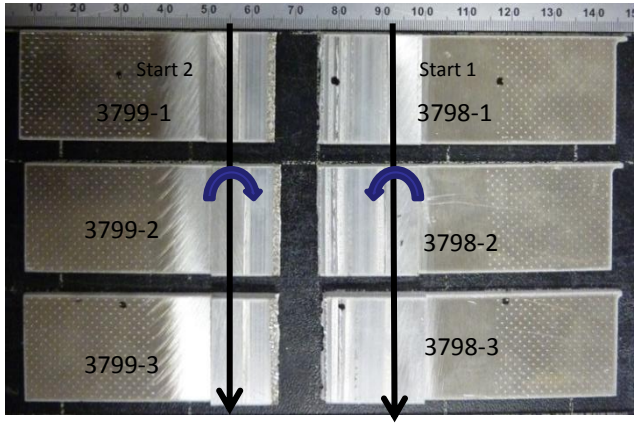

Top view

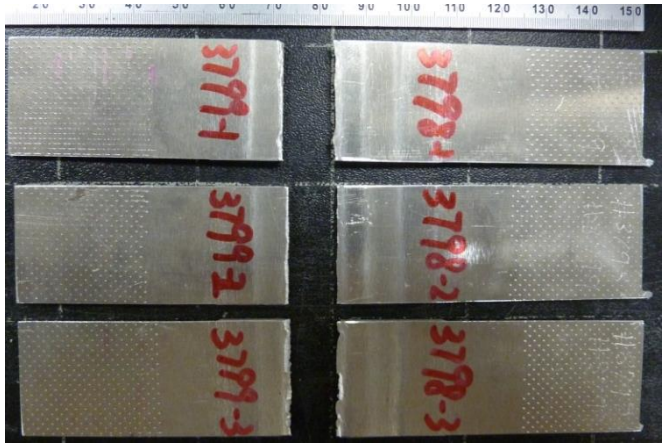

Bottom view

3797-3798 fractured tensile bars

Pin rotation speed: ±1500RPM, Welding speed:8.47mm/sec, Z-force:14.23kN by Tool 3

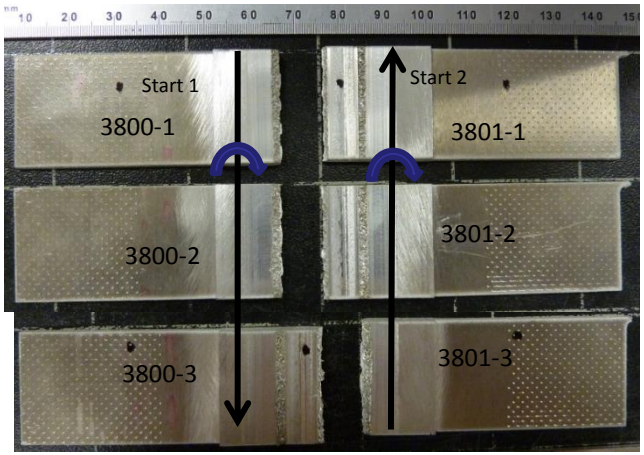

Top view

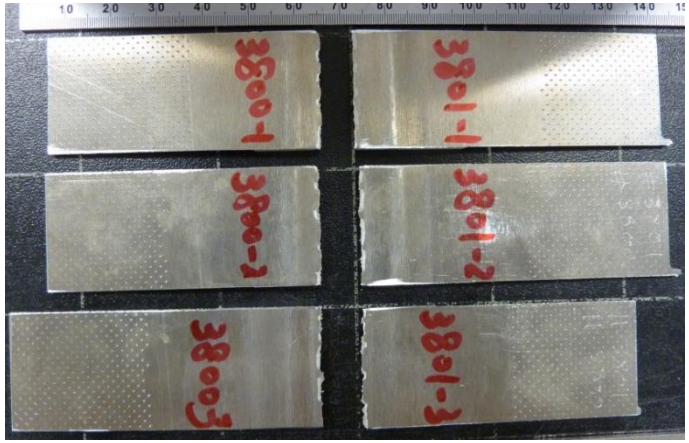

Bottom view

3800-3801 fractured tensile bars

Pin rotation speed:1500RPM, Welding speed:8.47mm/sec, Z-force:14.23kN by Tool 3

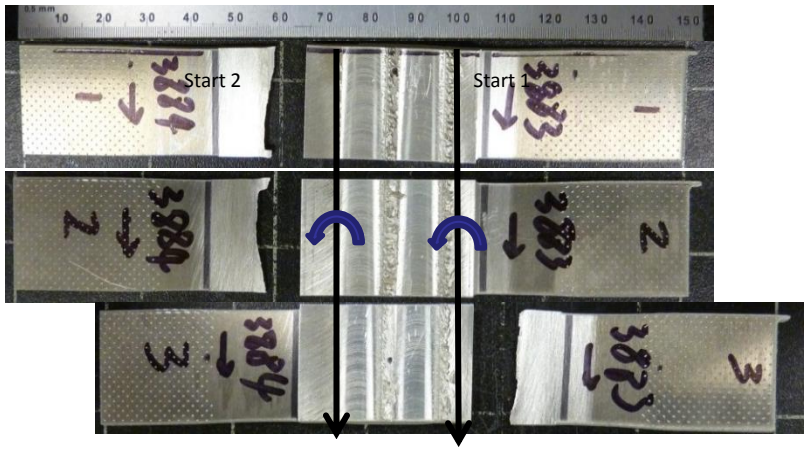

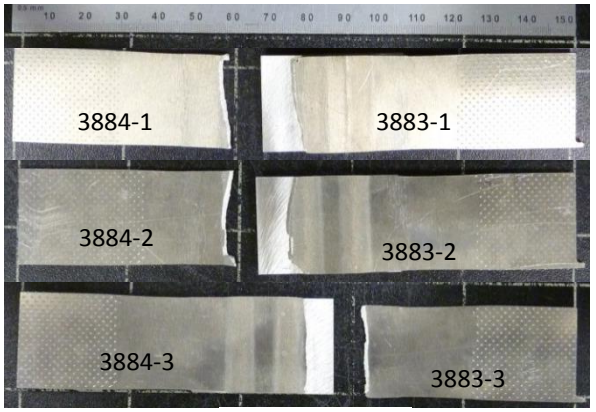

Top view 3883-3884 fractured tensile bars Bottom view

Pin rotation rate: -1500RPM, Welding speed:8.47mm/sec, Z-force:6.67kN by Tool 4

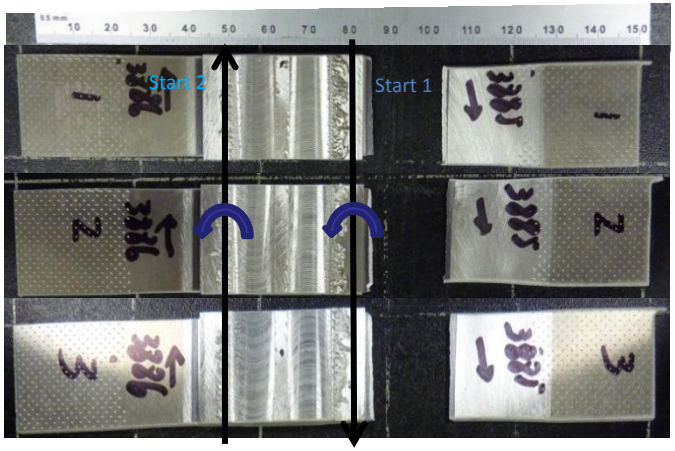

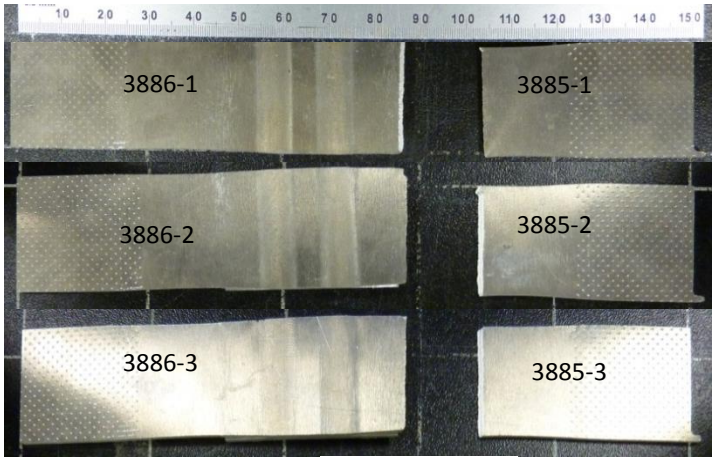

Top view 3885-3886 fractured tensile bars Bottom view

Pin rotation rate: -1500RPM, Welding speed:8.47mm/sec, Z-force:6.67kN by Tool 4